Fuel 371 (2024) 132125

Contents lists available at ScienceDirect

Fuel

journal homepage: www.elsevier.com/locate/fuel

Full Length Article

Clean co-combustion of glycerol and methanol blends using a novel fuel-flexible injector

Timothy Hall, Derek Williams, S M Rafiul Islam, Ishaan Patel, Caleb Chakmakjian, Lulin Jiang *

Department of Mechanical Engineering, Baylor University, Waco, TX 76798, USA

ARTICLE INFO

Keywords:
Swirl Burst (SB) injector
Lean-premixed combustion
Glycerol/methanol blends
High viscosity
Near-zero emissions

ABSTRACT

This study explores combustion of highly oxygenated fuel blends (glycerol/methanol, G/M) to mitigate carbon footprint using a novel fuel injector, called Swirl Burst (SB) injector. The recently developed SB injector yields fine droplets immediately rather than a breaking jet/film of conventional injectors. The advanced atomization resulted in ultra-clean combustion with high fuel flexibility even for viscous oils without fuel preheating. The present work investigates the effects of fuel composition and the atomizing air to liquid mass ratio (ALR) across the injector on the global combustion characteristics of G/M blends without fuel preheating in an uninsulated lab-scale combustor. Results show that the SB injection resulted in mainly clean lean-premixed and near complete combustion for the G/M mixes of 50/50, 60/40 and 70/30 by power with near-zero emissions of CO and NOx. Increase in ALR resulted in more radially distributed flames with slightly reduced flame lift-off height, with ultra-clean and near complete combustion for all the ALRs for the 50/50 and 70/30 blends. Clean and efficient G/M combustion without fuel preheating achieved by the fuel-flexible SB injection signifies the potential to combust crude glycerol – the largest oxygenated byproduct of biodiesel production – to enable biofuel cost effectiveness with near-zero emissions.

1. Introduction

In recent years, near-zero/net-zero-emission and efficient combustion and biofuel applications are urged by the changing climate due to the aggravating global warming. Biodiesel has become an emerging alternative fuel because of its closed carbon cycle and similar fuel properties to conventional diesel. In the European Union (EU), biodiesel production increased from 6.129 millions of tons to 14.11 millions of tons over the year 2007–2018 [1,2]. To create this fuel, highly viscous source oils go through the costly trans-esterification process [3] to form the biodiesel with "drop-in" i.e., similar properties of conventional diesel to be adapted into the existing combustion systems [4]. These systems utilize conventional fuel injectors with a high sensitivity to even a slight variation in fuel properties [5,6]. In addition, the trans-esterification process creates large surplus of crude glycerol as a waste byproduct, though the crude glycerol can be refined in another expensive process to be used in various food and pharmaceutical products [4]. Cost related to coping with the abundant waste renders the biodiesel production less cost effective, hence limiting its broad application for decarbonization. On the other hand, the waste crude glycerol can become an extremely low-cost potential fuel [7–9]. Glycerol has a moderate heating value and a high oxygen (O_2) content, and thus, has the potential to be burned as biofuel to mitigate carbon footprint for power generation [4,6,10,11]. However, the high ignition temperature and high viscosity of glycerol and the low-viscosity tolerance of conventional injectors have made it difficult to burn [4,12,13].

Clean and complete combustion of liquid fuels is not only determined by its chemical composition (such as a closed-carbon cycle of biofuels) but also by the complicated physicochemical process of spray combustion [4]. Effective atomization results in fine sprays that evaporate fast, leading to homogenous mixing of fuel vapor and air and thus the clean premixed combustion of liquid fuels with near-zero emissions or net-zero emissions when fuels are biobased with closed carbon cycle. Unfortunately, conventional airblast (AB) and pressure swirl (PS) injectors, widely used in gas turbines and other industrial burners generate a liquid jet core/film first that gradually disintegrates into ligaments and ultimately droplets even for low-viscosity water [4,14–16]. Moreover, the jet-breaking atomization is highly sensitive to slight fuel property variations. High viscosity further suppresses the atomization capability

* Corresponding author.
E-mail address: lulin_jiang@baylor.edu (L. Jiang).

https://doi.org/10.1016/j.fuel.2024.132125
Received 11 March 2024; Received in revised form 2 June 2024; Accepted 4 June 2024
Available online 8 June 2024
0016-2361/© 2024 Elsevier Ltd. All rights are reserved, including those for text and data mining, AI training, and similar technologies.

Nomenclature

CO	carbon monoxide
NO_X	nitrogen oxides
SB	swirl burst
VO	vegetable oil
H	the height between the injector exit and the internal liquid tube tip
D	the inside diameter of the internal liquid tube tip
AA	atomizing air
PA	primary air
d_h	hub diameter
d_t	tip diameter
α	angle of swirl (swirl vane angle)
ISN	injector swirl number
SN	swirl number for the combustion swirl of the gas turbine combustor
ALR	atomizing air to liquid mass ratio
LPM	lean premixed
G/M	glycerol/methanol

and elongates the atomization process, resulting in ligaments and large droplets [15]. These large ligaments/droplets of viscous fuels burn incompletely and/or in diffusion mode, yielding high pollutant emissions such as soot, toxic carbon monoxide (CO), nitrogen oxides (NO_X), and unburned hydrocarbons [4]. For instance, alternative jet fuel C-3 with only 3x higher viscosity than diesel resulted in the poorest ignition and high pollutant emissions compared to other jet fuels by using conventional AB injector [17]. As high-viscosity fuels burn incompletely using the conventional injectors, more fuel mass must be burned to achieve the same heat output compared to conventional low-viscosity fuels such as diesel, or more energy will be needed to preheat the fuels to reduce the viscosity [4]. This effect is further compounded in glycerol combustion because of its relatively low heating value, 15.8 MJ/kg, which is half that of biodiesel [4,7,12,13]. The high viscosity and relatively low energy density signify that novel fine atomization concept with high-viscosity tolerance and/or blending glycerol with fuels with higher heating values are necessitated to enable glycerol as a potential clean renewable fuel and achieve heat output comparable to conventional fuels via co-combustion of glycerol-based blends [4].

In the last two decades, Gañán-Calvo first developed flow-blurring (FB) atomizer which can generate 5–50 times greater surface area than an AB atomizer, via using a novel primary atomization mechanism by bubble bursting that is fundamentally distinct from the typical AB/PS jet/film breaking [18]. In FB, at a unique simple internal geometry, a small quantity of the atomizing air (AA) that passes through an annular channel around the center liquid channel penetrates into the liquid fuel and rapidly forms bubbles at the inner liquid tube tip [18]. These bubbles burst due to a large pressure drop while leaving the atomizer exit, defined as the primary atomization, shattering the surrounding liquid into fine spray immediately at the injector exit [19], rather than a typical AB/PS jet core/film. The remaining larger portion of AA directly leaves the injector exit and leads to the secondary atomization of liquid by shear layer instabilities developed at the interface of the liquid parts and the high-velocity air [20]. FB can generate ultra-fine sprays for various liquids [15] ranging from low-viscosity water, to high-viscosity alternative jet fuel C-3 [21], and even extremely viscous pure glycerol [22] without fuel preheating. Simmons et al. observed that for atomizing air to liquid mass ratio (ALR) of 2.5, with the injector exit diameter (D) of 1.5 mm, FB can generate more uniform final water droplets with the Sauter Mean Diameter (SMD) of 5–15 μm, compared to SMD of 5–25 μm for the AB injector with the injector orifice *D* of 0.15 mm at >2 cm downstream the exit [15]. Qavi et al. found that FB injector, with the injector *D* of 1.5 mm, generated fine droplets with the size of 90 % < 45–70 μm for the ALRs of 1.00 to 2.5 respectively within 6 mm downstream of the injector exit for the viscous alternative jet fuel C-3 (blends of farnesane and JP-5) [21]. Even for the high-viscosity glycerol (~>200x more viscous than diesel), FB injector generates thin ligaments and fine droplets with the thickness or diameter <40 μm at 0–2 mm located at the downstream direction from the injector exit [22]. Thus, it has enabled ultra-clean, complete, and lean-premixed combustion of distinct fuels including diesel, biodiesel, straight vegetable oil and straight glycerol [10,23–25]. However, relatively larger droplets occur at the FB injector spray periphery [26]. Also, while atomizing the extremely viscous pure glycerol by using an FB atomizer, the thin ligaments undergo secondary atomization by shear layer instabilities [22], yielding a longer atomization completion length compared to the lower viscosity liquids. Hence, though complete, ultra-clean and lean-premixed combustion was even achieved for the non-preheated straight glycerol by FB injection, the flame lift-off height was increased compared to the lower-viscosity fuels, compromising its flame stability [19].

To further improve the secondary atomization with a wide range of viscosity tolerance, our group recently developed a novel Swirl Burst (SB) injector [27,28]. The SB injector integrates the bubble-bursting primary atomization mechanism of the FB and novel swirling channels on the chamfered exit to guide the AA to leave the injector exit in a swirling pattern (as a combined radial and axial swirl) to rigorously enhance the interaction between the liquid parts and the swirling AA, resulting in more robust secondary breakup. Fig. 1 (a)-(c) show the

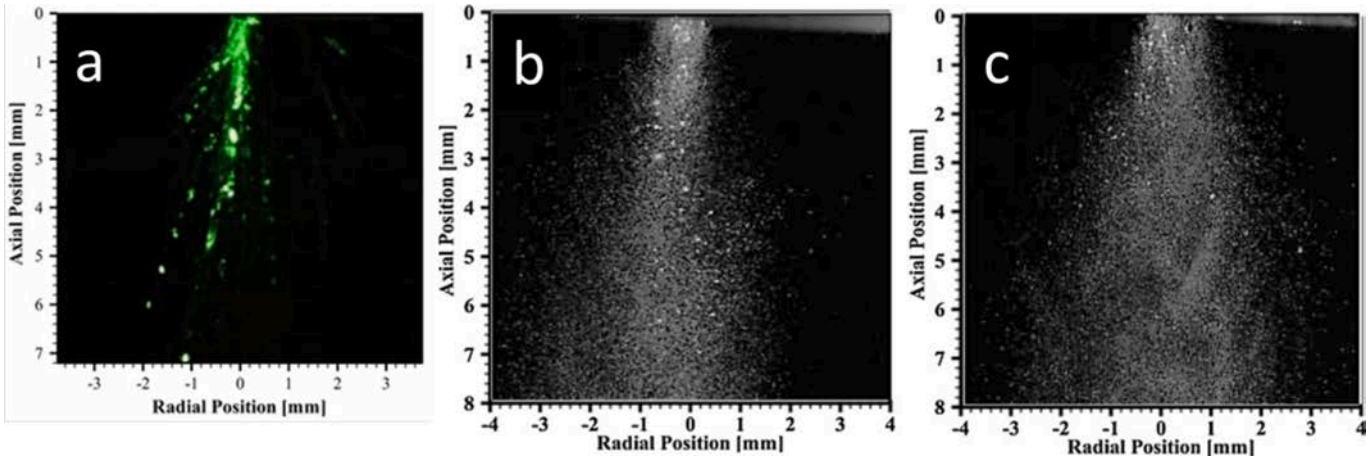

Fig. 1. Comparison of water spray images from (a) AB injector [26] (b) FB injector and (c) SB injector [27].

water spray images by AB, FB and SB injectors respectively [26,27]. Compared to the AB jet core, both FB and SB injectors generate fine droplets at the injector immediate exit with more diverged spray angle for the SB injection. Advanced laser diagnostics in the injector near field also quantitatively substantiated that the SB injector generates finer droplets at the spray periphery with more uniform droplet size distribution and halved atomization completion length than that of an FB injector [27–29]. Thus, the SB injector enabled lean-premixed and complete combustion with ultra-low emissions for fuels including diesel, biodiesel, viscous straight vegetable oil (VO), and straight algae oil (AO), without fuel preheating nor hardware modification [4,19,20]. The VO and AO are approximately 15 times or 16 times more viscous than diesel [4,19,20]. The flame lift-off height of the straight VO sprays formed by the SB injection was also shortened compared to that of the FB atomizer, enhancing the spray combustion stability, as over-lifted flames are subjective to blow out [4,19]. A previous version of the novel two-phase injector with high-viscosity tolerance but a longer atomization length [21,27,29] also resulted in clean and complete combustion of straight glycerol (>200 times more viscous than diesel) without fuel preheating, though an insulation layer was used to minimize heat loss [4,10]. This novel injector design transforms the conventional jet-breaking atomization into ultra-fast and fine atomization with high fuel flexibility [4]. Compared to a sooty flame with droplets incompletely burned by jet-breaking conventional injection, the SB injector thereby not only enables complete and lean-premixed combustion of low-viscosity liquid fuels, but also enables the ultra-clean and efficient combustion of highly viscous waste glycerol, transforming it into a potential cost-effective biofuel and making the biodiesel production more economically friendly.

On the other hand, crude glycerol formed as a biodiesel byproduct contains a major impurity in the form of methanol [4,6,11,30,31]. Methanol is an extremely low viscosity liquid that is used in excess during the trans-esterification process to help convert reactants to biodiesel [4,7]. Besides, methanol has high octane number that could prevent engine from knocking and reduce greenhouse gas emissions [32]. While it can be removed and reused in the trans-esterification process, methanol is typically left with the crude glycerol and disposed of because it is easier and cheaper to use a pure supply [4,7,31]. Also, energy consumption for extracting methanol from biodiesel production is almost 48 % of total energy consumption of biodiesel production [33]; hence, it is a highly energy expensive process. Compared to glycerol, glycerol/methanol blends, the main components of crude glycerol, can achieve a significantly lower viscosity that is comparable to that of diesel, easing the fuel atomization when using it as a fuel source [4,7,34]. Crude glycerol from the transesterification process of biodiesel production contains 60–70 % glycerol and 23.4–37.5 % methanol by weight [6]. Thus, the current study examines glycerol and methanol blends with the composition representing the crude glycerol to avoid the need for possible further refinement of crude glycerol, which could enhance its cost-effectiveness as a potential waste-based biofuel to produce renewable energy [4]. Furthermore, methanol blended with glycerol helps to avoid heat loss, lower the fuel viscosity, and benefit carbon mitigation as an oxygenated fuel [4,7].

The combustion performance of glycerol/methanol (G/M) blends is rarely investigated. Agwu et al. [7] investigated the G/M flame characteristics (luminosity, stability etc.) but not the emissions using a conventional pressure swirl injector that is based on jet/film breaking atomization, which generated sooty orange flames. Jin et al. showed that, for Spark Ignition Engine (SIE), by adding 5 % glycerol with methanol by volume can increase the thermal efficiency from 38.3 % to 43.1 %, while NOx emissions and soot in the exhaust gas remain unchanged compared to the 100% methanol fuel [35]. Oliveria et al. combusted glycerol by chemical looping combustion process and achieved 90 % combustion efficiency at oxygen to fuel molar ratio of 7, water/glycerol ratio of 0.75 and with reactor temperature of 1023 K [36]. In the current study, the swirl burst (SB) injector, with the preliminary results that proved high viscosity tolerance [19,20], is expected to achieve complete, clean, and stable combustion of glycerol-methanol blends without fuel preheating [4]. The objective of this experiment is to discover the impacts of fuel composition of glycerol and methanol and the atomizing air to liquid mass ratios (ALR) on the global combustion characteristics using the novel SB injector in a lab-scale swirl-stabilized gas turbine combustor [4]. The flame features of interest include visual flame images, product gas temperatures, and emissions (CO and NO_X) to assess global combustion completeness, cleanness, and flame stability [4]. The novelty of the current study is thus focused on potentially enabling direct use of crude glycerol for waste to energy with minimal processing by achieving clean and nearly complete combustion of different non-preheated high-viscosity glycerol and methanol blends representing crude glycerol using the SB injector.

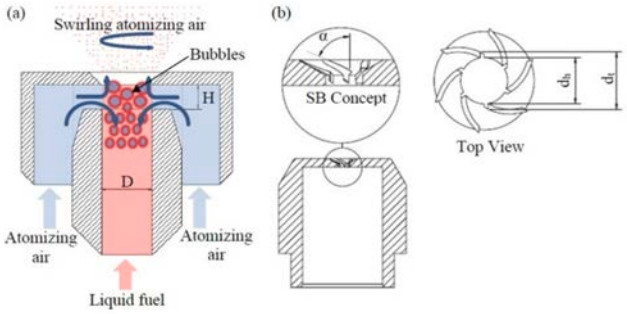

Fig. 2. (a) working principle of the SB injector (b) SB concept [4,19,20].

2. Experimental setup

2.1. Swirl burst injector

The working principle and concept of the swirl burst injector are illustrated in Fig. 2, which are detailed in Ref. [4,19,20,27,28]. The SB injector has two stages of atomization [4]. The first stage occurs while the AA in the annulus channel surrounding the liquid tube bifurcates and incurs the backflow of a small amount of AA into the liquid tube tip, when the geometric conditions are met: (1) D of the internal liquid tube is equal to that of the injector exit; (2) the gap, H, between the liquid tube tip and the injector exit is $\leq 1/4D$ [4]. The AA backflow rapidly forms a bubble zone with pockets of air enclosed by liquid at the liquid tube tip [4]. The bubbles expand and burst, causing the surrounding liquid to shatter into fine droplets while exiting the injector, due to a quick pressure drop [4]. The remaining AA exits the chamfered injector orifice through small grooves in a swirling motion [4]. This causes increased shearing between the liquid and AA around it, further breaking down the liquid into smaller droplets [4,27,28]. The swirling grooves in the orifice are defined by three parameters called the hub diameter (d_h), tip diameter (d_t), and swirl vane angle (α) [4]. The hub and tip diameter describe the volume of air/fuel mixture that passes through the grooves, while the swirl angle describes the angle at which the liquid (fuel mixture) is swirled as it exits the injector [4]. The swirl burst injector exit orifice is defined using a non-dimensional injector swirl number (ISN) as in Eq. (1) [4,27,28,37]. It is a non-dimensional number representing the axial flux of swirl momentum divided by the axial flux of axial momentum times equivalent nozzle radius [4,37]. The current study uses the SB injector with D of 1.5 mm, H of 0.375 mm, and ISN of 2.4 [4].

$$ISN = \frac{2}{3} \times \frac{1-(d_h/d_t)^3}{1-(d_h/d_t)^2} \times tan\alpha \quad (1)$$

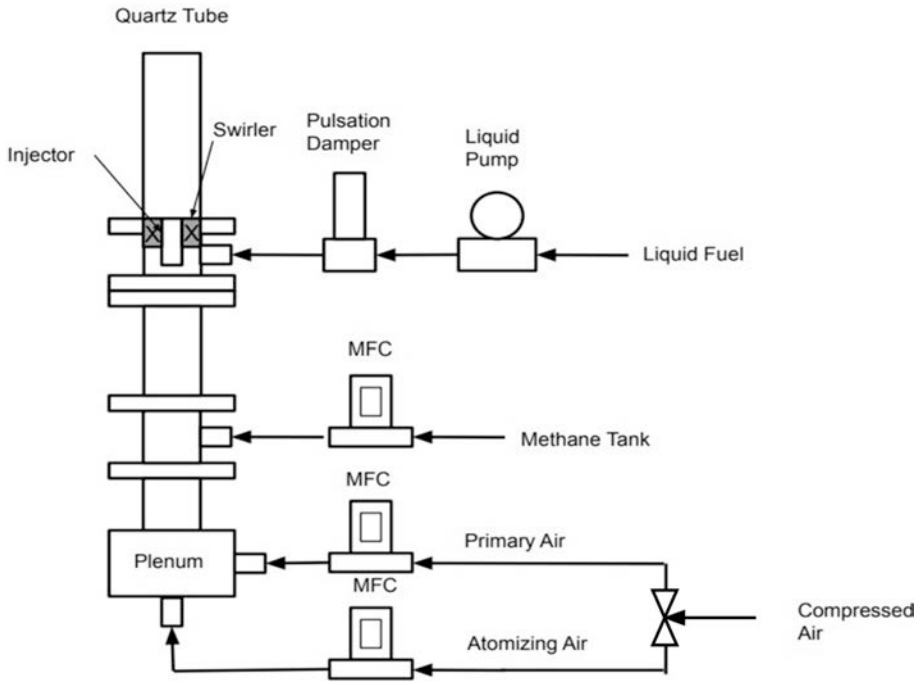

Fig. 3. Schematic of the experimental set-up [4].

2.2. Combustion system

Fig. 3 shows the experimental setup of the lab-scale swirl-stabilized gas turbine combustion system [4]. The in-house compressed air, after passing through water traps and filters to ensure clean air, is split into two lines [4]. The first line is the primary air for combustion [4]. The second line, atomizing air, connects to the SB fuel injector that is installed in the center of the downstream dump plane [4]. Both lines are controlled with mass flow controllers (MFC) [4]. The mass flow controllers are both Alicat MC-series controllers with a range of 0–100 SLPM for the atomizing air and a range of 0–250 SLPM for the primary air [4]. Both mass flow controllers have an uncertainty of 0.8 % of the reading ±0.2 % of the full range [4]. The primary air flows into a mixing chamber filled partially with marbles to ensure a laminar and even flow [4]. Methane flows into the mixing chamber from a compressed natural gas tank [4]. The flow is controlled with another Alicat MC-series controller with a range of 0–50 SLPM [4]. For air and methane flow control, all the MFCs use standard conditions and the set value of the standard condition is 25℃ temperature and 1 atm pressure. Also, the ambient temperature of the laboratory is 22℃ throughout the experiment. To ensure the repeatability of the experiment, preliminary test is conducted by taking emission and temperature data at the combustor exit to ensure the injector and combustor system is function well without leakage. In the mixing chamber, methane is premixed with the primary air which then enters a quartz combustor tube through an axial swirler with a swirl number (SN) of ~0.75 [4]. The quartz tube is 45 cm long and 7.62 cm wide [4]. The methane/air flame is used to preheat the chamber before switching the gaseous fuel to fully liquid fuel blends [4]. The liquid fuel blend is delivered through a pulsation damper by a peristaltic pump [4]. The peristaltic pump is a Cole-Parmer Masterflex L/S (EW-77921-75) with a range of 0–88 mLPM and an uncertainty of ±0.1 % of the reading [4]. The liquid fuel then enters the fuel injector before entering the quartz combustor as a fine spray [4]. The fuel blends are atomized using the swirl burst injector with the ISN of 2.4 [4].

2.3. Experimental conditions

The fuel blends of glycerol and methanol in this experiment are 50/50, 60/40, and 70/30 of glycerol/methanol by percent heat output at a constant theoretic heat release rate (HRR) of 7 kW and a constant equivalence ratio (ER) of 0.75 [4]. Table 1 provides physical properties of glycerol and methanol compared to conventional diesel fuel [4]. The experimental conditions and the properties of the fuel mixes are listed in Table 2 [4]. The viscosity calculations for the fuel blends in Table 2 are calculated with the method detailed by O. Agwu et al in [4,7]. The fuel blends are fed into the twin-fluid SB injector at ALR of 1.5, 2.0, 2.5, and 3.0 for the spray combustion in the 7-kW swirl stabilized gas turbine

Table 1
Selected properties of the relevant fuels [4,7,10,12,13,38–40].

Property	Diesel	Methanol	Glycerol
Approximate chemical formula	$C_{11.125}H_{19.992}$	CH_4O	$C_3H_8O_3$
Lower Heating Value, LHV (MJ/kg)	44.6	19.9	15.8
Density at 25 °C (kg/m^3)	834.0	791	1260
Kinematic viscosity at 25 °C (mm^2/s)	3.88	0.59	965.8
Auto-ignition temperature (°C)	260	464	370
Vaporization temperature (°C)	160–370	64.7	290
Heat of vaporization (kJ/kg)	250	726.1	662
Stoichiometric air/fuel ratio (mol/mol)	16.12	7.14	16.66

Table 2
The experimental conditions and fuel properties of the tested fuel blends [4].

Property		50/50	60/40	70/30
Percent heat output	Glycerol	50 %	60 %	70 %
	Methanol	50 %	40 %	30 %
Mass flow rate (g/min)	Glycerol	13.29	15.95	18.61
	Methanol	10.53	8.44	6.33
	Total	23.84	24.39	24.94
Volume flow rate (mLpm)	Glycerol	10.55	12.66	14.77
	Methanol	13.34	10.67	8.01
	Total	23.89	23.33	22.77
Atomizing air flow rate (SLPM)		56.09	57.37	58.66
Primary air flow rate (SLPM)		87.96	86.99	86.02
Density at 25 °C (kg/m^3)		998.09	1045.46	1095.15
Kinematic viscosity (mm^2/s) at 25 °C		4.16	8.02	18.02

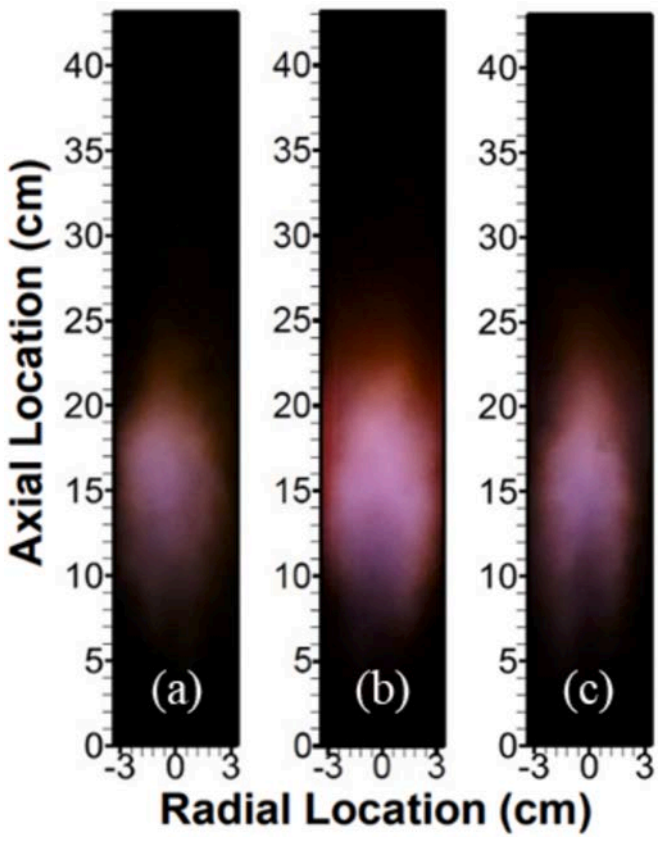

Fig. 4. Flame images of glycerol/methanol fuel mixes by power of (a) 50/50 (b) 60/40 and (c) 70/30 at the constant ALR of 3 and constant HRR of 7 kW [4].

combustor [4]. The combustion of the three fuel blends also remains at the constant equivalence ratio of 0.75 [4]. The combustion products including NOx, CO, carbon dioxide (CO_2) and O_2 are measured using an ENERAC (700 series) emission gas analyzer [4]. The analyzer can detect NOx in dual range mode of the low range 0–50/150 ppm and 0–1500 ppm with a resolution of 0.1 ppm and an uncertainty of $< \pm 1\%$ of measurement [4]. For CO, the measurement range is low range 0–50/150 ppm and 0–2000 ppm with a resolution of 0.1 ppm, an uncertainty of ±1–2 % of measurement [4]. The O_2 sensor has a range of 0–25 % with 0.1 % resolution, an uncertainty of ±0.2 % of the reading [4]. The catalytic sensor that detects the combustibles has a range of 0–5 % with an uncertainty of ±2 % [4]. The temperature of the exhaust gas is measured with a type K thermocouple plugged into the emissions analyzer with a range of 0–1100 degrees Celsius and an uncertainty of 2 degrees Fahrenheit [4]. The thermocouple is placed inside of a thin hollow probe that also collects a continuous sampling of exhaust gas for the emissions analyzer [4]. The emissions are collected at the combustor exit, i.e., 1 in. upstream the quartz opening, to assess the combustion completeness and cleanness [4].

3. Results and discussion

3.1. Effect of fuel blends on global combustion characteristics

3.1.1. Global flame characteristics

This study first investigates the effect of various fuel mixtures [4]. The largest apparent difference is the kinematic viscosity of each mixture shown in Table 2 [4]. The density for 70/30 G/M increases up to 10 % from the density of G/M 50/50. The viscosity varies from 4.16 mm^2/s for 50/50 G/M, which is only slightly more viscous than diesel in Table 1, to 18.02 mm^2/s for 70/30 G/M, i.e., >5x more viscous than diesel [4]. Flow rates are similar at the constant HRR of 7 kW as illustrated in Table 2. Visual flame images are taken to qualitatively analyze the cleanness and structure of the flame [4]. Flame lift-off heights and flame lengths are estimated [4]. Flame color indicate flame cleanness related to the chemiluminescence [4,12,32]. For example, blue flames represent chemiluminescence of complete combustion of CH* [24]. The flame images of G/M fuel blends with a ratio of 50/50, 60/40 and 70/30 by HRR are illustrated in Fig. 4. In all the three cases the equivalence ratio and the ALR are maintained at 0.75 and 3.0 respectively. Fuel atomization, fuel pre-vaporization, and fuel–air mixing occurs in the dark area near the injector exit and upstream the flame front, indicating that the mainly lean-premixed (LPM) combustion has achieved for all the three fuel blends [4]. The main blue color in all the flames qualitatively signifies that all the fuel blends are combusted cleanly. The overall physical flame structure is similar for all the flames, signifying the high fuel flexibility of the novel SB injection regardless of the distinct variation of the fuel viscosity [4]. The visual flame begins near the axial location of y = 10 cm (with y = 0 for the dump plane) in each fuel mix [4]. However, the 50/50 mixture creates a slightly more compact and faint flame than the other two mixtures [4]. The 50/50 mixture's visual flame is located slightly further downstream than the other two mixes at y = 11 cm [4]. It ends at y = 23 cm, while the other two end further downstream at 24-cm [4]. The flame lengths are ~12 cm (y = ~11–23 cm), 15 cm (y = ~ 9–24 cm) and 15 cm (y = ~ 9–24 cm) respectively for the 50/50, 60/40 and 70/30 glycerol/methanol (G/M) mixes [4]. The slight variation is possibly due to (1) the higher viscosity of the 60/40 and 70/30 fuel mixtures causing large droplets to penetrate deeper into the reaction zone more often which increases the residence time of combustion, thus a slightly elongated flames, and (2) more glycerol for the 60/40 and 70/30 resulting in slower vaporization, ignition, and thus slower oxidation due to the high vaporization and auto-ignition temperature of glycerol [4]. The slightly increased flame lift-off height of the G/M 50/50 is likely due to the higher AA flow rate causing a higher injection velocity for the fuel mixture [4].

From the flame images in Fig. 4, it is observed that the flame area of 50/50 G/M is most compact. The 60/40 G/M is with the largest flame area with the longest and widest flame among the three cases. The 70/30 G/M flame has a slightly shorter length than 60/40 G/M flame but the narrowest flame among the three. The flame structure variation is possibly attributed to the combined effects of (1) the fuel blend viscosity; (2) the composition of the glycerol component that has high evaporation and ignition temperatures; (3) the fuel injection velocity determined by the AA flow rate. Among the three blends, 50/50 G/M is the least viscous with the lowest AA thus lowest injection/droplet velocity, and the least glycerol amount as shown in Tables 1 and 2. The lowest viscosity could result in the finest droplets, with the least glycerol amount, which lead to the most rapid fuel evaporation, ignition and thus the fastest oxidation rate, yielding the most compact flame. The lowest injection velocity further enhances the fuel residence time to ensure more complete combustion as substantiated in the later combustion efficiency estimate. The more viscous 60/40 G/M may result in larger droplets than those of 50/50 G/M, plus with more glycerol component, the evaporation rate and thus the subsequent ignition and fuel oxidation rate are all slower than those of the 50/50 G/M droplets, resulting in an elongated flame zone with less completed combustion. The in-between injection velocity ensures more residence time of most of the fuel in the combustor than the 70/30 G/M flame, with less glycerol, yielding the longest flame among the three. The largest width of the 60/40 G/M flame also suggests that though the viscosity is higher than that of the 50/50 G/M, droplets are still fine enough to be burned at the near wall zone due to the fine SB atomization. However, for the 70/30 G/M blend, the viscosity is >2x higher than 60/40 G/M, which might generate more larger droplets at the spray periphery. Those large droplets closer to the wall with the highest glycerol component and highest injection velocity undergo incomplete evaporation and combustion, and rapidly escape from the combustor, leading to the lowest reaction rate at the wall and hence the narrowest flame. As the result, it generates the lowest combustor surface

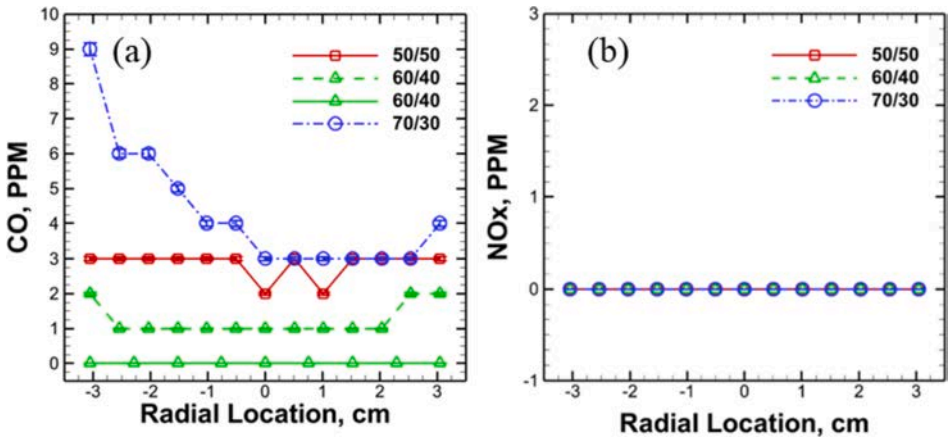

Fig. 5. Radial profiles of (a) CO and (b) NOx emissions at the combustor exit for all the tested fuel mixes [4].

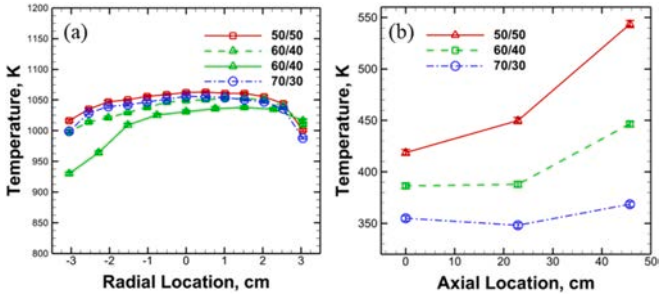

Fig. 6. (a) Radial temperature profile of combustion products (uncorrected) at the combustor exit, and (b) combustor surface temperature [4].

temperature substantiated later in Fig. 6 (b). Compared to the larger fuel drops at the spray periphery, the relatively finer droplets in the combustor center experience slow evaporation, ignition and oxidation, leading to a long flame. The comparable flame length of 70/30 G/M to that of the 60/40 G/M blends again suggests that the sizes of the droplets generated at the combustor center are comparable to those of 60/40 G/M, though more larger ones at the periphery. This again shows the fine atomization and high-viscosity tolerance of the SB injection. This is consistently validated by the comparable combustion efficiency of the 60/40 G/M and 70/30 G/M blends (90.3 % vs 90 %) in the later section, which also indicates most of fuel is atomized in the center regardless of the discrepancy at the spray periphery and closer to the wall. It is worth mentioning that compared to the mainly lean-premixed G/M flames by the novel SB injector, even at 7 kW for G/M 70/30 (by power), a standard pressure swirl injector resulted in mainly diffusion combustion for G/M 30/70 (by volume) at 6 kW that has less glycerol [4,6]. This suggests the significantly improved SB atomization with considerably finer sprays that evaporated rapidly, mixed more homogeneously with air and burned at premixed mode, even for G/M 70/30, which is ~9x more viscous than the G/M 30/70 (by volume) [7] and more difficult-to-evaporate glycerol [4]. Note that the representative visual flame images are intended for qualitative information only and flame fluctuation due to turbulence causes variation within the flame [4]. The quantitative data displayed below may be used for a more detailed analysis of fuel combustion [4].

Fig. 5 illustrates the radial profiles of CO and NOx emissions at the combustor exit for each fuel mixture at a constant ALR, equivalence ratio, and HRR [4]. The experiment repeatability is depicted using two experimental data sets of gas temperature and emissions measurements of the 60/40 G/M blends at the combustor exit, shown in Figs. 5 and 6 (a). The discrepancy of 1–2 ppm is acquired for the CO emissions with 0 ppm of NOx concentrations measured for both cases, suggesting the repeatability. For both tests, the temperature profiles are following similar trend with uncertainty of 5–18 K for the main flame zone, though a higher discrepancy of ~65 K is observed at one side of the combustor zone. This is highly likely due to the uncertainty of the mass flow controllers (MFCs), shown in Section 2.2. The MFCs measure the actual flow rates based on the setpoint. Though the setpoint of both cases are identical (57.37 SLPM and 86.99 SLPM for AA and PA respectively as shown in Table 2), the actual AA and PA flow rates are 56.09 SLPM and 88.06 SLPM respectively for the test 1 (dashed green line in Fig. 5). For test 1, the lower AA flow rate might lead to some slightly larger droplets at the spray periphery. Those larger drops combust at local diffusion mode without full vaporization, resulting in slightly higher local temperature at the near wall zone in Fig. 6 (a), and slightly higher CO concentration consistently shown in Fig. 5(a). The asymmetry is mainly due to the imperfect injector manufacturing that results in asymmetric droplet size distribution on both sides as shown in previous studies [4,27,28]. Regardless of the temperature discrepancy near the wall, the experiment is repeatable with the measurement uncertainties for NOx, CO emissions, and temperature of 0, 1–2 ppm, 5–18 K respectively for the main flame.

All the three fuel mixtures yielded low emissions of CO (<10 ppm) and no NOx emissions indicating ultra-clean combustion [4]. The CO emissions for 50/50 and 60/40 mixes are within the measurement uncertainty [4]. The 70/30 mixture of glycerol/methanol by percent HRR tends to have slightly higher CO emissions mainly close to the combustor wall [4]. This is possibly due to (1) the higher viscosity of the mixture which resulted in larger droplets, especially on the spray periphery [4]. The larger droplets tend to penetrate the reaction zone without complete evaporation, thus burning in diffusion mode and yielding the slightly higher CO emissions; and/or (2) the lower combustion gas temperature thus lower CO oxidation rate closer to wall, as in Fig. 6 due to heat loss of the uninsulated quartz combustor to the surrounding by convection and thermal radiation [4]. NOx is not present for the tested fuel mixes mainly due to the low flame temperature as shown in Fig. 6 [4]. Without any nitrogen content in the fuels, thermal NOx favoring high temperature is mainly from N_2 in air at temperature higher than 1800 K [4,41]. In summary, the global thermal and emission characteristics of the combustion exhaust gases quantitatively suggest clean combustion achieved for all the tested fuel mixes by the SB injection without fuel preheating, regardless of the wide discrepancy in the fuel viscosity and the high evaporation and auto-ignition temperatures of the glycerol component [4].

3.1.2. *Combustion efficiency*

Combustion completeness is estimated by considering the energy transfer from the combustor as detailed in [4,10]. Low surface temperatures at the outside of the quartz combustor are due to the heat loss via

convection and radiation from the combustor surface to the surroundings [4]. To get an accurate assessment of heat loss from the combustor, the gas temperatures measured by the thermocouples are corrected as the thermocouple bead also experiences heat losses through conduction and radiation [4]. Heat loss from the thermocouple bead causes readings to be lower than the true gas temperature [4]. Radiation correction of the gas temperature can be found using Eq. (2) below [4].

$$h_t\left(T_g - T_t\right) = \varepsilon_b \sigma (T_t^4 - T_s^4) \tag{2}$$

where T_g is the true gas temperature, T_t is the temperature measured by the thermocouple, T_s is the ambient temperature, σ is the Stefan-Boltzmann constant, $\varepsilon_b = 0.89$ is the type K thermocouple bead emissivity, and finally $h_t = 174$ W/m^{2}K is the estimated forced convective heat transfer coefficient over the thermocouple bead [4,19,42]. The difference between the thermocouple reading and the calculated true gas temperature is about 340 K for each of the three mixtures [4]. Solving Eq. (2) for T_g allows a more accurate estimate for the energy released during combustion [4].

To analyze the combustion completeness of each fuel blend, the total energy released during combustion is estimated by adding up the leaving energy carried by exhaust gases using the correct gas temperatures at the combustor exit, and the heat losses from the combustor wall to the surrounding using Eqs. (3)–(5) as below [4].

$$Q_{total} = Q_{gas} + Q_{losses} \tag{3}$$

$$Q_{gas} = m_g C_{P_{air}} T_g \tag{4}$$

$$Q_{losses} = h_a A_s (T_w - T_{surr}) + \varepsilon_{glass} \sigma A_s (T_w^4 - T_{surr}^4) \tag{5}$$

where Q_{total} is the total energy released from the combustion process, Q_{gas} denotes energy carried by the leaving combustion gases, calculated in Eq. (4), and Q_{losses} are energy losses from the combustion gases through the combustor outer wall to the surroundings, via convection and thermal radiation, calculated in Eq. (5). m_g is the mass flow rate of the combustion gases, calculated by summing the liquid fuel mass flow rate and the total air mass flow rate [4]. T_g stands for the true gas temperature calculated previously using the measured temperature by the thermocouple in Eq. (2). Specific heat capacity of the combustion product gases, $C_{P_{air}}$, is estimated for the exhaust gas products of gas mixtures: CO_2, steam (H_2O), O_2 and N_2, approximating complete combustion for lean conditions at the combustion gas temperature, T_g [4]. The $C_{P_{air}}$ for each mixture at the average combustion gas temperature is 1.383 kJ/kg K, 1.372 kJ/kg K, and 1.375 kJ/kg K for the 50/50, 60/40, and 70/30 fuel mixtures respectively [4]. The value of $C_{P_{air}}$ is estimated from the calculated C_P value of exit gas CO_2, N_2, O_2 and H_2O [43] at average corrected exit gas temperature T_g. A_s is the combustor surface area, which is equal to 1077.25 cm^2, σ is the Stefan-Boltzmann's constant, and T_w and T_{surr} are the temperatures of the combustor outer wall surface and the surrounding respectively [4]. Combustor outer wall temperature (T_w) is taken in 3 different sections (1 in. downstream of the dump plane, i.e. the quartz combustor bottom, combustor center, 1 in. upstream from the combustor exit) along the combustor gas flow direction, i.e., the axial direction. ε_{glass} is the emissivity of quartz glass, varies along the length of the combustor as a function of the surface temperature and glass thickness [4]. This value is estimated by using [44]. The emissivity is extrapolated for each fuel mixture at the three surface temperature measurements taken in Fig. 5 (b) [4]. For 50/50 G/M blend, the estimated emissivity values for the three corresponding temperature and segments of the combustor wall are 0.6782, 0.7032 and 0.7121 from bottom to top. Estimated emissivity for 60/40 blend are 0.7042, 0.7212 and 0.7217, and for 70/30 blend are 0.7272, 0.7336 and 0.7315. These values are used to estimate the heat loss from the outside surface of the quartz glass by thermal radiation in 3 segments of the combustor quartz glass, based on the quartz combustor wall temperature at bottom, middle and top of the combustor [4]. Natural convective heat transfer co-efficient, h_a is estimated by using the natural convective heat transfer equations [45]. Adding the heat loss through each segment of the combustor outer wall, total heat loss to the surrounding by the combustor wall is estimated.

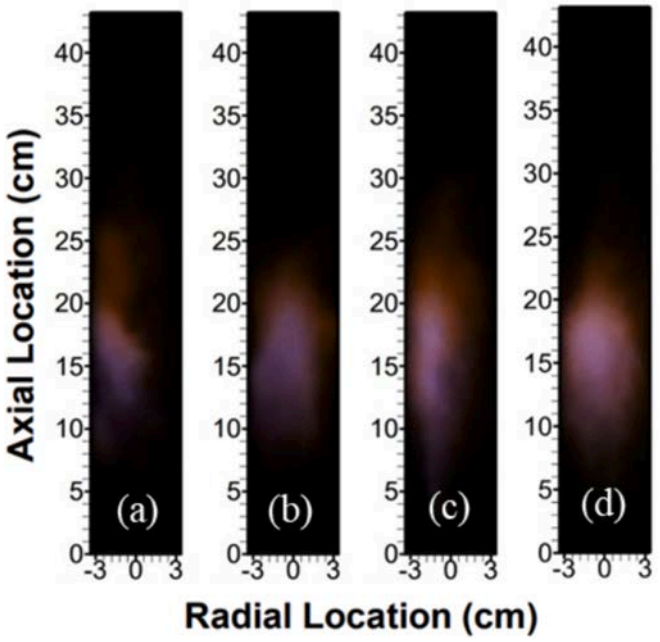

Fig. 7. Flame images for glycerol/methanol (G/M) fuel mixture of 50/50 at ALRs (a) 1.5 (b) 2.0 (c) 2.5 and (d) 3.0 at the constant HRR of 7 kW and equivalence ratio of 0.75 [4].

The released heat of each mixture is estimated to be 6.63 kW, 6.32 kW, and 6.30 kW for the 50/50, 60/40, and 70/30 fuel mixtures, at an ALR of 3, respectively by summing the enthalpy of the exhaust gas leaving the combustor end and the heat loss through the quartz tube outer wall [4]. Thus, the estimated combustion efficiencies are 94.9 %, 90.3 %, and 90 % respectively for the G/M mixtures at the ratios of 50/50, 60/40, and 70/30 at an ALR of 3 and the constant theoretical HRR of 7 kW. In comparison, straight glycerol with extremely high viscosity was completely burned in the same 7 kW but insulated combustor owing to the fine FB atomization in our prior studies [4,12,22]. With further enhanced atomization, the SB injector integrating the FB injection concept [46,47] led to complete combustion of other straight oils including algae oil and vegetable oil [19,48] that are more viscous than the most viscous fuel blend (70/30 G/M) in the current study [4]. Therefore, the unburned fuel is (1) may be mainly due to the high ALR and thus high injection velocity resulting in some fuel leaving without sufficient residence time to be completely combusted; (2) and also possibly due to the high evaporation and auto-ignition temperatures of glycerol and the currently uninsulated combustor, which dissipates heat loss, reducing temperatures and thus fuel evaporation and oxidation rates in the combustor; and (3) some unburned larger droplets at the more viscous blends 60/40 and 70/30 compared to the G/M 50/50 case; (4) increased glycerol component in G/M 60/40, 70/30 than that of 50/50 [4]. Despite the more unburned fuels for the glycerol-denser fuel blends, the 50/50 G/M mix is near complete combustion at ALR of 3 owing to the effective SB atomization yet without fuel preheating nor insulation [4].

3.2. *The effect of ALR on the global combustion characteristics*

Previous studies have indicated that an increase in ALR results in finer atomization that might further benefit fuel evaporation, fuel–air mixing, and efficient combustion [4,46–48]. The present work also

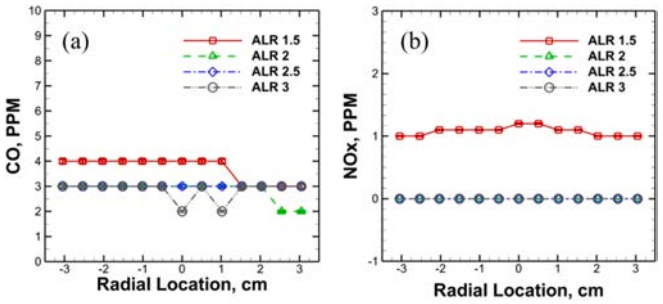

Fig. 8. Radial profiles of (a) CO and (b) NOx emissions for fuel mix G/M of 50/50 [4].

investigated the effect of ALR on the overall combustion characteristics of glycerol/methanol fuel blends, while keeping constant equivalence ratio, HRR and total air flow rate by varying the AA and PA flow rates [4]. The ALRs of 1.5, 2.0, 2.5, and 3.0 are employed to explore the combustion performance for the fuel blend 50/50 that is most comparable to diesel in terms of fuel properties [4] and G/M 70/30 that represents crude glycerol.

3.2.1. *Global flame characteristics for 50/50 G/M*

Fig. 7 displays the visual flame images of 50/50 at each of the four ALRs previously mentioned [4]. Each of the images show relatively similar flame structure with the visual flame beginning at the axial location of around y = 10 cm and ending before y = 25 cm [4]. As the ALR increases, flame width increases while flame length and flame lift-off slightly decrease [4]. This is possibly because of the finer droplets due to the increased ALR that evaporate faster and mix more homogenously with air, yielding a more radially distributed flame within the combustor at the highest ALR of 3.0 [4]. This also means that the injector with higher AA can quickly break down larger particles at the higher ALR so that they can begin to combust sooner and in a shorter residence time than those at the lower ALRs, resulting in a slightly less limited flame at the high ALR though the droplet velocity is higher [4]. Despite the slight discrepancy, at all the ALRs, mainly lean-premixed flames are obtained indicative of the upstream dark region of fuel evaporation and mixing as the result of the fine SB atomization [4].

Fig. 8 shows the radial emissions profiles of CO and NOx at the combustor exit for the 50/50 fuel mixture at ALRs ranging from 1.5 to 3.0 [4]. The SB injector achieved ultra-low emissions at every ALR tested with CO < 5 ppm and NOx at nearly 0 [4]. With no nitrogen element in the fuel, NOx is mainly created by the thermal NOx mechanism that takes place at temperatures above 1800 K [4,19]. As shown in Fig. 9, the glycerol/methanol fuel mixtures did not reach temperatures near that mainly due to the high evaporation and auto-ignition temperature of the glycerol component and heat loss of the uninsulated combustor as aforementioned [4]. The 50/50 fuel mixture creates very low CO emissions which indicates near complete combustion for each ALR [4]. The CO emission readings are also ultra-low, even near the combustor walls indicating clean combustion possibly owing to the more uniform size distribution of droplets generated by the SB injector [4,46,47] compared to the FB injection and conventional atomizers such as air-blast and pressure swirl injectors [4]. Decrease in ALR resulted in a slight increase in CO emissions, which is likely due to some slightly larger droplets burn locally at diffusion mode or incompletely. However, it is within the uncertainty range of CO measurement. Fig. 9 illustrates that the increase in ALR resulted in slightly lowered combustion exhaust gas temperature at the combustor exit [4]. This is possibly attributed to the increased injection velocity at the higher ALR that slightly shortens the residence time of the fuel blend in the combustor [4]. On the other hand, at the lower ALR, though the droplets might be slightly larger, fuel stayed longer in the combustor to further approach complete combustion and release more energy to raise up the gas product temperature

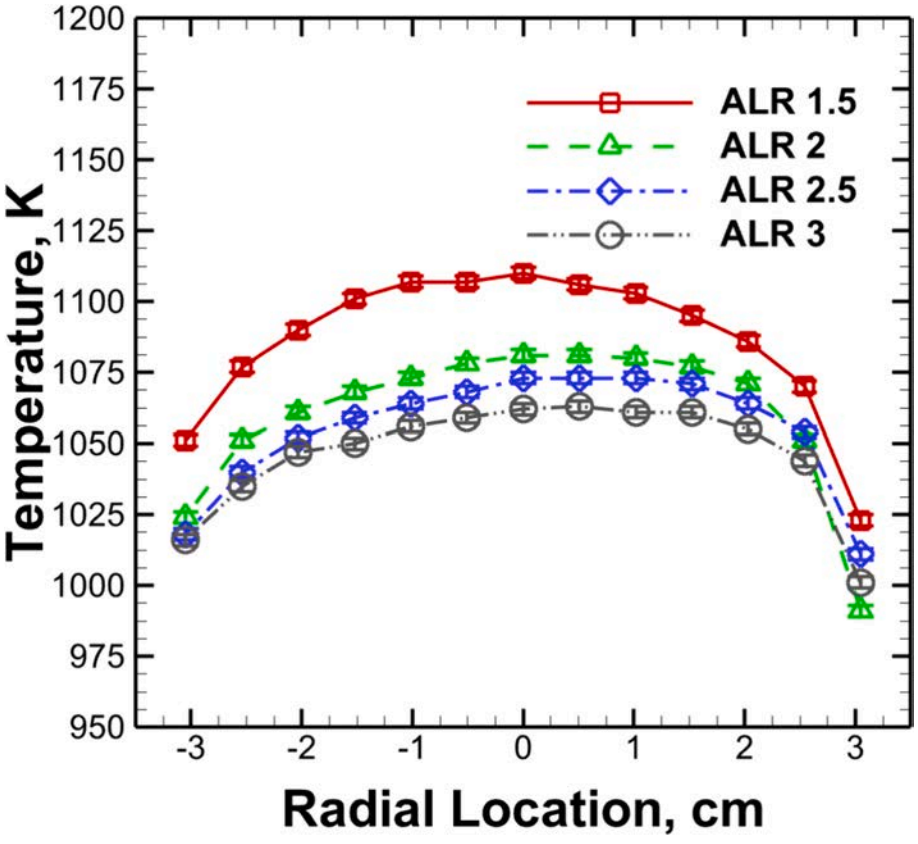

Fig. 9. Radial temperature profile of combustion products at the combustor exit at various ALRs for the G/M blend of 50/50 [4].

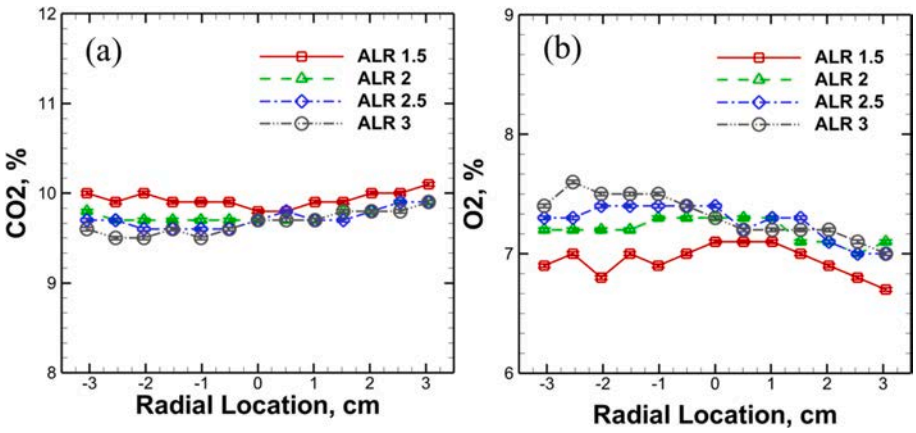

Fig. 10. Radial profiles of (a) CO_2 and (b) O_2 concentrations at the combustor exit for the G/M blend of 50/50 [4].

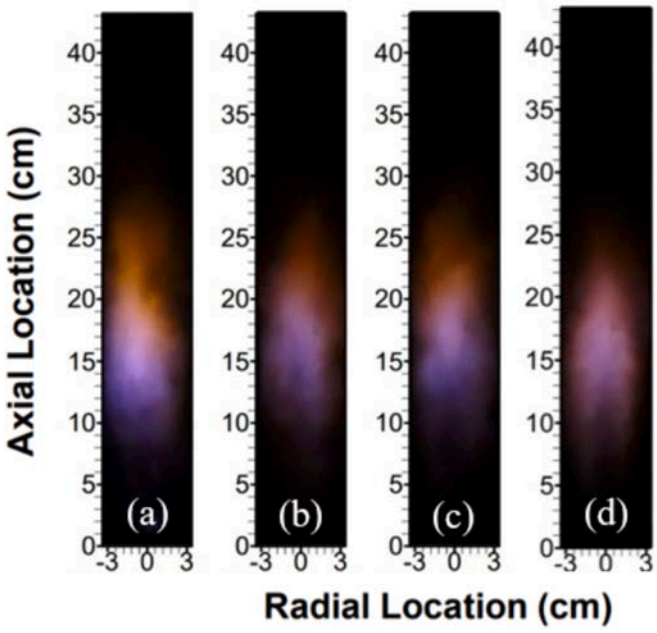

Fig. 11. Flame images for the glycerol/methanol (G/M) fuel mixture of 70/30 at ALRs of (a) 1.5 (b) 2.0 (c) 2.5 and (d) 3.0 at the constant HRR of 7 kW and equivalence ratio of 0.75.

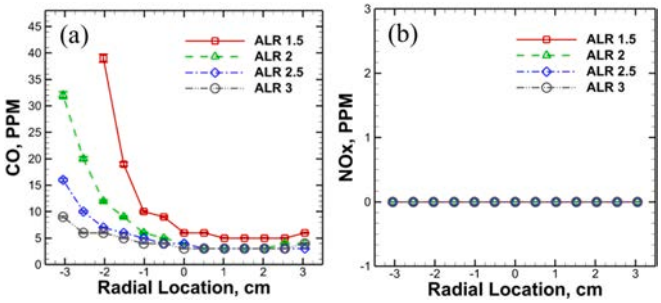

Fig. 12. Radial profiles of (a) CO and (b) NOx emissions for the fuel mix G/M of 70/30.

[4]. Consistently, in Fig. 10, higher CO_2 and lower O_2 concentrations are measured at a lower ALR, again indicating more complete combustion at the lower ALR [4]. At ALR of 3, the previous estimate indicated near complete combustion for the 50/50 blend, signifying near complete combustion for all the tested ALRs owing to the fine SB atomization [4].

3.2.2. *Global flame characteristics for 70/30 G/M*

The effect of ALRs on the combustion characteristics of the 70/30 G/M by HRR is also investigated, which contains G/M ratio of 74.6/25.4 by weight and is also representative to crude glycerol from the trans-esterification process that contains ~62–76 % glycerol [49] and ~23–38 % methanol by weight [6]. The 70/30 G/M mix is ~4.5x viscous than conventional diesel as in Tables 1 and 2. Hence, it becomes difficult to combust effectively by conventional AB atomizer. Flame images of the ALRs of 1.5, 2.0, 2.5 and 3.0 for G/M 70/30 ratio by HRR are shown in Fig. 11. For all the ALRs, the dark region from the combustor dump plane to the upstream the flame suggests mainly LPM combustion. At the ALR of 1.5 more orange color reflects the soot chemiluminescence. With the increase in ALRs, probably due to enhanced atomization, mainly blue flames were observed indicating clean combustion is achieved. Flames become more compact with the increase in ALR due to finer atomization that quickens fuel evaporation, mixing, and oxidation. At ALR of 1.5, the flame starts at around y = 8 cm and ends at y = 27 cm, with an approximate flame length of 19 cm. Whereas, at the higher ALR of 3.0, flame starts at y = 10 cm and ends at y = 23 cm, with a compact flame length of around 13 cm. It is also observed that the flames are slightly shifted to one side of the combustor. This may be attributed to (1) the turbulence nature of flame; (2) imperfect manufacturing of the SB injector that results in more larger droplets at one side than those on the other side [19]. More uniform distributed flame is observed at the increased ALR, which is likely due to finer droplets that rapidly and fully evaporate and result in homogenous fuel vapor-air mixture and thus combustion. Fig. 12 (a) and (b) exhibit the radial profiles of CO and NOx emissions at 1 in. upstream the combustor exit. It is seen that CO concentration of one side of the combustor is higher. In one side of the combustor, CO concentration is more than 100 ppm for ALR of 1.5, which is not shown in Fig. 12 (a). In consistent to the visual flame images, this is likely due to (1) more larger droplets at one side of the injector at the lower ALRs (1.5 and 2.0) which penetrate into the reaction zone without complete evaporation, resulting in less homogenous fuel air mixing in the near wall zone; (2) at the near wall zone, temperature is lower than the center zone of the combustor, which may lead to slower CO oxidation. Nevertheless, for ALR of 3.0, CO concentration is less than 10 ppm. This indicates that very fine and uniform size droplets are generated by the SB injector, which leads to rapid, complete evaporation with homogeneous fuel–air mixing. Thus, the novel SB injector achieved clean combustion even for a very high-viscosity G/M blend of 70/30 ratio, without fuel preheating.

Fig. 13 represents radial profiles of the exhaust gas temperature located at 1 in. upstream of the combustor exit. All the ALRs share similar temperature distribution. At the center of the combustor the

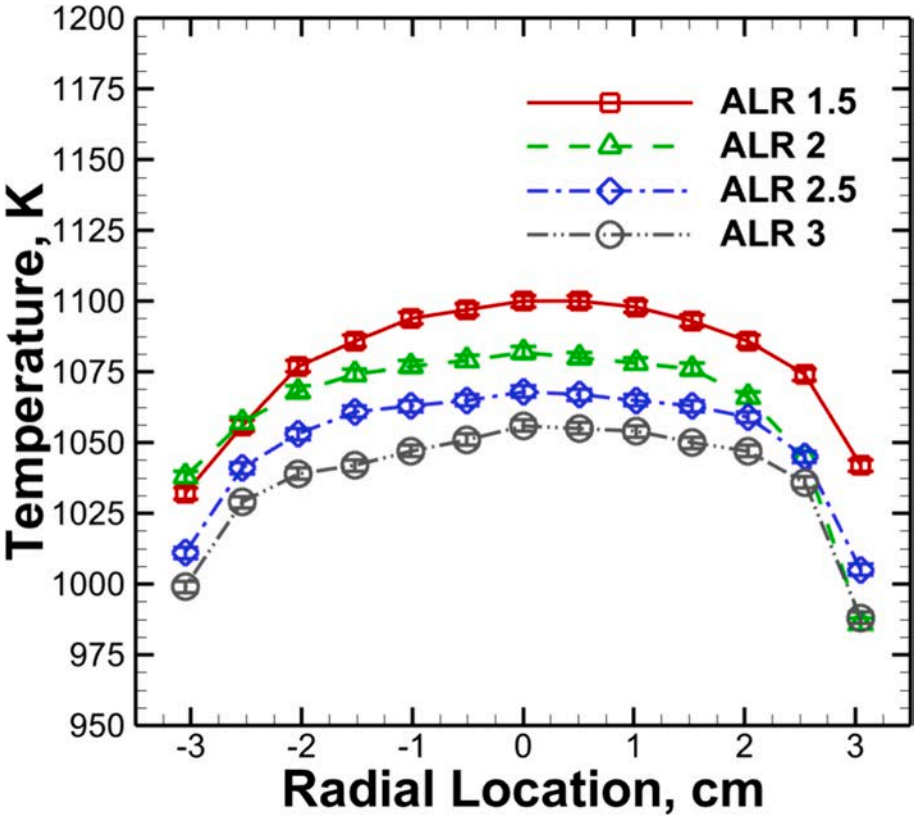

Fig. 13. Radial temperature profile of combustion products at the combustor exit at various ALRs for the G/M blend of 70/30.

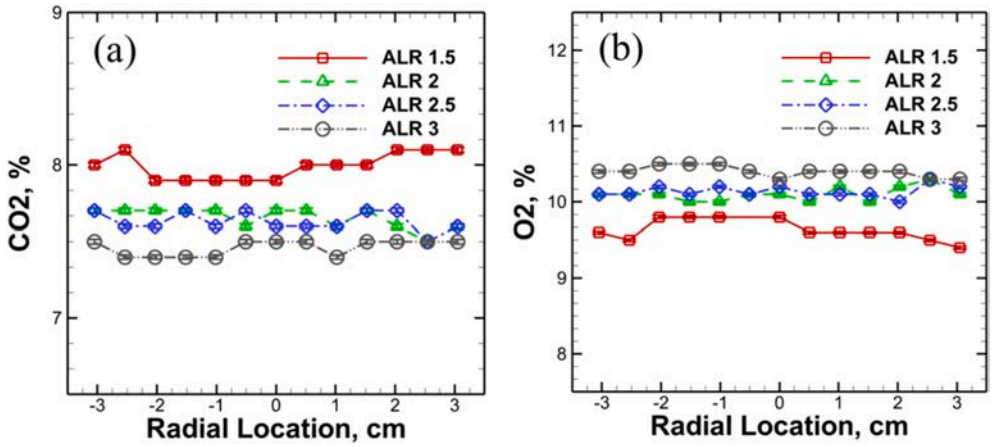

Fig. 14. Radial profiles of (a) CO_2 and (b) O_2 concentrations at the combustor exit for the G/M blend of 70/30.

temperature is higher compared to the near wall zone due to the heat loss through convection and radiation heat transfer in the near wall zone by the combustor quartz glass. Exhaust gas temperature is higher for lower ALRs. Again, this may be due to the lower ALR, injection velocity is lower at the decreased AA, which provides higher residence time to combust more completely. Besides, for the 70/30 G/M blend, the generated droplets may be slightly larger compared to the 50/50 and 60/40 G/M blends. These slightly larger droplets get more time to burn more completely and release more energy at lower ALRs when the injection velocity is reduced. For the lower ALR of 1.5, concentration of CO_2 is higher than that at the higher ALRs as per Fig. 14 (a), which consistently indicates that more complete combustion incurred for lower ALR of 1.5. Fig. 14 (b) illustrates O_2 concentration in exhaust gas, again substantiating that the completeness of combustion is higher for lower ALRs, concentration of the remaining O_2 in exhaust gas is thus lower.

3.2.3. *Combustion efficiency*

Combustion completeness is estimated as aforementioned by summing the energy of the exhaust gas and the convection and radiation heat loss of the quartz combustor wall to the surrounding [19,50]. To minimize the thermocouple error, convection and radiation heat loss by the bead of thermocouple to the surrounding is taken into consideration and Eq. (2) is used to estimate the corrected exhaust gas temperature [19]. Estimated temperature difference between the thermocouple reading and true gas temperature is 346–402 K for ALR of 1.5–3.0 for 50/50 G/M and 334–391 K for ALRs of 1.5–3.0 for 70/30 G/M blends. To estimate total energy released by the combustion Eqs. (3)–(5) are used [19,45]. Theoretical input power is 7 kW. The estimated Cp of the

combustion exhaust gas are 1.4002, 1.3893, 1.3871 and 1.3834 for the ALRs of 1.5, 2.0, 2.5 and 3.0 for 50/50 G/M, based on the corrected gas temperature [43]. Similarly, the estimated Cp values are 1.3932, 1.3858, 1.3812 and 1.3753 for the ALRs of 1.5, 2.0, 2.5 and 3.0 for 70/30 G/M [43].

The estimated heat release for ALRs of 1.5, 2.0, 2.5 and 3.0 of G/M 50/50 blend are 6.97 kW, 6.81 kW, 6.61 kW and 6.64 kW respectively, signifying 99.5 %, 97.2 %, 94.5 % and 94.9 % combustion efficiency respectively. Our previous study found that an increase in ALR leads to a finer SB spray that is expected to evaporate faster for homogeneous fuel-vapor and air mixing and thus clean and complete combustion [19,28]. It is interesting that with the increase in ALR, the combustion completeness degree decreases. This is attributed to the higher injection velocity at the higher ALR [4], at which the atomizing air flow rate is increased at the constant liquid flow. Hence, fuel residence time reduces, and fuel leaves the combustor without complete burn. This also signifies that the fine atomization already achieved at ALR of 1.5 by the SB injection. Also, this again substantiates that the incomplete combustion observed at ALR of 3 for the 50/50 G/M mix in the previous section 3.1 is due to the insufficient fuel residence time, rather than ineffective atomization, as increase in ALR further enhances atomization. From Fig. 10, it is also observed that at the lower ALR, CO_2 concentration in exhaust gas is higher and O_2 concentration is lower compared to those at a higher ALR. This again substantiates that at a lower ALR, more fuel is burnt with higher O_2 consumed and more CO_2 generated and thus less excess O_2 concentration in exhaust gas. Similar trend of completeness of combustion is observed for the different ALRs for 70/30 G/M blend. The estimated heat release rate for the ALRs of 1.5, 2.0, 2.5 and 3.0 of 70/30 G/M blend are 6.80 kW, 6.55 kW, 6.39 kW and 6.24 kW respectively, indicating the efficiency of 97.2 %, 93.6 %, 91.3 % and 90 % respectively. At the lower ALR of 1.5 for the least and most viscous blends of G/M 50/50 and 70/30, the combustion is nearly completed despite of using uninsulated combustor and highly viscous fuel without pre-heating, reflecting the ultra-fine spray generation for the viscous mix by the SB injector. The viscosity range of the blends varied almost 5 times of diesel, which proves a very wide range of viscosity tolerance of the SB injector to combust fuel cleanly and efficiently with high fuel flexibility. Also, the SB injection at ALR of 1.5 results in complete combustion of all the G/M blends regardless of the distinct viscosity variations.

4. Conclusion

The current study investigates the combustion characteristics of glycerol/methanol blends using a novel twin-fluid injector with proved high-viscosity tolerance and fuel flexibility [4]. Biofuels, as oxygenated fuels, are highly desired to mitigate carbon footprint in energy generation [4]. The so-called SB injector utilizes a novel two-phase atomization concept to generate fine sprays immediately rather than a typical breaking jet/film of conventional atomizers such as air-blast or pressure swirl injectors widely used in gas turbine engines [4]. In the present study, the SB injection has yielded mainly lean-premixed combustion with ultra-low emissions of CO and NOx regardless of the wide range of fuel viscosity for the 50/50, 60/40, and 70/30 (~5x higher viscosity than diesel) of glycerol/methanol blends by percent HRR without fuel preheating nor insulation [4]. Estimate of energy released from the combustion indicates that the fuel blends of 50/50, 60/40, and 70/30 at an ALR of 3, achieve 94.9 %, 90.3 %, and 90 % complete combustion respectively [4]. The unburned fuel is mainly due to the high evaporation and auto-ignition temperature of the glycerol component in the uninsulated combustor [4]. For the fuel mix of 50/50 and 70/30, the increase in ALR results in more radially distributed flame and slightly reduced flame lift-off height due to the improved atomization at the higher ALR [4]. On the other hand, more complete combustion with higher product gas temperatures is acquired at lower ALRs due to lower injection velocity and thus longer residence time of fuels [4]. Estimated combustion completeness for ALRs of 1.5, 2.0, 2.5 and 3.0 of 50/50 G/M blends are 99.5 %, 97.2 %, 94.5 % and 94.9 % respectively; and for ALRs of 1.5, 2.0, 2.5 and 3.0 of 70/30 G/M blends are 97.2 %, 93.6 %, 91.3 % and 90 % respectively. The SB injection at the ALR of 1.5 results in complete combustion for the least and most viscous G/M blends regardless of the distinct viscosity variations, showing its powerful atomization capability and high fuel flexibility for ultra-clean and efficient combustion. Each ALR achieves ultra clean and near-complete combustion with near zero emissions of CO and NOx [4]. Overall, the SB injection has enabled clean and near complete combustion of glycerol and methanol mixes representing crude glycerol with minimal waste processing without fuel preheating nor combustor insulation, signifying that the SB injector can enable the use of cost-effective biofuels for power generation with reduced carbon footprint [4].

CRediT authorship contribution statement

Timothy Hall: Writing – original draft, Methodology, Investigation, Formal analysis, Data curation. **Derek Williams:** Methodology, Investigation, Data curation. **S M Rafiul Islam:** Writing – original draft, Methodology, Formal analysis. **Ishaan Patel:** Methodology, Investigation, Data curation. **Caleb Chakmakjian:** Methodology, Data curation. **Lulin Jiang:** Writing – review & editing, Supervision, Resources, Project administration, Methodology, Funding acquisition, Formal analysis, Conceptualization.

Declaration of competing interest

The authors declare that they have no known competing financial interests or personal relationships that could have appeared to influence the work reported in this paper.

Data availability

Data will be made available on request.

Acknowledgments

The current research is funded by the Startup fund of Baylor University, NSF CIVIC award No. 2228311 by US National Science Foundation, and NSF CIVIC award No. 2322319 cofunded by US National Science Foundation and Department of Energy. We would also like to express our gratitude to Mr. Ashely Orr who helped manufacture the combustion system and Mr. Joseph Breerwood for helping set up the system.

References

[1] Pasha MK, Dai L, Liu D, Guo M, Du W. An overview to process design, simulation and sustainability evaluation of biodiesel production. Biotechnol Biofuels 2021;14:129. https://doi.org/10.1186/s13068-021-01977-z.
[2] UFOP. Report on Global Market Supply: 2019/2020, Berlin, 2020. 2020. https://library.wur.nl/WebQuery/titel/2289027 (accessed February 7, 2024).
[3] Farag HA, El-Maghraby A, Taha NA. Transesterification of esterified mixed oil for biodiesel production; 2012.
[4] Jiang L, Hall T, Williams D, Swinney R. Global Combustion Characteristics of Glycerol and Methanol Blends Using a Novel Fuel-Flexible Injector. In: AIAA SCITECH 2023 Forum. National Harbor, MD & Online: American Institute of Aeronautics and Astronautics; 2023. https://doi.org/10.2514/6.2023-0495.
[5] Leung DYC, Wu X, Leung MKH. A review on biodiesel production using catalyzed transesterification. Appl Energy 2010;87:1083–95. https://doi.org/10.1016/j.apenergy.2009.10.006.
[6] Quispe CAG, Coronado CJR, Carvalho Jr JA. Glycerol: Production, consumption, prices, characterization and new trends in combustion. Renew Sustain Energy Rev 2013;27:475–93. https://doi.org/10.1016/j.rser.2013.06.017.
[7] Agwu O, Valera-Medina A, Katraśnik T, Seljak T. Flame characteristics of glycerol/methanol blends in a swirl-stabilised gas turbine burner. Fuel 2021;290:119968. https://doi.org/10.1016/j.fuel.2020.119968.
[8] Okoye PU, Abdullah AZ, Hameed BH. Synthesis of oxygenated fuel additives via glycerol esterification with acetic acid over bio-derived carbon catalyst. Fuel 2017;209:538–44. https://doi.org/10.1016/j.fuel.2017.08.024.

[9] Spataru D, Soares Dias AP, Vieira Ferreira LF. Acetylation of biodiesel glycerin using glycerin and glucose derived catalysts. J Clean Prod 2021;297:126686. https://doi.org/10.1016/j.jclepro.2021.126686.

[10] Jiang L, Agrawal AK. Combustion of straight glycerol with/without methane using a fuel-flexible, low-emissions burner. Fuel 2014;136:177–84. https://doi.org/10.1016/j.fuel.2014.07.027.

[11] Zhang J, Wang Y, Muldoon VL, Deng S. Crude glycerol and glycerol as fuels and fuel additives in combustion applications. Renew Sustain Energy Rev 2022;159:112206. https://doi.org/10.1016/j.rser.2022.112206.

[12] Ferreira AGM, Egas APV, Fonseca IMA, Costa AC, Abreu DC, Lobo LQ. The viscosity of glycerol. J Chem Thermodyn 2017;113:162–82. https://doi.org/10.1016/j.jct.2017.05.042.

[13] Seljak T, Katrašnik T. Emission reduction through highly oxygenated viscous biofuels: use of glycerol in a micro gas turbine. Energy 2019;169:1000–11. https://doi.org/10.1016/j.energy.2018.12.095.

[14] Pillai AL, Nagao J, Awane R, Kurose R. Influences of liquid fuel atomization and flow rate fluctuations on spray combustion instabilities in a backward-facing step combustor. Combust Flame 2020;220:337–56. https://doi.org/10.1016/j.combustflame.2020.06.031.

[15] Simmons BM, Panchasara HV, Agrawal AK. A Comparison of Air-Blast and Flow-Blurring Injectors Using Phase Doppler Particle Analyzer Technique. Volume 2: Combustion, Fuels and Emissions, Orlando, Florida, USA: ASMEDC; 2009, p. 981–92. https://doi.org/10.1115/GT2009-60239.

[16] Zhang T, Dong B, Chen X, Qiu Z, Jiang R, Li W. Spray characteristics of pressure-swirl nozzles at different nozzle diameters. Appl Therm Eng 2017;121:984–91. https://doi.org/10.1016/j.applthermaleng.2017.04.089.

[17] Hendershott TH, Stouffer S, Monfort JR, Diemer J, Busby K, Corporan E, et al. Ignition of Conventional and Alternative Fuel at Low Temperatures in a Single-Cup Swirl-Stabilized Combustor. In: 2018 AIAA Aerospace Sciences Meeting. Kissimmee, Florida: American Institute of Aeronautics and Astronautics; 2018. https://doi.org/10.2514/6.2018-1422.

[18] Gañán-Calvo AM. Enhanced liquid atomization: From flow-focusing to flow-blurring. Appl Phys Lett 2005;86:214101. https://doi.org/10.1063/1.1931057.

[19] Akinyemi OS, Jiang L. Development and combustion characterization of a novel twin-fluid fuel injector in a swirl-stabilized gas turbine burner operating on straight vegetable oil. Exp Therm Fluid Sci 2019;102:279–90. https://doi.org/10.1016/j.expthermflusci.2018.11.014.

[20] Akinyemi OS, Jiang L, Hernandez R, McIntyre C, Holmes W. Combustion of straight algae oil in a swirl-stabilized burner using a novel twin-fluid injector. Fuel 2019;241:176–87. https://doi.org/10.1016/j.fuel.2018.12.006.

[21] Qavi I, Jiang L, Akinyemi OS. Near-field spray characterization of a high-viscosity alternative jet fuel blend C-3 using a flow blurring injector. Fuel 2021;293:120350. https://doi.org/10.1016/j.fuel.2021.120350.

[22] Jiang L, Agrawal AK. Investigation of glycerol atomization in the near-field of a flow-blurring injector using time-resolved PIV and high-speed visualization. Flow Turbulence Combust 2015;94:323–38. https://doi.org/10.1007/s10494-014-9572-2.

[23] Simmons BM, Agrawal AK. Flow blurring atomization for low-emission combustion of liquid biofuels. Combust Sci Technol 2012;184:660–75. https://doi.org/10.1080/00102202.2012.660222.

[24] Jiang L, Agrawal AK, Taylor RP. Clean combustion of different liquid fuels using a novel injector. Exp Therm Fluid Sci 2014;57:275–84. https://doi.org/10.1016/j.expthermflusci.2014.05.002.

[25] Panchasara HV, Sequera DE, Schreiber WC, Agrawal AK. Emissions reductions in diesel and kerosene flames using a novel fuel injector. J Propul Power 2009;25:984–7. https://doi.org/10.2514/1.37165.

[26] Jiang L, Agrawal AK. Spray features in the near field of a flow-blurring injector investigated by high-speed visualization and time-resolved PIV. Exp Fluids 2015;56:103. https://doi.org/10.1007/s00348-015-1973-z.

[27] Danh V, Jiang L, Akinyemi OS. Investigation of water spray characteristics in the near field of a novel swirl burst injector. Exp Therm Fluid Sci 2019;102:376–86. https://doi.org/10.1016/j.expthermflusci.2018.12.014.

[28] Danh V, Akinyemi OS, Taylor CE, Frank JT, Jiang L. Effect of injector swirl number on near-field spray characteristics of a novel twin-fluid injector. Exp Fluids 2019;60:80. https://doi.org/10.1007/s00348-019-2721-6.

[29] Qavi I, Jiang L. Optical characterization of near-field sprays for various alternative and conventional jet fuels using a flow-blurring injector. Flow Turbulence Combust 2022;108:599–624. https://doi.org/10.1007/s10494-021-00276-9.

[30] Chilakamarry CR, Mimi Sakinah AM, Zularisam AW, Pandey A, Vo D-V-N. Technological perspectives for utilisation of waste glycerol for the production of biofuels: a review. Environ Technol Innov 2021;24:101902. https://doi.org/10.1016/j.eti.2021.101902.

[31] He Q (Sophia), McNutt J, Yang J. Utilization of the residual glycerol from biodiesel production for renewable energy generation. Renew Sustain Energy Rev 2017;71:63–76. https://doi.org/10.1016/j.rser.2016.12.110.

[32] Deka TJ, Osman AI, Baruah DC, Rooney DW. Methanol fuel production, utilization, and techno-economy: a review. Environ Chem Lett 2022;20:3525–54. https://doi.org/10.1007/s10311-022-01485-y.

[33] Marulanda VF. Biodiesel production by supercritical methanol transesterification: process simulation and potential environmental impact assessment. J Clean Prod 2012;33:109–16. https://doi.org/10.1016/j.jclepro.2012.04.022.

[34] Gülüm M, Bilgin A. A comprehensive study on measurement and prediction of viscosity of biodiesel-diesel-alcohol ternary blends. Energy 2018;148:341–61. https://doi.org/10.1016/j.energy.2018.01.123.

[35] Jin C, Sun T, Xu T, Jiang X, Wang M, Zhang Z, et al. Influence of glycerol on methanol fuel characteristics and engine combustion performance. Energies 2022;15:6585. https://doi.org/10.3390/en15186585.

[36] De Oliveira GS, Lobo CES, Padilha CEA, Souza DFS, Ruiz JAC. Glycerin combustion through chemical looping. Fuel 2023;352:129038. https://doi.org/10.1016/j.fuel.2023.129038.

[37] Lilley DG. Swirl flows in combustion: a review. AIAA J 1977;15:1063–78. https://doi.org/10.2514/3.60756.

[38] Duraisamy G, Rangasamy M, Govindan N. A comparative study on methanol/diesel and methanol/PODE dual fuel RCCI combustion in an automotive diesel engine. Renew Energy 2020;145:542–56. https://doi.org/10.1016/j.renene.2019.06.044.

[39] Li Z, Wang Y, Geng H, Zhen X, Liu M, Xu S, et al. Effects of diesel and methanol injection timing on combustion, performance, and emissions of a diesel engine fueled with directly injected methanol and pilot diesel. Appl Therm Eng 2019;163:114234. https://doi.org/10.1016/j.applthermaleng.2019.114234.

[40] Wang Y, Wang H, Meng X, Tian J, Wang Y, Long W, et al. Combustion characteristics of high pressure direct-injected methanol ignited by diesel in a constant volume combustion chamber. Fuel 2019;254:115598. https://doi.org/10.1016/j.fuel.2019.06.006.

[41] Turns SR. An introduction to combustion: concepts and applications. 3rd ed. New York: McGraw-Hill; 2012.

[42] Çengel YA, Ghajar AJ. Heat and mass transfer: fundamentals & applications. 5th ed. New York, NY: McGraw Hill Education; 2015.

[43] Çengel YA, Boles MA. Thermodynamics: an engineering approach. 8th ed. New York: McGraw-Hill Education; 2015.

[44] Petrov V, Reznik V. Measurement of the emissivity of quartz glass. High Temperatures-High Pressures 1972;4:687–93.

[45] Çengel YA. Heat Transfer: A Practical Approach. Second Edition. McGraw-Hill Companies; 2002.

[46] Lefebvre AH. Airblast atomization. Prog Energy Combust Sci 1980;6:233–61. https://doi.org/10.1016/0360-1285(80)90017-9.

[47] Simmons BM, Agrawal AK. Spray characteristics of a flow-blurring atomizer. Atomiz Spr 2010;20:821–35. https://doi.org/10.1615/AtomizSpr.v20.i9.60.

[48] Institute of Mechanics and Thermodynamics, Chemnitz University of Technology, Chemnitz, Germany, Roudini M, Wozniak G. Investigation of the Secondary Atomization in Prefilming Air-Blast Atomizers. IJCEA 2019;10:138–43. https://doi.org/10.18178/ijcea.2019.10.5.757.

[49] Thompson JC, He BB. Characterization of crude glycerol from biodiesel production from multiple feedstocks. Appl Eng Agric 2006;22:261–5. https://doi.org/10.13031/2013.20272.

[50] Shannon KS, Butler BW. A review of error associated with thermocouple temperature measurement in fire environments. In: 2nd International Wildland Fire Ecology and Fire Management Congress and the 5th Symposium on Fire and Forest Meteorology; 2003.

clean technologies

MDPI

Article

Effect of Methane on Combustion of Glycerol and Methanol Blends Using a Novel Swirl Burst Injector in a Model Dual-Fuel Gas Turbine Combustor

S M Rafiul Islam [1], Ishaan Patel [1] and Lulin Jiang [1,*]

[1] Department of Mechanical Engineering, Baylor University, Waco, TX 76798, USA; smrafiul_islam1@baylor.edu; ishaan_patel1@baylor.edu
* Correspondence: lulin_jiang@baylor.edu

Abstract: Glycerol, a byproduct of biodiesel, has moderate energy but high viscosity, making clean combustion challenging. Quickly evaporating fine fuel sprays mix well with air and burn cleanly and efficiently. Unlike conventional air-blast atomizers discharging a jet core/film, a newly developed swirl burst (SB) injector generates fine sprays at the injector's immediate exit, even for high-viscosity fuels, without preheating, using a unique two-phase atomization mechanism. It thus resulted in ultra-clean combustion for glycerol/methanol (G/M) blends, with complete combustion for G/M of 50/50 ratios by heat release rate (HRR). Lower combustion efficiencies were observed for G/M 60/40 and 70/30, representing crude glycerol. Hence, this study investigates the effect of premixed methane amount from 0–3 kW, and the effect of atomizing gas to liquid mass ratio (ALR) on the dual-fuel combustion efficiency of G/M 60/40-methane in a 7-kW lab-scale swirl-stabilized gas turbine combustor to facilitate crude glycerol use. Results show that more methane and increased ALR cause varying flame lift-off height, length, and gas product temperature. Regardless, mainly lean-premixed combustion, near-zero CO and NOx emissions (≤2 ppm), and ~100% combustion efficiency are enabled for all the cases by SB atomization with the assistance of a small amount of methane.

Keywords: swirl burst (SB) injector; lean-premixed combustion; dual-fuel combustion; high viscosity; near-zero emissions

Citation: Islam, S.M.R.; Patel, I.; Jiang, L. Effect of Methane on Combustion of Glycerol and Methanol Blends Using a Novel Swirl Burst Injector in a Model Dual-Fuel Gas Turbine Combustor. *Clean Technol.* **2024**, *6*, x. https://doi.org/10.3390/xxxxx

Academic Editor(s): Name

Received: 31 August 2024
Revised: 28 September 2024
Accepted: 10 October 2024
Published: date

Copyright: © 2024 by the authors. Submitted for possible open access publication under the terms and conditions of the Creative Commons Attribution (CC BY) license (https://creativecommons.org/licenses/by/4.0/).

1. Introduction

As fossil fuel reserves continue to deplete, researchers in the field of biodiesel combustion research have turned their focus towards developing alternative sources of energy [1]. Consequently, the production of biodiesel is steadily on the rise. As biodiesel production increases, so does the generation of its byproducts. The primary and most commonly used biodiesel production process is transesterification, in which the raw material is oils and fats from plants or animals [2,3]. Biodiesel can be combusted cleanly and efficiently without preheating and further modification due to its properties similar to those of diesel. Biodiesel primarily yields glycerol ($C_3H_8O_3$) as its main byproduct [4]. The quantity of glycerol produced during biodiesel production constitutes approximately 10% of its total weight [5]. Glycerol has limited use in a few industrial sectors of cosmetics, food processing, packing material, etc. The excess glycerol production can be treated as waste, which is a challenging task to dispose of in the environment [5]. Due to the high viscosity, high surface tension, and low calorific value of glycerol, it is difficult to burn [6] with conventional injectors such as air-blast (AB) atomizers that are highly sensitive to slight variations in fuel properties. However, due to its substantial oxygen content and moderate heat output, glycerol is a feasible biofuel option for combustion, aiming to decrease carbon emissions [7,8]. On the other hand, crude glycerol from biodiesel contains

methanol [9–12], which has a high octane number, high performance, and low emissions [8,13]. Additionally, methanol can be produced from biomass [8,13]. Efficiently combusting glycerol and methanol blends can reduce the cost of purifying crude glycerol, which contains 60–70% glycerol and 23.4–37.5% methanol by weight [5]. Moreover, by blending methanol with glycerol, the viscosity of the blend reduces significantly compared to pure glycerol [8]. However, it is ~3× viscous than diesel [14], which is difficult to burn by using the AB injector [8].

In the present era, there is a worldwide inclination towards implementing strict emissions regulations to reduce global warming [8]. Scientists are actively engaged in efforts to minimize emissions through the implementation of clean and efficient combustion approaches [8]. Fine spray generation, which helps to evaporate the spray quickly and mix with air homogeneously, is a pre-requisite for clean and complete combustion [8]. However, the atomization capability of the conventional AB atomizer is limited. The AB atomizer introduces a fuel at a relatively lower velocity while injecting air at a higher velocity through the injector [8,15]. It first produces a liquid jet core or film at the injector exit, which breaks further downstream by creating long ligaments, short streaks, and large droplets gradually by shear layer instabilities between the liquid fuel and the high-velocity air [8,15–17]. When ligaments and larger droplets move further in the flow direction, aerodynamic forces by the relative velocity of the ligaments and droplets with the surrounding air break the ligaments and droplets into smaller droplets, which is called secondary atomization [8,18,19]. However, for liquid fuels with even a slight increase in viscosity and surface tension force, shear layer instabilities are suppressed, hindering the liquid disintegration to yield larger droplets and ligaments that do not fully vaporize [19,20]. Hence, they burn in diffusion mode locally, resulting in high local flame temperature and pollutant emissions [7,8,16,17,21]. For instance, sustainable aviation fuel C-3 has almost 2.5 times higher viscosity of conventional jet fuel Jet A [22,23]. Due to the limited atomization capability of AB injector while atomizing C-3, it exhibited the lowest ignition capability among the tested fuels, including Jet A-1, A-2, A-3, C-1, C-2, C-3, C-4, C-5, and C-7 [23].

Ganán-Calvo (2005) developed the flow-blurring (FB) atomizer with a significantly enhanced atomization efficiency [8,24]. Compared to the conventional AB atomizers that atomize by external air-liquid interaction, the FB atomizer uses a unique internal geometry to incur rapidly formed internal two-phase flow with entrapped air bubbles. While crossing the injector exit, the air bubbles expand and burst robustly due to the dramatic pressure drop. This tears the surrounding liquid into fine droplets immediately at the injector exit, defined as primary atomization. Hence, the FB atomizer offers a significantly larger total droplet surface area, ranging from five to fifty times greater than the AB atomizer [24]. Due to the fundamentally varied primary atomization mechanism, the FB atomizer has a broader range of fine spray generation capability irrespective of viscosity [8,16,22,25]. It generates droplets with smaller diameter and more uniform droplet size distribution. For water, the Sauter mean diameter (SMD) is 5–25 μm for FB and 5–45 μm for AB ≥2 cm downstream of the injector exit [8,21]. This creates a shorter atomization complete length (for FB ~2.67 D downstream from the injector exit with diameter of D and AB > 50D from the injector exit) [26]. FB generates fine droplets for a variety of liquids: water [26], diesel [27], biodiesel [28], vegetable oil [27], Jet A-2 [29], JP-5 [29], viscous sustainable aviation fuel C-3 [22,29], and even thin ligaments for extremely viscous glycerol at the injector immediate exit [30]. As a result, the FB injection resulted in clean, lean-premixed, and complete combustion of diesel [31], biodiesel [31], vegetable oil (VO) [31], and even straight glycerol [7] (~>200× more viscous than diesel) without preheating the fuel or the air. However, though the primary atomization generates fine droplets for distinct fuels, thin ligaments are observed for extremely viscous glycerol at the injector immediate exit [8,30]. Jiang et al. (2015) observed that larger droplets are generated at the spray periphery while atomizing water by using the FB injector [26]. Additionally, for high-viscosity glycerol, small ligaments, in addition to droplets, are

generated at the injector exit. These ligaments and larger droplets undergo a longer secondary atomization length than low-viscosity water [8,30]. This causes a long fuel pre-vaporization and fuel–air mixing zone, leading to a further-lifted-off flame that is subject to blow-off [8]. Sharma et al. (2024) investigated the effects of atomizing air to liquid mass ratio (ALR) and swirl number for preheated glycerol at 400 K and preheated air at 500 K in a swirl stabilized combustor by using the FB injector [32]. They found the lift-off height increases with the increase of ALR and swirl number [32]. FB was also utilized to combust preheated vegetable oil and glycerol at 400 K with preheated air at 500 K in a swirl stabilized combustor [33]. It was observed that with the increase in swirl number, flame stability increases [33] with cleaner combustion compared to the counter-swirl AB injector.

In order to further enhance the secondary atomization, our group recently developed a novel twin-fluid injector called a swirl burst (SB) injector by innovatively introducing swirling atomizing air (AA) with the FB concept [17,34,35]. It creates stronger shear layer interactions by forming the radial and tangential velocity components of the AA via uniquely designed swirling vane channels to disintegrate the large droplets and/or ligaments rapidly at the injector nearfield by secondary atomization [8,17,36,37]. Thus, the SB injector generates more uniform and finer droplets with diverged spray angles [8,35,37–40] than an FB injector [29,34,35]. The atomization length of the SB injector is half of the FB injector; thus, the SB yielded lower lifted-off and more compact flames of straight VO, signifying enhanced flame stability and compactness [8,34]. In addition, combustion efficiency is further improved for SB compared to FB: for non-preheated straight VO, completeness of combustion was found to be 98% by using the SB injector whereas 95% completeness was found by using the FB injector [8,17]. The SB injector achieved complete, lean-premixed combustion of straight algae oil (AO) (~16× more viscous than diesel) with ultra-low CO (6–8 ppm) and NOx (6 ppm) emissions at an equivalence ratio of 0.65 and air-to-liquid mass ratio (ALR) of 4.34, proving the fine atomization capability of the SB injector [8,36]. Furthermore, computational simulation and modeling provide insight into the fundamental two-phase atomization mechanism underlying the ultra-fine spray formation and clean combustion using the FB injection concept that shares the same primary atomization mechanism with the SB atomization. Murugan et al. (2020) found that the two-phase flow pattern of the FB injector is investigated numerically by large eddy simulation (LES) [41]. They observed that the threshold ALR for the working principle of FB injector is 0.6 [41]. Ling and Jiang (2024) investigated the internal two-phase flow dynamics and break-up mechanism of the FB atomization concept using a two-dimensional (2D) rectangular section [42]. They identified the threshold Weber number and dynamic pressure ratio at which a bubbly-jet region is generated, which is a transition regime between the AB-jet regime and the FB-jet regime formed near the liquid tube tip inside the atomizer [42]. Nasim et al. (2023) found that air penetration depth upstream of the liquid channel tip increases as the ratio of the gap between the liquid flow tube exit and atomizer exit (H) to the center liquid channel's inner diameter (D) decreases for the SB injector [43]. In addition, the numerical method utilized by Cravero et al. (2024) has the potential to establish the correlation between the injector swirl geometry and the turbulence phenomena of the two-phase atomization [44]. The recirculation length of the two-phase flow, if any, can also be numerically simulated by the 3-dimensional large eddy simulation [45].

To reduce NOx and particulate matter emissions, dual-fuel combustion is being explored in combustion systems. Papagiannakis et al. (2004) used natural gas (NG) in a dual-fuel diesel engine with the pilot diesel ignition and observed ~50–200 ppm less NOx while running at 2500 rpm and ~100–800 ppm less NOx while running at 1500 rpm compared to direct diesel combustion in a compression ignition (CI) engine [46]. By using methane (CH_4) in a dual-fuel diesel-methane combustion Guido et al. (2018) found less soot and almost a 40% reduction in particles found in the combustion gas products [47]. They also observed ~0.02–0.35 mg/L less soot concentration of dual-fuel compared to diesel combustion [46]. Moreover, in spark-ignition (SI) engines, dual-fuel combustion can

reduce emissions and enhance performance by reducing fuel consumption [48]. Iorio et al. (2013) discovered ~0.012 g/kg lower CO, ~15 g/kg lower NOx and ~2–5 g/kg less particulate emission by utilizing methane–gasoline dual fuel combustion compared to gasoline combustion in a SI engine [49]. Similarly, by utilizing biodiesel and NG dual-fuel combustion in a radial swirl gas turbine at an equivalence ratio of 0.5, found ~10 ppm less NOx compared to biodiesel combustion [50]. Chong et al. (2020) demonstrated ~1.5 g/kWh less NO at an equivalence ratio of 0.65 by using diesel-NG dual fuel combustion compared to diesel combustion in a model gas turbine combustor [51]. Additionally, using an FB injector, Jiang et al. (2014) combusted pure glycerol with methane in a 7 kw model gas turbine combustor and found that flame length becomes almost half when methane flow is increased from 4.14 slpm to 7.12 slpm with a constant heat release rate (HRR) of 7.9 kW [7,8]. Also, due to the high temperature, ~1800–2000 K, at a distance of 8 cm from the injector exit for 55% of methane by HRR, fuel pre-vaporization is faster compared to the 32% methane by HRR in glycerol and methane co-combustion at an ALR of 2.23, resulting in more homogeneous air–fuel mixing and more complete combustion with less pollutant emissions [7]. Thus, for 55% methane by HRR in the co-combustion of glycerol and methane, carbon monoxide (CO) emission is ~20 ppm and NOx emission is ~10 ppm less than the 32% methane by HRR [7].

In our previous study, by using an SB injector, we achieved ultra-low CO and NOx concentrations and promising combustion efficiency of G/M blends in the ratios of 50/50, 60/40, and 70/30, as well as at different ALRs for 50/50 ratio of G/M (1.5–3.0) [8,52]. Near-complete combustion was achieved for 50/50 with relatively lower combustion efficiency for 60/40 and 70/30 by HRR [8,52]. To further improve the combustion efficiency, the present study is concentrated on analyzing the effect of methane amount through the combustion swirler on the dual-fuel combustion performance (methane and 60/40 G/M blend by HRR) at a constant ALR of 3.0 using the SB injector for the liquid portion [8]. G/M blend of 60/40 ratio represents crude glycerol [5]. Additionally, the impact of ALRs on the G/M of 60/40 methane main flame of the dual-fuel combustion is investigated with the small quantity of premixed methane of 1 kW [8]. The equivalence ratio and total HRR are kept constant at 0.75 and 7.0 kW, respectively [8]. Flame images, concentration of CO and NOx in the combustion gas products, and combustion gas products and combustor wall temperature are also studied to determine the global combustion characteristics of the dual-fuel G/M of 60/40 methane combustion [8]. The novelty of this work mainly resides in (1) achieving lean premixed combustion with near zero NOx and CO emissions of the dual-fuel G/M 60/40-methane with the methane amount of 0–3.0 kW, without fuel nor air preheating, (2) investigating the optimum methane amount to enhance the efficiency of the duel-fuel combustion of G/M 60/40-methane blends, and (3) acquiring complete combustion of G/M 60/40-methane blends with a small amount of methane at 1 kW by using the novel SB injector at two-phase mass ratio of 2, enabling use of waste crude glycerol as a biofuel.

2. Experimental Setup

2.1. Working Principle of Swirl Burst Injector

Figure 1 illustrates the SB injector's working principle [8,17,36]. Key geometrical properties of the SB injector are provided in Table 1. Liquid fuel passes through the center channel, and atomizing air (AA) flows through the annulus around the center liquid channel [8,24]. The geometric conditions are: (i) center liquid channel inner diameter, D is equal to the exit orifice diameter; (ii) the gap between the liquid flow tube exit and atomizer exit (H) will be equal to or less than 0.25 times of the center liquid channel diameter [8,24]. While leaving the gap H, AA flows in the radial direction [8]. When the geometric conditions are achieved [12,24,36], a stagnation point develops between the center liquid fuel tube tip and the injector exit, and a small part of the AA penetrates a very short distance of the liquid fuel flow channel, which creates turbulence and forms

bubbles slightly downstream of the liquid fuel flow exit channel, resulting in significantly turbulent two-phase flow passing through the injector exit [8,24]. The air bubbles leaving the atomizer exit in the flow direction burst and break into fine droplets due to a significant pressure drop [8,17]. The remaining major portion of AA flows through the injector exit with a very high momentum which helps the secondary atomization by shear layer instabilities at the interface of the liquid parts and fast-moving air [8,36]. This process was first introduced in the FB atomization concept. In the SB injector, it innovatively integrates the advantage of the FB injection and the swirling flow to further enhance the secondary atomization. Like the FB injector, a stagnation point is developed at the same location. From the stagnation point, a small amount of air penetrates the liquid channel, and the remaining larger quantity of air moves toward the injector exit with a swirling motion through the swirl grooves and helps with the secondary atomization through shearing between the surface of droplets and swirling air [8,17,36]. The swirling flow is characterized by the injector swirl number (SN), which is a non-dimensional number determined by Equation (1) [8,53,54].

$$N = \frac{2}{3} \times \frac{1 - (d_h/d_t)^3}{1 - (d_h/d_t)^2} \times tan\,\alpha \quad (1)$$

where swirler hub diameter is denoted by d_h, tip diameter is denoted by d_t, α represents the exit vane angle of the swirler. The vane angle α is the angle between the axial plane of the curved vane and tangent to the exit of the curved vane.

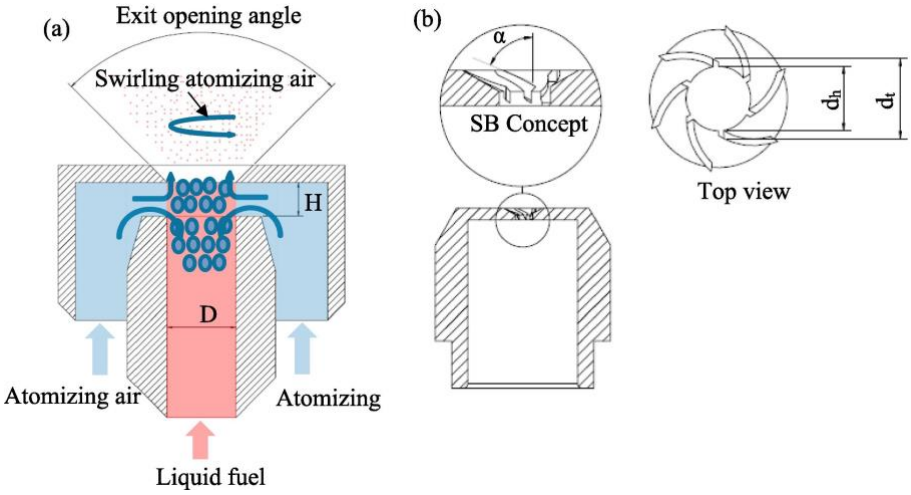

Figure 1. (**a**) Working principle of SB injector, (**b**) SB concept [8,17,36].

Table 1. Key geometrical parameters of the SB injector.

Parts	Dimensions
Center channel diameter, *D*	1.5 mm
The gap between the liquid flow tube exit and atomizer exit, *H*	0.375 mm
Hub diameter, d_h	1.5 mm
Tip diameter, d_t	2.1 mm
Exit vane angle, α	70°
Injector swirl number, ISN	2.4

2.2. Experimental Setup of the Model Dual-Fuel Gas Turbine Combustor

The objectives of the current study are to investigate (1) the effect of methane amount (0 to 3 kW by HRR) on the combustion performance of the dual-fuel (gaseous and liquid fuel) flame when methane is introduced through the combustor swirler and G/M of 60/40 (by HRR) is used as the liquid fuel blend and atomized by an SB injector at a constant ALR of 3.0; and (2) the effect of ALR on the dual-fuel G/M of 60/40-methane combustion by using the SB injector at a constant 1 kW of methane [8]. All the experiments are conducted at the constant equivalence ratio of 0.75 and the total HRR of 7.0 kW [8]. Global flame characteristics are investigated by analyzing the visual flame images, carbon monoxide (CO), and nitrogen oxide (NOx) concentrations in the combustion gas products at the combustor exit [8]. The combustion gas product temperature and the combustor outer wall temperature are measured to evaluate the combustion completeness [8].

For our current investigation, a lab-scale 7-kW swirl-stabilized gas turbine combustor was used as per Figure 2a,b [8]. To ensure dry, clean air supply to the combustor, the compressed air goes through water traps and filters, and then is divided into PA and AA [8]. The Mass Flow Controller (MFC) from Alicat MC-series controls the PA and AA supply with an uncertainty of 0.8% of the reading and ±0.2% of the full range [8]. The MFC model number for PA is MCP-250SLPM-D with a range of 0–250 SLPM, and for AA, the model number is MCP-100SLPM-D with a range of 0–100 SLPM [8]. The AA is introduced through a check valve, located at the downstream of the MFC to prevent the backflow. Before starting the experiment, methane gas is used to preheat the combustor [8]. Methane flows from the source tank and is introduced through a valve [8]. Flow was controlled by MFC of model no. MCP-50SLPM-D with a range of 0–50 SLPM [8]. Methane is mixed with PA in the mixing chamber. A ball valve is used to flow methane to the mixing chamber, while a second ball valve remains closed to prevent methane flow to the atomizer. Finally, the mixture of PA and methane passes through a 45° straight vane swirler with SN of 0.77 to the quartz combustor. It is to be mentioned that throughout the experiment, methane is premixed with the PA in the mixing chamber shown in Figure 2a and then introduced to the quartz combustor through a combustor swirler. The cylindrical quartz tube of the combustor has a length of 45 cm and a diameter of 7.62 cm [8]. Glycerol and methanol are stirred by using a magnetic stirrer with a speed of up to 3000 rpm for the mixing. The mixed fuel is introduced to the atomizer via a peristaltic pump: Cole-Parmer Masterflex L/S (EW-77921-75), Masterflex LLC, Barrington, Illinois, USA, with a range of 0–88 mLPM and an uncertainty of ±0.1% of the range, is used [8]. A pulsation damper is used between the fuel pump and the SB injector [8].

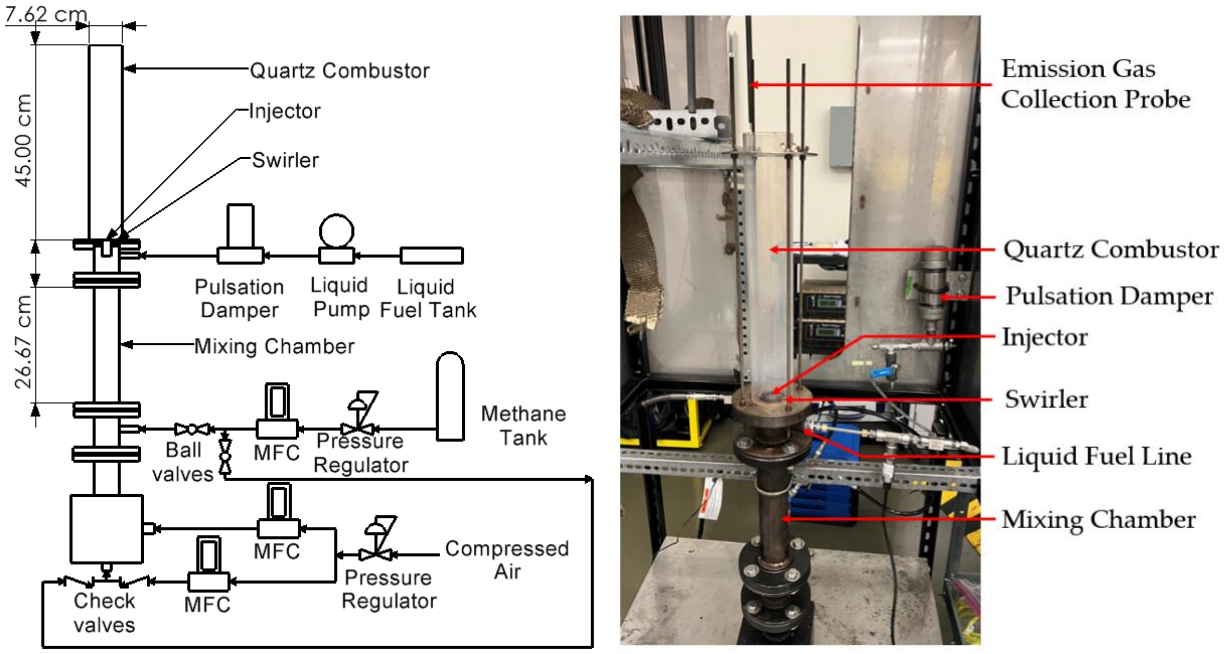

(**a**) (**b**)

Figure 2. (**a**) Schematic [8] and (**b**) the test rig of the model dual-fuel gas turbine combustor**.**

The research objectives of the current study are twofold: (1) it investigates the effect of premixed methane amount (0 to 3 kW by HRR) on the combustion performance of G/M of 60/40-methane dual-fuel combustion, and (2) it explores the impact of ALRs on the G/M of 60/40-methane dual-fuel combustion with 1 kW methane by using SB injector [8]. A comparison of the physical and chemical properties of pure glycerol, methanol, and G/M of 60/40 blend with diesel is provided in Table 2 [8]. Table 3 exhibits the experimental conditions for different amounts of premixed methane in the G/M of 60/40-methane dual-fuel combustion with a constant ALR of 3.0 and equivalence ratio of 0.75 [8]. Constant HRR of 7 kW and an equivalence ratio of 0.75 are maintained throughout the process for the tested cases [8]. For the effect of ALR through the liquid fuel injector on the dual fuel combustion, the AA flow rate is varied to achieve ALRs of 2.0, 2.5, and 3.0 while keeping an HRR of 7 kW and an equivalence ratio of 0.75 as constant.

Table 2. Selected physical and chemical properties of the fuels used [7,8,12,14,29,54–59].

Property	Diesel	Methanol	Glycerol	G/M of 60/40 Blend
Chemical formula	$C_{11.125}H_{19.992}$	CH_4O	$C_3H_8O_3$	N/A
Lower heating value, LHV (MJ/kg)	44.60	19.90	15.80	17.22
Density at 25 °C (kg/m^3)	834.00	791.00	1260.00	1045.46
Kinematic viscosity at 25 °C (mm^2/s)	3.88	0.59	965.80	8.02
Auto-ignition temperature (°C)	260.00	464.00	370.00	N/A
Vaporization temperature (°C)	160.00–370.00	64.70	290.00	N/A
Heat of vaporization (kJ/kg)	250.00	726.10	662.00	N/A
Stoichiometric air/fuel ratio (mol/mol)	16.12	7.14	16.66	10.92

Table 3. Experimental conditions for G/M of 60/40-methane dual-fuel combustion at ALR of 3.0.

ALR	HRR of G/M of 60/40 Fuel	HRR of Methane (kW)	G/M of 60/40 Blend Volume Flow Rate (MLPM)	Methane Flow Rate (SLPM)	Atomizing Air Flow Rate (SLPM)	Primary Air Flow Rate (SLPM)

	(kW)					
3.0	7.0	0	23.33	0	57.37	86.99
3.0	6.8	0.2	22.67	0.33	55.74	88.05
3.0	6.6	0.4	22.00	0.67	54.10	89.12
3.0	6.4	0.6	21.33	1.00	52.46	90.18
3.0	6.2	0.8	20.67	1.33	50.82	91.25
3.0	6.0	1.0	20.00	1.67	49.18	92.33
3.0	5.5	1.5	18.33	2.50	45.08	94.97
3.0	5.0	2.0	16.67	3.34	40.98	97.64
3.0	4.5	2.5	15.00	4.17	36.88	100.30
3.0	4.0	3.0	13.33	5.00	32.79	102.96
2.5	6.0	1.0	20.00	1.67	40.98	100.51
2.0	6.0	1.0	20.00	1.67	32.79	108.70

To analyze global combustion characteristics, CO and nitrogen oxides (NOx) concentrations in the combustion gas products are measured by an ENERAC (700 series) emission gas analyzer. For NOx detection, the range is 0–150 ppm and 0–1500 ppm (dual mode) with a resolution of 0.1 ppm and an uncertainty of <±1% of the reading. CO is measured by a four-electrode electrochemical sensor with a range of 0–150 ppm and 0–2000 ppm (dual mode), the resolution of 0.1 ppm, and the uncertainty of ±1–2% of the reading [8]. The flame images are meticulously captured by using a Canon EOS M50 Mark II, Canon U.S.A. Inc., Huntington, NY, USA, with an aperture setting f/4.5, light sensitivity settings of International Organization for Standardization (ISO)-6400 (ISO)-6400 [60], an exposure time of 1/125 s, and a focal length of 17 mm [8]. A R-type thermocouple with a range of -50–1480 °C and uncertainty of ±1.5 °C or ±0.25% of the reading is used to measure the combustion products gas temperature at 2.54 cm upstream of the combustor exit in the radial direction of the quartz combustor tube [8]. To measure the surface temperature of the quartz combustor tube, a LS-84D thermometer with a J-type thermocouple (Omega HPS-HT-J-12-SMP-M) with a range of 0–760 °C and uncertainty of (±0.5% of reading + 0.7 °C) is used [8]. The temperature of the combustion products gas is measured at the combustor exit (2.54 cm upstream the opening) at nine equidistant radial locations. Combustor wall temperature is measured at nine equidistant axial locations. Both temperatures are continuously monitored. At each measured location, the temperature stabilizes after several minutes within a fluctuating range with ~6–8 K variation from the lowest to the peak value. To minimize thermocouple error, the average of the upper and lower bounds of the fluctuating temperature data is recorded.

3. Results and Discussion

3.1. The Effect of Methane Amount in the Dual-Fuel Combustion

3.1.1. Global Flame Characteristics for Various Methane Amount in the Dual-Fuel Combustion

The Effect of Methane Amount on Visual Flame Images

In this study, the effect of methane amount on global combustion characteristics of the dual-fuel flames is analyzed in terms of visual flame image, thermal characteristics and CO, and NOx concentrations of the combustion gas products. Properties of 60/40 G/M are illustrated in Table 2 [8]. The kinematic viscosity of 60/40 G/M is ~2× that of diesel fuel, making it difficult to be finely atomized using a conventional AB injector due to the AB injector's sensitivity to small change in fuel properties [8]. Instead, the current work employs the SB injection that has demonstrated high viscosity tolerance as aforementioned [8]. Figure 3 shows the flame images of 60/40 G/M and 60/40 G/M methane dual-fuel with the varying methane amount of 0.2 kW to 3.0 kW, where total HRR is maintained at 7 kW with ALR of 3.0 and equivalence ratio of 0.75 [8]. Each visual

flame image is captured at an exposure time of 0.008 s, which significantly exceeds the chemical time scales of elementary reactions, e.g., at the order of magnitude of ~10^{-4}s for OH* [61]. Hence, each flame image is an ensemble flame image of a time averaging process of fast-changing chemical kinetics and varying flame stages within the exposure time. The ensemble flame images thus illustrate average flame lift-off height and flame length. The image brightness is increased by 50% to analyze the flame qualitatively [8]. Blue chemiluminescence of the flames reflects complete combustion of CH* [35,61]. Therefore, in all cases, the predominant blue flames suggest that the complete and clean combustion is achieved for the high-viscosity pure-liquid 60/40 G/M fuel blend and the dual-fuel combustion of G/M of 60/40 and methane by using a powerful SB injector even without fuel or air pre-heating and with an uninsulated combustor [8]. It is to be noted that the red color on the quartz combustor is the result of the reflection of the flame zone on the quartz combustor wall. Fuel pre-vaporization and fuel–air mixing likely occurs in the dark region upstream of the flame which signifies mainly lean-premixed combustion attained by the ultra-fine SB atomization [8]. The highly illuminated portion at the middle of the flame illustrates the high-temperature primary reaction zone [8]. It is observed that the lift-off height of the pure-liquid G/M of 60/40 fuel is ~10 cm, for G/M of 60/40 methane dual-fuel at 0.2 kW methane is ~8 cm, which decreases gradually with the increase in the amount of the methane and becomes ~5 cm for the flame with 3 kW premixed methane [8]. Flame length also becomes shorter with the increment of methane amount with more radially distributed flame: pure-liquid G/M of 60/40 fuel flame length is ~12 cm (y = ~10–22 cm); for G/M of 60/40-methane dual-fuel at 0.2 kW methane, flame length is ~11 cm (y = ~8–19 cm); and at 3 kW, methane length is ~8 cm (y = ~5–13 cm) [8]. The possible reasons mainly contributing to these trends are: (1) the addition of highly reactive methane enhances the reaction rates resulting in less lift-off height with a shorter flame length; (2) thus the local flame temperature is also increased in return, vaporizing the liquid droplets faster by quickly providing more thermal feedback that expedites complete pre-vaporization of droplets; (3) the rapidly vaporized liquid fuel mixes with oxidizer quickly and more homogeneously, thus leading to rapid reactions with a higher flame temperature in return; and (4) to keep the HRR constant, with the increase in methane, liquid fuel flow rate, and AA flow rate decrease for the constant ALR of 3.0 [8]. Hence, the injection velocity decreases, causing less lift-off height [62,63]. Thus, the flame is stabilized closer to the combustor swirl with more residence time for complete combustion [8]. Note that high-fidelity measurements of the flow-turbulence-chemistry interaction in the combustion field are needed to further validate these possible reasons, which is beyond the scope of the current global flame characterization. The flames are not radially symmetric, possibly due to the turbulent nature of the flame and/or imperfections in the manufacturing of the combustion swirler vanes, leading to uneven primary air flow.

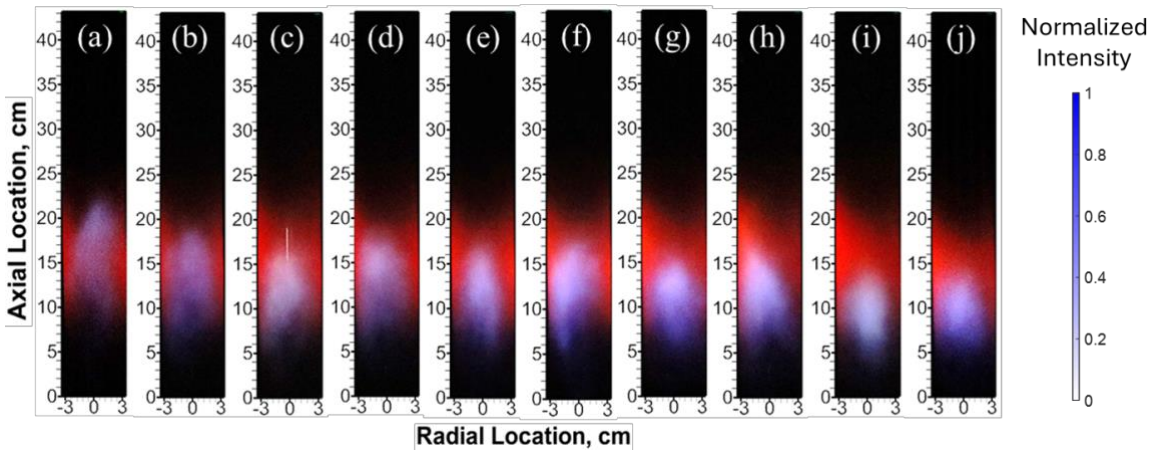

Figure 3. Flame images for (**a**) pure-liquid G/M of 60/40, and dual-fuel combustion of G/M of 60/40-methane with the methane quantity of (**b**) 0.2, (**c**) 0.4, (**d**) 0.6, (**e**) 0.8, (**f**) 1.0, (**g**) 1.5, (**h**) 2.0, (**i**) 2.5, and (**j**) 3.0 kW at a constant ER of 0.75, ALR of 3 and total HRR of 7 kW using the SB injector [8].

Figure 4 exhibits the quartz glass outer wall uncorrected surface temperature [8]. From Figure 3, it is observed that the most illuminating zone, representing the primary reaction zone is at the middle of the flame which is consistently substantiated by the quartz glass outer wall temperature profile [8]. Temperature increases from the dump plane up to the middle of the quartz combustor and then decreases in the downstream direction of the combustor [8]. It is also observed that the location of the highest wall temperature shifts in the downstream direction with the decrease of methane amount in the combustor supporting the increased lift-off height and shorter flame length with the decrease in methane amount, as per Figure 3 [8].

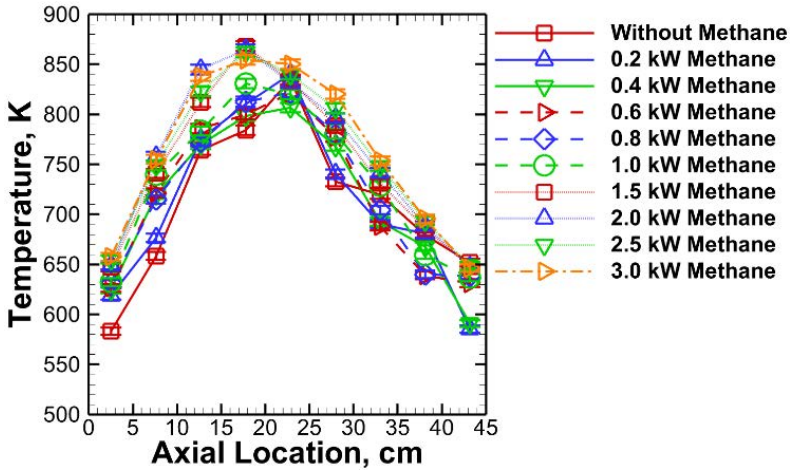

Figure 4. Axial profile of combustor outer wall surface temperature of pure-liquid G/M mix of 60/40 and G/M of 60/40-methane dual fuel combustion at a constant ER of 0.75, ALR of 3 [8].

The Effect of Methane Amount on Emissions in Combustion Gas Products

Figure 5a presents the radial temperature profile (uncorrected) of the combustion gas products at the combustor exit [8]. For all cases, temperature profiles follow a similar trend with lower temperature in the near wall zone compared to the middle of the combustor due to the convection and radiation heat loss of the uninsulated combustor wall to the surrounding [8]. The temperature profiles are not perfectly symmetric on both sides of the combustor, possibly due to the unevenly distributed primary air through the imperfectly manufactured combustion swirl and/or the turbulent nature of the flame. Temperature increases slightly with the increase in premixed methane mainly due to the high reactivity and flame speed of the methane [8]. This trend can also be substantiated by the estimated adiabatic flame temperature in Figure 6, which is 1887.7 K without methane, whereas with 3.0 kW methane, it increases up to 1909.6 K [8]. Though the difference in estimated adiabatic flame temperature from the case without methane to the dual-fuel flame with 3 kW methane is 21.9 K, the difference in gas product temperature at the combustor exit is higher than 21.9 K. This can be likely attributed to (1) the different volumes and length of the flame without methane and those with varying amounts of methane, as in Figure 3, at the constant total HRR of 7 kW, resulting in various local flame temperature, gas product temperature, and combustor wall temperature; (2) various amounts of heat loss from the uninsulated combustor to the surroundings through convective and radiative heat transfer. Figure 5b shows the CO emissions are ≤2 ppm irrespective of the methane amount in the combustor for all the tested cases [8]. Figure 5c illustrates NOx

concentration in the combustion products. Estimated adiabatic flame temperature from without methane to 3 kW methane in the dual-fuel combustion of glycerol/methanol–methane is 1887.7 K to 1909.6 K. Additionally, the uninsulated combustor wall temperature ranges approximately between 750 K to 900 K for all the cases in the reaction zone, where the flame temperature and the combustor wall temperature peak shown in Figure 4. Hence, there is considerable heat loss through the quartz combustor wall to the ambient air by radiation and convection. As a result, the flame temperature is significantly lower than 1800 K, above which thermal NOx forms [61]. Note that there might be minimal thermal NOx, less than the resolution (0.1 ppm) of the NOx measurement capacity of the emission gas analyzer. Therefore, the thermal NOx is ~0 in the current study without fuel nitrogen. Thus, the near-zero concentrations of CO and NOx suggest nearly complete and thus clean combustion achieved for the highly viscous G/M blends with/without methane. This can be again explained by the fact that the SB injector generates very fine droplets, leading to fast pre-evaporation and thus subsequently mainly lean-premixed and complete combustion [8,40]. CO_2 concentration in the gas products at the combustor exit is illustrated in Figure 5d. From pure-liquid G/M of 60/40 fuel to G/M of 60/40 methane dual-fuel combustion, the radial profiles of CO_2 emissions almost overlap. CO_2 increases with an increase in premixed methane up to 2 kW, then reduces slightly at higher methane flows. This is likely due to the increment of highly reactive methane; more O_2 participates in the reaction, generating more CO_2 in the exhaust gas, with an increment in combustion completeness. Note that the CO_2 profiles qualitatively represent the trend and may not the exact values as the sensor of the emission analyzer detects and measures CO, NOx, and O_2 but calculates CO_2 using the O_2 values and the internal algorithm based on preset fuels that are not the current fuel blend.

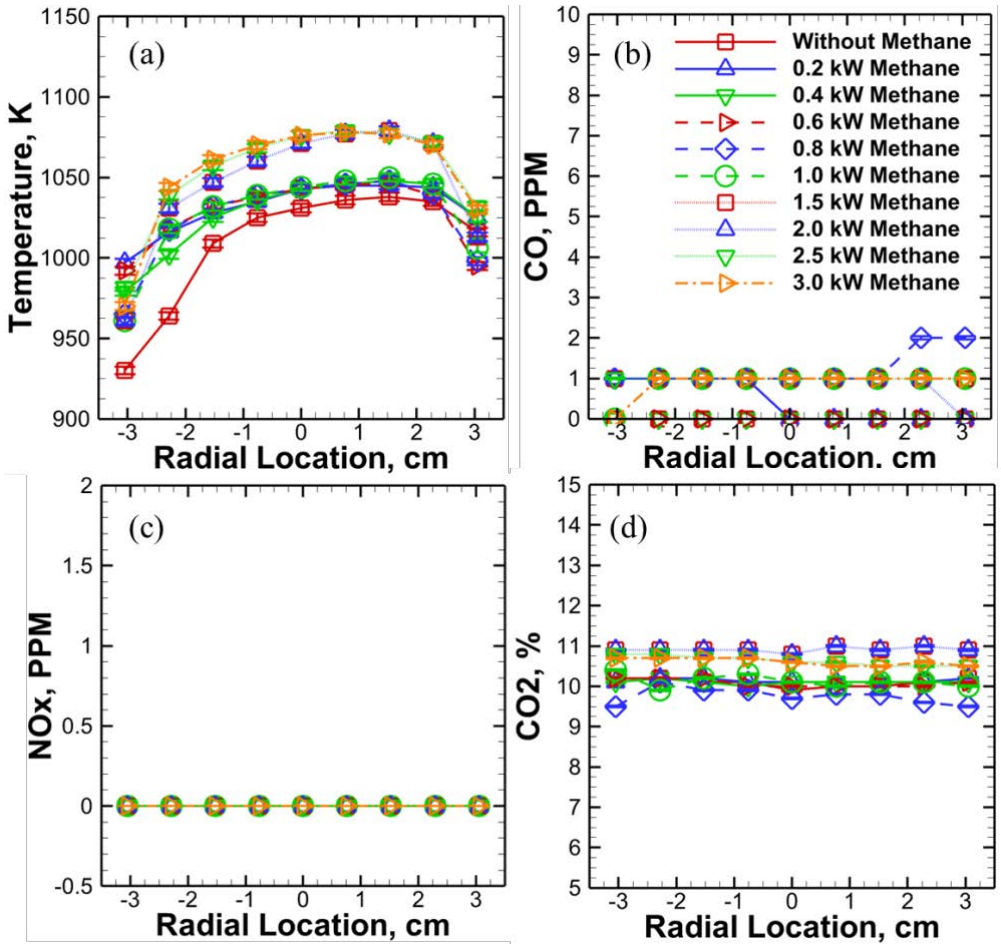

Figure 5. Radial profiles of (**a**) combustion product temperature [8] and (**b**) CO [8], (**c**) NOx, and (**d**) CO_2 concentrations at the combustor exit of pure-liquid G/M mix of 60/40 and G/M of 60/40 methane dual fuel combustion at a constant total HRR of 7 kW, ER of 0.75, and ALR of 3 using the SB injector.

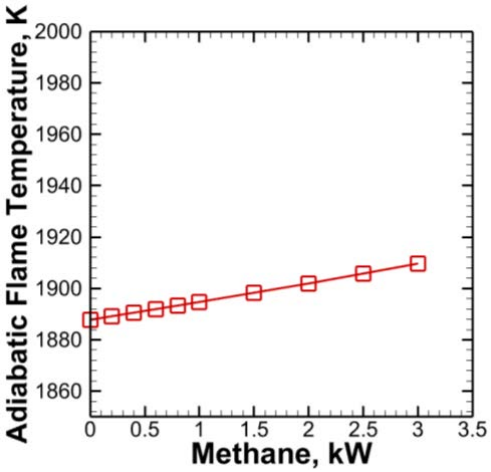

Figure 6. Adiabatic flame temperature of pure-liquid G/M blend of 60/40 and G/M of 60/40 methane dual fuel combustion at a constant ER of 0.75, ALR of 3 [8].

3.1.2. Combustion Completeness Estimation for the Varying Methane Amount

The temperature of the combustion gas products is measured by an R-type thermocouple, which is prone to error due to significant heat loss by the bead to the surrounding through radiation mostly [8,64]. To minimize the error of the thermocouple, corrected gas temperature is estimated by using Equation (2) [8,64].

$$h_t(T_g - T_t) = \varepsilon_b \sigma (T_t^4 - T_s^4) \quad (2)$$

where T_g is true gas temperature; T_t is thermocouple reading; T_s is ambient temperature, which is 22.2 °C, ε_b is the emissivity of the thermocouple bead, which is a function of combustion gas product temperature and thermocouple bead materials. It is estimated based on the correlation of R-type thermocouple and combustion gas products temperature, as per the referenced studies [65–67]; estimated values of the thermocouple bead emissivity are 0.136, 0.139, 0.138, 0.138, 0.138, 0.139, 0.141, 0.141, 0.142, and 0.142 without methane and 0.2 kW, 0.4 kW, 0.6 kW, 0.8 kW, 1.0 kW, 1.5 kW, 2.0 kW, 2.5 kW, and 3.0 kW with methane, respectively [65–67]. σ is the Stefan–Boltzmann constant, and forced convective heat transfer coefficient h_t of the combustion gas product flow is approximated using air properties [64]. The estimated values of h_t are 29.249 W/m²K, 29.828 W/m²K, 29.6989 W/m²K, 29.456 W/m²K, 29.329 W/m²K, 29.314 W/m²K, 29.420 W/m²K, 29.348 W/m²K, 29.265 W/m²K, and 29.076 W/m²K without methane and 0.2 kW, 0.4 kW, 0.6 kW, 0.8 kW, 1.0 kW, 1.5 kW, 2.0 kW, 2.5 kW, and 3.0 kW with methane, respectively [64].

Total energy released by the combustion is equal to the energy carried away by the combustion gas and heat loss to the surroundings by the combustor wall, as per Equations (3)–(5) [8,17].

$$Q_{total} = Q_{gas} + Q_{losses} \quad (3)$$

$$Q_{gas} = m_g C_{P_{air}} T_g \quad (4)$$

$$Q_{losses} = h_a A_s (T_w - T_{surr}) + \varepsilon_{glass} \sigma A_s (T_w^4 - T_{surr}^4) \quad (5)$$

where, Q_{total} is the total energy released from the combustion process; Q_{gas} is the energy carried away by the combustion gases; Q_{losses} are the energy losses by convection and radiation heat transfer from the combustion gases through the combustor outer wall to

the surroundings; m_g is the mass flow rate of the combustion gases which is equal to the total mass of fuel and gas; $C_{P_{air}}$ is the isobaric specific heat capacity of the combustion gases at the combustion gas temperature, T_g; air properties are used for the combustion products in this simple estimate. The estimated values of $C_{P_{air}}$ are 1.255 kJ/kgK, 1.262 kJ/kgK, 1.261 kJ/kgK, 1.260 kJ/kgK, 1.259 kJ/kgK, 1.259 kJ/kgK, 1.265 kJ/kgK, 1.265 kJ/kgK, 1.265 kJ/kgK, and 1.263 kJ/kgK without methane and 0.2 kW, 0.4 kW, 0.6 kW, 0.8 kW, 1.0 kW, 1.5 kW, 2.0 kW, 2.5 kW, and 3.0 kW with methane, respectively [64]; T_w is the combustor outer wall surface temperature of corresponding surface area A_s; σ is the Stefan–Boltzmann's constant; T_{surr} is the surrounding or ambient temperature, which is 22.2 °C, the ambient temperature of the laboratory environment where experiment is conducted; ε_{glass} is the emissivity of quartz glass that is a function of combustor wall temperature T_w and quartz glass average thickness of 2.136 mm [68]; for the wall temperature in 9 axial locations as illustrated in Figure 4, for each case from 0 kW methane to 3 kW methane, 9 estimated emissivity data points are obtained by using Ref. [68]; h_a is the natural convective heat transfer coefficient of the surrounding air for the heat loss from the combustor wall to the ambient air [69] and is a function of temperature; again, for the wall temperature in 9 axial locations as illustrated in Figure 4, for each case from without methane to 3 kW methane, 9 estimated the natural convective heat transfer coefficient data points are obtained by using Ref. [69].

Irrespective of the methane amount in the dual-fuel combustion, this simple estimation indicates a combustion completeness of ~100% compared to the lower efficiency of pure-liquid fuel combustion of G/M 60/40 [14]. It is to be mentioned that air properties were used for the combustion products in this simple estimate. Due to the above assumptions made, this estimation serves as a qualitative indicator rather than an absolute measure. In addition, the asymmetry of the flame in the radial direction might affect the combustor product gas temperature at the combustor exit and the combustor wall temperature measurement, thus the estimation of combustion completeness. The actual degree of combustion completeness may vary slightly. Regardless of this simple estimate, the measured combustion exhaust temperature and concentration, as well as the blue flame chemiluminescence for complete combustion of CH* [36,61], combinedly suggest the ~100% complete combustion achieved in the current study. In addition, our previous study showed that owing to the fine atomization capability of FB injector, sharing the same primary atomization by bubble bursting with the SB injection, highly viscous pure glycerol (~250 times more viscous than diesel) was atomized finely [30] and a relatively low CO (<40 ppm) was achieved in an insulated lab scale 7-kW combustor while co-combusting 68% or 45% of pure glycerol by HRR with the remaining HRR from methane at the ALR of 2.23 [7]. With further advanced atomization capability of the SB injector, clean, lean premixed (LPM), and near-complete combustion was achieved for straight algae oil and vegetable oil which are more viscous than 60/40 G/M blend [17,36]. In our present study, it is observed that ~100% combustion completeness is achieved by introducing premixed methane through the combustor swirler. This is due to the high reactivity and adiabatic flame temperature of methane [61] that helps to fully vaporize the droplets in addition to the fine atomization capability of the powerful SB injector.

3.2. The Effect of ALR

3.2.1. Global Flame Characteristics for Various ALRs of G/M of 60/40 Methane Dual-Fuel Combustion

The Effect of ALR on Visual Flame Images

Prior studies showed that an increase in ALR leads to finer atomization with very low CO emissions, ≤4 ppm, for ALR values of 3.0 for 50/50 G/M ratio fuel combustion [8,14]. In this study, the effect of ALR is observed for high-viscosity G/M of 60/40 blend with methane (1 kW) dual-fuel combustion by using a novel SB injector at a constant total HRR of 7 kW and an equivalence ratio of 0.75 [8]. For all the ALRs, the main blue flame

indicates clean combustion [35] of high-viscosity 60/40 G/M blend [8]. In the dark region upstream of the flame, pre-vaporization and fuel-air mixing occurs, which indicates the achievement of lean premixed combustion [8]. Thus, the SB injector finely atomizes high-viscosity fuel without pre-heating [8]. It is observed that an increase in ALR results in a shorter flame length [8] and a slightly shorter flame lift-off height. Figure 7 shows that for ALR of 2.0, flame length is ~16 cm (y = ~7–23 cm), at ALR of 2.5, it becomes ~15 cm (y = ~5–20 cm), and for ALR of 3.0 it becomes 11 cm (y = ~5–16 cm) [8]. The probable main reasons behind this trend are: (1) for the low ALRs, droplets are slightly bigger than those at a higher ALR and may travel further downstream along the combustor due to a higher momentum, leading to a longer flame length; (2) at the higher ALR, droplets become smaller, evaporate faster, and combust with a shorter residence time resulting in a less lifted and more compact flame [8]. Figure 8 depicts the uninsulated quartz combustor outer wall temperature (uncorrected) [8]. Quartz combustor outer wall temperature increases to the peaks and then decreases along the axial direction. Note that the flames are radially asymmetric as per Figure 7, which may result in an increased uncertainty of the combustor outer wall temperature.

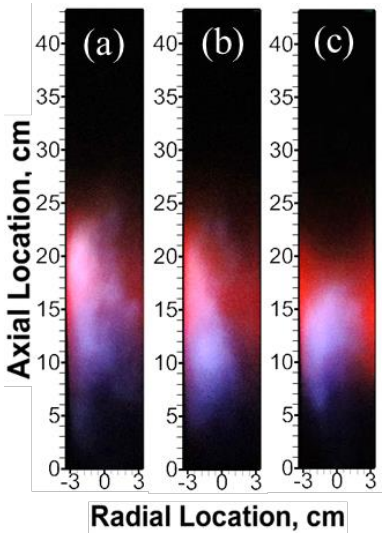

Figure 7. Flame images for dual-fuel combustion of G/M (60/40)-methane (1 kW) at ALRs of (**a**) 2.0 (**b**) 2.5 and (**c**) 3.0 at a constant HRR of 7 kW and the equivalence ratio of 0.75 [8].

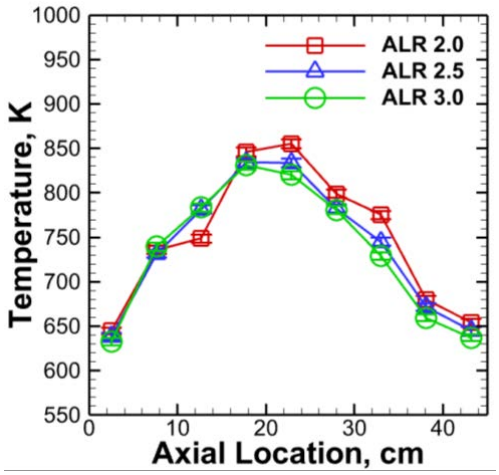

Figure 8. Axial profile of combustor outer wall surface temperature of dual-fuel combustion of G/M (60/40) methane (1 kW) for various ALRs across the SB injector at a constant ER of 0.75 [8].

The Effect of ALR on Emissions in Combustion Gas Products

Figure 9a shows that a slight decrease in ALR results in higher temperature compared to higher ALRs [8]. This might be due to (1) some of the slightly larger droplets at ALR of 2.0 burn at diffusion combustion mode without complete vaporization, resulting in slightly higher local temperature and thus higher local CO and NOx concentrations, as in Figure 9b,c compared to ALR of 2.5 and 3.0; (2) for the lower ALR of 2.0, the lower AA at the constant liquid flow rate compared to that of ALRs of 2.5 and 3.0 results in a lower injection velocity, i.e., the droplet velocity [8]. This allows a longer residence time of the droplets in the combustor, though they might be relatively larger [8]. Thus, the fuel may burn more completely with higher heat released, leading to higher combustion product temperatures [8]. For all the ALRs the CO concentrations are less than 3 ppm and NOx < 2 ppm which are illustrated in Figure 9b and Figure 9c respectively. The ultra-low CO and NOx emissions are achieved for a high-viscosity 60/40 G/M blend by using the novel SB injector, indicating near complete combustion [8]. Additionally, CO emission is uniform throughout the radial direction of the combustor exit again suggesting the generation of very fine and/or uniform droplet size by the SB injector [8]. For the ALR of 2.0, the combustion gas product temperature is slightly higher compared to the ALRs of 2.5 and 3.0, which possibly led to a slight increase in NOx at ALR of 2.0.

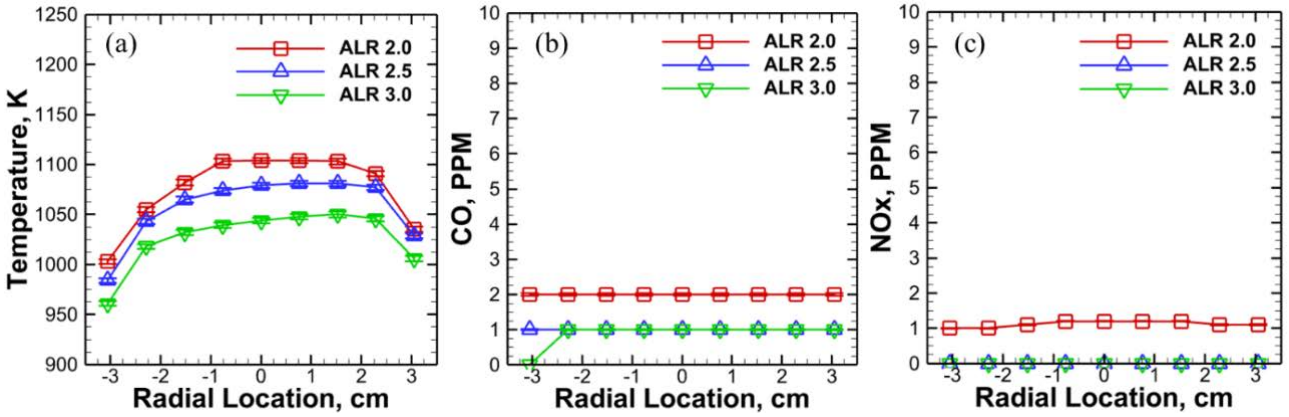

Figure 9. Radial profiles of (**a**) combustion product temperature and concentrations of (**b**) CO and (**c**) NOx at the combustor exit of dual-fuel combustion of G/M (60/40) methane (1 kW) for various ALRs across the SB injector at a constant ER of 0.75 and a constant total air flow [8].

From Figure 10a, it is evident that carbon dioxide concentration is higher for an ALR of 2.0 compared to ALRs of 2.5–3.0. This trend signifies more complete combustion at an ALR of 2.0. This may be because at the lower ALR, the injection velocity is lower, which leads to more residence time for the fuel to combust completely. Figure 10b represents oxygen concentrations in the gas products at the combustor exit. Oxygen composition is lower for an ALR of 2.0 compared to other ALRs, showing an adverse trend compared to the CO_2 profiles as expected. More oxygen consumption generates more complete combustion with increased CO_2 in the product, with less remaining oxygen in the combustion gas products.

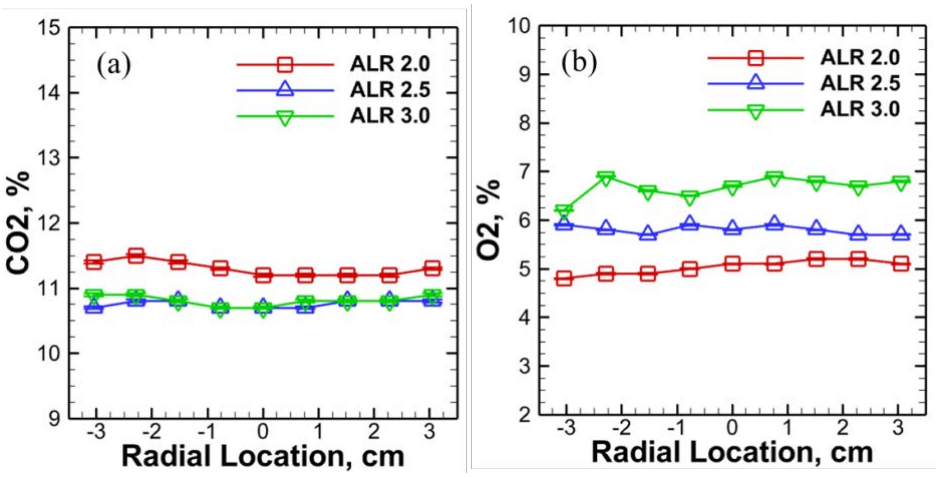

Figure 10. Radial profiles of (**a**) CO_2 and (**b**) O_2 emissions at the combustor exit of dual-fuel combustion of G/M (60/40)-methane (1 kW) for various ALRs across the SB injector at a constant ER of 0.75 and a constant total air flow.

3.2.2. Combustion Completeness Estimation for the Varying ALRs

The total generated heat is estimated by adding the heat loss to the surroundings through an uninsulated quartz combustor by radiation and convection with the energy carried away by the combustion gas products [8,17,70]. Thermocouple error is minimized by considering thermocouple bead heat loss to the surroundings through radiation as per Equation (2) [8,17]. Total energy produced is estimated by using Equations (3)–(5) [8,17]. The specific heat capacity of the combustion gases $C_{P_{air}}$ is estimated at the true gas temperature, T_g [8]. For the ALRs of 2.0, 2.5 and 3.0, the simple combustion completeness estimation results in ~100%. Again, this estimation provides qualitative information due to the assumptions made. However, again in combination of the simple estimation and the very low CO and NOx emissions as per Figure 9b,c, it can be concluded that due to a very fine atomization capability of the SB injector, at ALRs of 2.5 to 3.0, more complete combustion is achieved.

4. Conclusions

In the present study, glycerol/methanol (G/M) blends, representing waste crude glycerol from biodiesel production, are co-combusted with methane to achieve clean and complete combustion, compared to the baseline case of pure-liquid G/M combustion. This simultaneously allows us to explore renewable energy and minimize the burden of waste management. The novel SB injector is utilized to finely atomize the highly viscous G/M 60/40 blend for clean combustion without fuel preheating. Methane is added due to its high reactivity and high energy density to facilitate thermal feedback to vaporize the fine droplets quickly and combust cleanly [8], further overcoming the high evaporation and auto-ignition temperature of the glycerol component. In this study, the SB injector achieved ultra-clean combustion with CO concentration ≤ 2 ppm and ~0 ppm NOx concentration without preheating the viscous G/M and the dual-fuel burner, irrespective of methane amount from 0–3.0 kW at the total HRR of 7.0 kW. The visual flame images indicate that the increase in premixed methane via the combustion swirler results in shortened flame lift-off height and flame length with increased gas product temperature. Less lifted and more compact flames are obtained with the increase in ALR from 2.0 to 3.0. Near-zero CO and NOx concentrations are obtained for the ALRs of 2.0, 2.5, and 3.0 with a small amount of methane (1 kW), indicating the fine atomization capability of the SB injector. In addition, the simple estimate of combustion completeness, CO and NOx concentrations, and the blue flames combinedly suggest that with 1 kW of methane, at the ALRs of 2.5 and 3.0, almost-complete combustion is achieved for the main flame of

glycerol/methanol blend 60/40. Hence, the optimum ALR is 2.5 for the current experimental setup and conditions since an ALR of 2.5 has lower atomizing air flow compared to that at an ALR of 3.0. This requires less energy input for complete combustion. In summary, the dual-fuel combustor with the novel SB injector achieved lean-premixed, complete or near complete combustion of a highly viscous glycerol/methanol blend of 60/40 with/without methane and without fuel or air preheating in an uninsulated combustor. Thus, the novel SB injector coupled with/without co-combustion of a small amount of premixed methane potentially enables direct use of the crude glycerol for ultra-clean energy generation from the biofuel production waste, eliminating the expenditure of post-processing of waste crude glycerol [8]. The primary advantages and limitations of the current study are summarized in Table 4.

Table 4. Advantages and limitations of the current study.

Advantages	Limitations
Without air nor fuel pre-heating, achieving lean-premixed combustion with near zero NOx and CO emissions of the dual-fuel G/M 60/40-methane with the methane amount of 0–3.0 kW.	Approximation of the properties of combustion products as air properties, that leads to the qualitative estimate of the combustion completeness.
Determining the optimum methane amount to enhance the efficiency of the dual-fuel combustion of G/M 60/40-methane blends.	Use of unburned hydrocarbon measurement device can provide more accurate results of combustion completeness.
Achieving complete combustion of G/M 60/40-methane blends with a small amount of methane at 1 kW by using the novel SB injector at an ALR of 2.5, enabling use of waste crude glycerol as a biofuel.	Current simple flame color imaging could not provide more insight into the flame characteristics compared to other advanced optical diagnostics.

Future work will further investigate the reacting spray physics including the droplet size and velocity distribution and correlate with the downstream combustion characteristics to elucidate the fundamental physicochemical characteristics of the spray combustion using the SB injection.

Author Contributions: S.M.R.I.: experimentation, methodology, formal analysis, and writing—original draft and writing—review and editing. I.P.: experimentation, methodology, data curation, and writing–revising original draft. L.J.: conceptualization, methodology, resources, project administration, supervision, funding acquisition, formal analysis, and writing—review and editing. All authors have read and agreed to the published version of the manuscript.

Funding: The current research is funded by the Startup fund of Baylor University and NSF CIVIC award No. 2228311 and No. 2322319 co-funded by US National Science Foundation and Department of Energy.

Institutional Review Board Statement: Not applicable for this study.

Informed Consent Statement: Not applicable for this study

Data Availability Statement: Data will be made available on request.

Acknowledgments: We would also like to express our gratitude to Ashely Orr, who helped manufacture the combustion system and Joseph Breerwood for helping set up the system and Tony Bui for partial data collection. The paper is the extended version of the conference contribution here: https://arc.aiaa.org/doi/10.2514/6.2024-0331, (8 January 2024).

Conflicts of Interest: The authors declare that there are no competing financial interests nor personal relationships that could influence the work reported in this paper.

Nomenclature

AA	atomizing air or gas
AB	air blast
ALR	air or gas to liquid mass ratio
AO	algae oil
CH_4	methane
CO	carbon monoxide
D	diameter of the center liquid fuel channel and the injector exit
FB	flow blurring
G/M	glycerol/methanol
LPM	lean premixed combustion
H	gap between the center liquid fuel channel tip and injector exit
HRR	heat release rate
MFC	mass flow controller
MLPM	milliliter per minute
NG	natural gas
NOx	nitrogen oxides (including NO and NO_2)
PA	primary air
SB	swirl burst
SLPM	standard liter per minute
SMD	Sauter mean diameter
SN	swirl number
VO	vegetable oil
d_h	hub diameter
d_t	tip diameter
α	exit vane angle

References

1. Suhara, A.; Karyadi; Herawan, S.G.; Tirta, A.; Idris, M.; Roslan, M.F.; Putra, N.R.; Hananto, A.L.; Veza, I. Biodiesel Sustainability: Review of Progress and Challenges of Biodiesel as Sustainable Biofuel. *Clean Technol.* **2024**, *6*, 886–906. https://doi.org/10.3390/cleantechnol6030045.
2. Leung, D.Y.C.; Wu, X.; Leung, M.K.H. A Review on Biodiesel Production Using Catalyzed Transesterification. *Appl. Energy* **2010**, *87*, 1083–1095. https://doi.org/10.1016/j.apenergy.2009.10.006.
3. Farag, H.A.; El-Maghraby, A.; Taha, N.A. Transesterification of Esterified Mixed Oil for Biodiesel Production. *Int. J. Chem. Biochem. Sci.* **2012**, *2*, 105–114.
4. Yuan, Z.; Xia, S.; Chen, P.; Hou, Z.; Zheng, X. Etherification of Biodiesel-Based Glycerol with Bioethanol over Tungstophosphoric Acid To Synthesize Glyceryl Ethers. *Energy Fuels* **2011**, *25*, 3186–3191. https://doi.org/10.1021/ef200366q.
5. Quispe, C.A.G.; Coronado, C.J.R.; Carvalho, J.A., Jr. Glycerol: Production, Consumption, Prices, Characterization and New Trends in Combustion. *Renew. Sustain. Energy Rev.* **2013**, *27*, 475–493. https://doi.org/10.1016/j.rser.2013.06.017.
6. Feng, C.; Zhang, M.; Wu, H. Combustion of Fuel Mixtures Containing Crude Glycerol (CG): Important Role of Interactions between CG and Fuel Components in Particulate Matter Emission. *Ind. Eng. Chem. Res.* **2018**, *57*, 4132–4138. https://doi.org/10.1021/acs.iecr.8b00441.
7. Jiang, L.; Agrawal, A.K. Combustion of Straight Glycerol with/without Methane Using a Fuel-Flexible, Low-Emissions Burner. *Fuel* **2014**, *136*, 177–184. https://doi.org/10.1016/j.fuel.2014.07.027.
8. Islam, S.M.R.; Patel, I.; Jiang, L. Effect of Methane in Global Combustion Characteristics of Glycerol and Methanol Blend by Using a Novel Swirl Burst Injector. In Proceedings of the 2024 AIAA SciTech Forum and Exposition, Orlando, FL, USA, 8–12 January 2024.
9. He, Q.; McNutt, J.; Yang, J. Utilization of the Residual Glycerol from Biodiesel Production for Renewable Energy Generation. *Renew. Sustain. Energy Rev.* **2017**, *71*, 63–76. https://doi.org/10.1016/j.rser.2016.12.110.
10. Zhang, J.; Wang, Y.; Muldoon, V.L.; Deng, S. Crude Glycerol and Glycerol as Fuels and Fuel Additives in Combustion Applications. *Renew. Sustain. Energy Rev.* **2022**, *159*, 112206. https://doi.org/10.1016/j.rser.2022.112206.
11. Chilakamarry, C.R.; Mimi Sakinah, A.M.; Zularisam, A.W.; Pandey, A.; Vo, D.-V.N. Technological Perspectives for Utilisation of Waste Glycerol for the Production of Biofuels: A Review. *Environ. Technol. Innov.* **2021**, *24*, 101902. https://doi.org/10.1016/j.eti.2021.101902.
12. Agwu, O.; Valera-Medina, A.; Katrašnik, T.; Seljak, T. Flame Characteristics of Glycerol/Methanol Blends in a Swirl-Stabilised Gas Turbine Burner. *Fuel* **2021**, *290*, 119968. https://doi.org/10.1016/j.fuel.2020.119968.

13. Deka, T.J.; Osman, A.I.; Baruah, D.C.; Rooney, D.W. Methanol Fuel Production, Utilization, and Techno-Economy: A Review. *Environ. Chem. Lett.* **2022**, *20*, 3525–3554. https://doi.org/10.1007/s10311-022-01485-y.
14. Jiang, L.; Hall, T.; Williams, D.; Swinney, R. Global Combustion Characteristics of Glycerol and Methanol Blends Using a Novel Fuel-Flexible Injector. In Proceedings of the 2023 AIAA SCITECH Forum, Online, National Harbor, MD, USA, 23–27 January 2023.
15. Lefebvre, A.H. Airblast Atomization. *Prog. Energy Combust. Sci.* **1980**, *6*, 233–261. https://doi.org/10.1016/0360-1285(80)90017-9.
16. Simmons, B.M.; Agrawal, A.K. Spray Characteristics of a Flow-Blurring Atomizer. *At. Sprays* **2010**, *20*, 821–835. https://doi.org/10.1615/AtomizSpr.v20.i9.60.
17. Akinyemi, O.S.; Jiang, L. Development and Combustion Characterization of a Novel Twin-Fluid Fuel Injector in a Swirl-Stabilized Gas Turbine Burner Operating on Straight Vegetable Oil. *Exp. Therm. Fluid Sci.* **2019**, *102*, 279–290. https://doi.org/10.1016/j.expthermflusci.2018.11.014.
18. Institute of Mechanics and Thermodynamics, Chemnitz University of Technology, Chemnitz, Germany; Roudini, M.; Wozniak, G. Investigation of the Secondary Atomization in Prefilming Air-Blast Atomizers. *IJCEA* **2019**, *10*, 138–143. https://doi.org/10.18178/ijcea.2019.10.5.757.
19. Guildenbecher, D.R.; López-Rivera, C.; Sojka, P.E. Secondary Atomization. *Exp. Fluids* **2009**, *46*, 371–402. https://doi.org/10.1007/s00348-008-0593-2.
20. Bhayaraju, U.; Hassa, C. Planar Liquid Sheet Breakup of Prefilming and Nonprefilming Atomizers at Elevated Pressures. *At. Sprays* **2009**, *19*, 1147–1169. https://doi.org/10.1615/AtomizSpr.v19.i12.50.
21. Simmons, B.M.; Panchasara, H.V.; Agrawal, A.K. A Comparison of Air-Blast and Flow-Blurring Injectors Using Phase Doppler Particle Analyzer Technique. In Proceedings of the ASME Turbo Expo, Orlando, FL, USA, 8–12 June 2009; pp. 981–992.
22. Qavi, I.; Jiang, L.; Akinyemi, O.S. Near-Field Spray Characterization of a High-Viscosity Alternative Jet Fuel Blend C-3 Using a Flow Blurring Injector. *Fuel* **2021**, *293*, 120350. https://doi.org/10.1016/j.fuel.2021.120350.
23. Hendershott, T.H.; Stouffer, S.; Monfort, J.R.; Diemer, J.; Busby, K.; Corporan, E.; Wrzesinski, P.; Caswell, A.W. Ignition of Conventional and Alternative Fuel at Low Temperatures in a Single-Cup Swirl-Stabilized Combustor. In Proceedings of the AIAA Aerospace Sciences Meeting, Kissimmee, FL, USA, 8–12 January 2018.
24. Gañán-Calvo, A.M. Enhanced Liquid Atomization: From Flow-Focusing to Flow-Blurring. *Appl. Phys. Lett.* **2005**, *86*, 214101. https://doi.org/10.1063/1.1931057.
25. Panchasara, H.V.; Sequera, D.E.; Schreiber, W.C.; Agrawal, A.K. Emissions Reductions in Diesel and Kerosene Flames Using a Novel Fuel Injector. *J. Propuls. Power* **2009**, *25*, 984–987. https://doi.org/10.2514/1.37165.
26. Jiang, L.; Agrawal, A.K. Spray Features in the near Field of a Flow-Blurring Injector Investigated by High-Speed Visualization and Time-Resolved PIV. *Exp. Fluids* **2015**, *56*, 103. https://doi.org/10.1007/s00348-015-1973-z.
27. Simmons, B.M.; Agrawal, A.K. Drop Size and Velocity Measurements in Bio-Oil Sprays Produced by the Flow-Blurring Injector. In Proceedings of the ASME Turbo Expo, ASMEDC, Vancouver, BC, Canada, 6–10 June 2011; pp. 701–710.
28. Panchasara, H.V.; Simmons, B.M.; Agrawal, A.K.; Spear, S.K.; Daly, D.T. Combustion Performance of Biodiesel and Diesel-Vegetable Oil Blends in a Simulated Gas Turbine Burner. In Proceedings of the ASME Turbo Expo, Berlin, Germany, 9–13 June 2008.
29. Qavi, I.; Jiang, L. Optical Characterization of Near-Field Sprays for Various Alternative and Conventional Jet Fuels Using a Flow-Blurring Injector. *Flow Turbul. Combust.* **2022**, *108*, 599–624. https://doi.org/10.1007/s10494-021-00276-9.
30. Jiang, L.; Agrawal, A.K. Investigation of Glycerol Atomization in the Near-Field of a Flow-Blurring Injector Using Time-Resolved PIV and High-Speed Visualization. *Flow Turbul. Combust.* **2015**, *94*, 323–338. https://doi.org/10.1007/s10494-014-9572-2.
31. Simmons, B.M.; Agrawal, A.K. Flow Blurring Atomization for Low-Emission Combustion of Liquid Biofuels. *Combust. Sci. Technol.* **2012**, *184*, 660–675. https://doi.org/10.1080/00102202.2012.660222.
32. Sharma, S.; Biswal, Y.; Drabo, M.; Kolhe, P.S. Effect of Flow Field on Glycerol Combustion in a Swirl Stabilized Combustor Employing Flow Blurring Atomizer. In Proceedings of the 9th Thermal and Fluids Engineering Conference (TFEC), Corvallis, OR, USA, 21–24 April 2024.
33. Biswal, Y.; Sharma, S.; Warghat, K.V.; Nayak, G.M.; Drabo, M.; Kolhe, P.S. Characterization of Flame Morphology for Twin Fluid Atomizer-Based Swirl Stabilized Combustor. In Proceedings of the AIAA SCITECH Forum, Orlando, FL, USA, 8–12 January 2024.
34. Jiang, L.; Akinyemi, O.S.; Danh, V. Investigation of Combustion Characteristics of Straight Vegetable Oil for a Novel Twin-Fluid Fuel Injector: Heterogeneous Combustion. In Proceedings of the 10th U. S. National Combustion Meeting Organized by the Eastern States Section of the Combustion Institute, College Park, MD, USA, 23–26 April 2017.
35. Danh, V.; Akinyemi, O.S.; Taylor, C.E.; Frank, J.T.; Jiang, L. Effect of Injector Swirl Number on Near-Field Spray Characteristics of a Novel Twin-Fluid Injector. *Exp. Fluids* **2019**, *60*, 80. https://doi.org/10.1007/s00348-019-2721-6.
36. Akinyemi, O.S.; Jiang, L.; Hernandez, R.; McIntyre, C.; Holmes, W. Combustion of Straight Algae Oil in a Swirl-Stabilized Burner Using a Novel Twin-Fluid Injector. *Fuel* **2019**, *241*, 176–187. https://doi.org/10.1016/j.fuel.2018.12.006.
37. Akinyemi, O.S.; Qavi, I.; Taylor, C.E.; Jiang, L. Effect of the Air-to-Liquid Mass Ratio on the Internal Flow and near-Field Spray Characteristics of a Two-Phase Swirl Burst Injector. *J. Aerosol Sci.* **2023**, *167*, 106092. https://doi.org/10.1016/j.jaerosci.2022.106092.
38. Breerwood, J.; Jiang, L.; Ahmed, M.S. Near-Field Spray Characteristics and Steadiness of a Novel Twin-Fluid Injector with Enhanced Primary Atomization. *J. Aerosol Sci.* **2024**, *180*, 106402. https://doi.org/10.1016/j.jaerosci.2024.106402.

39. Ahmed, M.S.; Cary, J.; Fezzaa, K.; Clark, S.; McClain, S.T.; Jiang, L. Effect of Internal and External Swirls on Near-Field Spray Characteristics of Swirl Burst Injectors Using High-Speed X-Ray Imaging. In Proceedings of the AIAA SCITECH Forum, Orlando, FL, USA, 8–12 January 2024.
40. Danh, V.; Jiang, L.; Akinyemi, O.S. Investigation of Water Spray Characteristics in the near Field of a Novel Swirl Burst Injector. *Exp. Therm. Fluid Sci.* **2019**, *102*, 376–386. https://doi.org/10.1016/j.expthermflusci.2018.12.014.
41. Murugan, R.; Kolhe, P.S.; Sahu, K.C. A Combined Experimental and Computational Study of Flow-Blurring Atomization in a Twin-Fluid Atomizer. *Eur. J. Mech.—B/Fluids* **2020**, *84*, 528–541. https://doi.org/10.1016/j.euromechflu.2020.07.008.
42. Ling, Y.; Jiang, L. A Detailed Numerical Investigation of Two-Phase Flows Inside a Planar Flow-Blurring Atomizer. *At. Sprays* **2024**, *34*, 1–20. https://doi.org/10.1615/AtomizSpr.2023049089.
43. Nasim, M.N.; Qavi, I.; Jiang, L. Effect of Varying Internal Geometry on the Near-Field Spray Characteristics of a Swirl Burst Injector. *Flow Turbul. Combust.* **2023**, *111*, 641–674. https://doi.org/10.1007/s10494-023-00441-2.
44. Cravero, C.; Marogna, N.; Marsano, D. A Numerical Study of Correlation Between Recirculation Length and Shedding Frequency in Vortex Shedding Phenomena. *WSEAS Trans. Fluid Mech.* **2021**, *16*, 48–62. https://doi.org/10.37394/232013.2021.16.6.
45. Shi, L.; Yang, G.; Yao, S. Large Eddy Simulation of Flow Past a Square Cylinder with Rounded Leading Corners: A Comparison of 2D and 3D Approaches. *J. Mech. Sci. Technol.* **2018**, *32*, 2671–2680. https://doi.org/10.1007/s12206-018-0524-y.
46. Papagiannakis, R.G.; Hountalas, D.T. Combustion and Exhaust Emission Characteristics of a Dual Fuel Compression Ignition Engine Operated with Pilot Diesel Fuel and Natural Gas. *Energy Convers. Manag.* **2004**, *45*, 2971–2987. https://doi.org/10.1016/j.enconman.2004.01.013.
47. Guido, C.; Alfè, M.; Gargiulo, V.; Napolitano, P.; Beatrice, C.; Del Giacomo, N. Chemical/Physical Features of Particles Emitted from a Modern Automotive Dual-Fuel Methane–Diesel Engine. *Energy Fuels* **2018**, *32*, 10154–10162. https://doi.org/10.1021/acs.energyfuels.8b01011.
48. Malaquias, A.C.T.; da Costa, R.B.R.; Netto, N.A.D.; Coronado, C.J.R.; Baêta, J.G.C. A Review of Dual-Fuel Combustion Mode in Spark-Ignition Engines. *J. Braz. Soc. Mech. Sci. Eng.* **2021**, *43*, 426. https://doi.org/10.1007/s40430-021-03156-5.
49. Di Iorio, S.; Sementa, P.; Vaglieco, B.M. Experimental Investigation of a Methane-Gasoline Dual-Fuel Combustion in a Small Displacement Optical Engine. In Proceedings of the 11th International Conference on Engines & Vehicles, Capri, Napoli, Italy, 15–19 September 2013.
50. Altaher, M.A.; Li, H.; Andrews, G.E. Co-Firing of Kerosene and Biodiesel With Natural Gas in a Low NOx Radial Swirl Combustor. In *Volume 1: Aircraft Engine; Ceramics; Coal, Biomass and Alternative Fuels; Controls, Diagnostics and Instrumentation, Proceedings of the ASME Turbo Expo 2012, Copenhagen, Denmark, 11–15 June 2012*; American Society of Mechanical Engineers: New York, NY, USA, 2012; pp. 557–567.
51. Chong, C.T.; Chiong, M.-C.; Ng, J.-H.; Tran, M.-V.; Valera-Medina, A.; Józsa, V.; Tian, B. Dual-Fuel Operation of Biodiesel and Natural Gas in a Model Gas Turbine Combustor. *Energy Fuels* **2020**, *34*, 3788–3796. https://doi.org/10.1021/acs.energyfuels.9b04371.
52. Hall, T.; Williams, D.; Islam, S.M.R.; Patel, I.; Chakmakjian, C.; Jiang, L. Clean Co-Combustion of Glycerol and Methanol Blends Using a Novel Fuel-Flexible Injector. *Fuel* **2024**, *371*, 132125. https://doi.org/10.1016/j.fuel.2024.132125.
53. Lilley, D.G. Swirl Flows in Combustion: A Review. *AIAA J.* **1977**, *15*, 1063–1078. https://doi.org/10.2514/3.60756.
54. Khandelwal, B.; Lili, D.; Sethi, V. Design and Study on Performance of Axial Swirler for Annular Combustor by Changing Different Design Parameters. *J. Energy Inst.* **2014**, *87*, 372–382. https://doi.org/10.1016/j.joei.2014.03.022.
55. Li, Z.; Wang, Y.; Geng, H.; Zhen, X.; Liu, M.; Xu, S.; Li, C. Effects of Diesel and Methanol Injection Timing on Combustion, Performance, and Emissions of a Diesel Engine Fueled with Directly Injected Methanol and Pilot Diesel. *Appl. Therm. Eng.* **2019**, *163*, 114234. https://doi.org/10.1016/j.applthermaleng.2019.114234.
56. Wang, Y.; Wang, H.; Meng, X.; Tian, J.; Wang, Y.; Long, W.; Li, S. Combustion Characteristics of High Pressure Direct-Injected Methanol Ignited by Diesel in a Constant Volume Combustion Chamber. *Fuel* **2019**, *254*, 115598. https://doi.org/10.1016/j.fuel.2019.06.006.
57. Duraisamy, G.; Rangasamy, M.; Govindan, N. A Comparative Study on Methanol/Diesel and Methanol/PODE Dual Fuel RCCI Combustion in an Automotive Diesel Engine. *Renew. Energy* **2020**, *145*, 542–556. https://doi.org/10.1016/j.renene.2019.06.044.
58. Seljak, T.; Katrašnik, T. Emission Reduction through Highly Oxygenated Viscous Biofuels: Use of Glycerol in a Micro Gas Turbine. *Energy* **2019**, *169*, 1000–1011. https://doi.org/10.1016/j.energy.2018.12.095.
59. Ferreira, A.G.M.; Egas, A.P.V.; Fonseca, I.M.A.; Costa, A.C.; Abreu, D.C.; Lobo, L.Q. The Viscosity of Glycerol. *J. Chem. Thermodyn.* **2017**, *113*, 162–182. https://doi.org/10.1016/j.jct.2017.05.042.
60. Exclusively Canon, Essential for EOS Users. Available online: https://www.eos-magazine.com/articles/eospedia/what-is/iso.html (accessed on 12 October 2024).
61. Turns, S.R. *An Introduction to Combustion: Concepts and Applications*, 3rd ed.; McGraw-Hill: New York, NY, USA, 2012; ISBN 978-0-07-338019-3.
62. Li, S.; Qian, W.; Liu, H.; Liu, G.; Zhu, M. Autoignition and Flame Lift-off Behavior of a Fuel Jet Mixing with Turbulent Hot Air Coflow. *Proc. Combust. Inst.* **2021**, *38*, 6385–6392. https://doi.org/10.1016/j.proci.2020.06.230.
63. Kalghatgi, T.G. Lift-off Heights and Visible Lengths of Vertical Turbulent Jet Diffusion Flames in Still Air. *Combust. Sci. Technol.* **1984**, *41*, 17–29. https://doi.org/10.1080/00102208408923819.
64. Çengel, Y.A.; Ghajar, A.J. *Heat and Mass Transfer: Fundamentals & Applications*, 5th ed.; McGraw Hill Education: New York, NY, USA, 2015; ISBN 978-0-07-339818-1.

65. Bradley, D.; Entwistle, A.G. Determination of the Emissivity, for Total Radiation, of Small Diameter Platinum-10% Rhodium Wires in the Temperature Range 600-1450 C. *Br. J. Appl. Phys.* **1961**, *12*, 708–711. https://doi.org/10.1088/0508-3443/12/12/328.
66. Hindasageri, V.; Vedula, R.P.; Prabhu, S.V. Thermocouple Error Correction for Measuring the Flame Temperature with Determination of Emissivity and Heat Transfer Coefficient. *Rev. Sci. Instrum.* **2013**, *84*, 024902. https://doi.org/10.1063/1.4790471.
67. Yan, W.; Panahi, A.; Levendis, Y.A. Spectral Emissivity and Temperature of Heated Surfaces Based on Spectrometry and Digital Thermal Imaging—Validation with Thermocouple Temperature Measurements. *Exp. Therm. Fluid Sci.* **2020**, *112*, 110017. https://doi.org/10.1016/j.expthermflusci.2019.110017.
68. Petrov, V.; Reznik, V. Measurement of the Emissivity of Quartz Glass. *High Temp.-High Press.* **1972**, *4*, 687–693.
69. Çengel, Y.A. *Heat Transfer: A Practical Approach*, 2nd ed.; McGraw-Hill Companies: New York, NY, USA, 2002; ISBN 0-07-245893-3.
70. Shannon, K.S.; Butler, B.W. A Review of Error Associated with Thermocouple Temperature Measurement in Fire Environments. In Proceedings of the 2nd International Wildland Fire Ecology and Fire Management Congress and the 5th Symposium on Fire and Forest Meteorology, Orlando, FL, USA, 16–20 November 2003.

Disclaimer/Publisher's Note: The statements, opinions and data contained in all publications are solely those of the individual author(s) and contributor(s) and not of MDPI and/or the editor(s). MDPI and/or the editor(s) disclaim responsibility for any injury to people or property resulting from any ideas, methods, instructions or products referred to in the content.

Clean Dual-Waste Fuel Combustion of Glycerol-Methanol Blend with Simulated Landfill Gas by Utilizing a Novel Fuel-Flexible Injector

Md Fahad Hossain Mishu[1], Opeyemi Samuel Eso[2], Yang Li[3], Alex Yokochi[4], Lulin Jiang[5*]

[1,2,4,5]*Department of Mechanical Engineering, Baylor University, Waco, TX 76798, USA*

[3] *Department of Environmental Science, Baylor University, Waco, TX 76798, USA*

This study investigates the co-combustion characteristics of dual-waste fuel composition i.e., liquid and gaseous waste fuel, glycerol/methanol (G/M) blend with varying amounts of simulated landfill gas (LFG), to mitigate the carbon footprint and greenhouse gas effect using a novel fuel-flexible injector. Glycerol, the largest oxygenated byproduct of biodiesel production, with moderate energy density makes clean and efficient combustion very challenging due to its high viscosity. Extracting pure glycerol from crude glycerol, which contains a significant amount of methanol, is expensive. A recently developed Swirl Burst (SB) injector employs a two-phase atomization mechanism, generating fine sprays immediately even for highly viscous G/M blends without preheating, rather than a typical jet core/film by a conventional air-blast atomizer. Thus, the SB atomization has achieved ultra-clean combustion for G/M 60/40 ratios by heat release rate (HRR), effectively representing crude glycerol. On the other hand, LFG is a natural byproduct of the decomposition of organic material in landfills, with major component of methane, rendering it as a biofuel candidate. Hence, this study explores the co-combustion performance of G/M 60/40 with simulated LFG (50%/50% CH_4/CO_2 by volume) in a 7-kW lab-scale swirl-stabilized gas turbine combustor. The effects of varying simulated LFG HRR (0-7 KW) on combustion characteristics of G/M 60/40 flame by using a SB injector are investigated at a constant atomizing gas to liquid mass ratio (ALR) of 2.5 and an equivalence ratio of 0.75. The global flame characteristics investigated include the visual flame images, concentrations of carbon monoxide (CO) and nitrogen oxide (NOx), and temperature of the combustion gas product and the combustor outer wall. The clean and efficient co-combustion of dual waste fuel - G/M with LFG, achieved without fuel preheating, highlights the potential for simultaneously or independently utilizing liquid and gaseous waste fuels enabled by the fuel-flexible injector. This approach not only promotes fuel flexibility and biofuel cost-effectiveness but also reduces greenhouse gas emissions by utilizing LFG, a potent greenhouse gas, for clean combustion.

[1] Graduate Assistant, Department of Mechanical Engineering, Mdfahadhossain_Mish1@baylor.edu
[2] Graduate Assistant, Department of Mechanical Engineering, Opeyemi_Eso1@baylor.edu
[3] Assistant Professor, Department of Environmental Science, Yang_Li3@baylor.edu
[4] Professor, Department of Mechanical Engineering, Alex_Yokochi@baylor.edu
[5] Assistant Professor, Department of Mechanical Engineering, AIAA Senior member, Lulin_Jiang@baylor.edu
* Corresponding Author Email: Lulin_Jiang@baylor.edu

Nomenclature

AA	=	atomizing air or gas
AB	=	air blast
ALR	=	air or gas to liquid mass ratio
AO	=	algae oil
CH_4	=	methane
CO	=	carbon monoxide
D	=	center liquid fuel channel diameter
FB	=	flow blurring
G/M	=	glycerol/methanol
LPM	=	lean pre-mixed combustion
LFG	=	Landfill Gas
H	=	gap between the center liquid fuel channel tip and injector exit
HRR	=	heat release rate
MFC	=	Mass Flow Controller
MLPM	=	milliliter per minute
NG	=	natural gas
NOx	=	nitrogen oxide (included NO and NO_2)
PA	=	primary air or gas
SAA	=	swirling atomizing air
SB	=	swirl burst
SLPM	=	standard liter per minute
SMD	=	Sauter mean diameter
SN	=	swirl number
VO	=	vegetable oil
d_h	=	hub diameter
d_t	=	tip diameter
α	=	exit vane angle

I. Introduction

Alternative and sustainable energy sources, particularly biodiesel, are becoming more and more vital as fossil fuel reserves continue to be depleted. Transesterification, which uses oils and fats sourced from plants or animals, is the primary process to produce biodiesel [1]. Biodiesel, an attractive sustainable drop-in fuel, can replace diesel in current combustion systems due to its similarities to conventional diesel [2,3]. The production of biodiesel in the European Union (EU) increased significantly from 6.129 million tons in 2007 to 14.11 million tons in 2018 [4,5]. Crude glycerol, which makes up around 10% of the entire weight of biodiesel, is often treated as waste byproduct of biodiesel production, due to the high cost of purification [6]. Glycerol is a viable biofuel option due to its significant oxygen content and moderate heat release, even though it has a low calorific value, high viscosity, and high surface tension [7]. Crude glycerol also contains methanol [8–10], which has high octane value, low emission profile, and can be sourced from biomass [11]. Methanol lowers glycerol's viscosity but not sufficiently for conventional AB injector that has low viscosity tolerance [7]. Efficient combustion of glycerol-methanol blends (G/M) may reduce purification costs and improve fuel utilization. However, with a nearly neutral balance of CO_2 emissions, biogas is the most affordable renewable energy source. Landfill gas (LFG), a form of biogas that may find application in industrial furnaces, gas turbines, and internal combustion engines [12]. LFG produced from the anaerobic decomposition of municipal solid waste, primarily consists of about 50-55% methane (CH_4), 40-45% carbon dioxide (CO_2) along with other trace gases [13]. Because of its potential for pollution, flammability, and greenhouse gas emissions, LFG poses significant environmental risks [12–14]. Traditionally, landfill gas is managed by flaring, effectively wasting its substantial energy potential [13]. Although LFG can provide both environmental and economic benefits while used in engines and gas turbines, its high CO_2 content challenges flame stability and combustion [14]. Combining LFG with G/M blends could support sustainable and cleaner energy applications.

Nowadays, there is a global push to prevent global warming by enforcing stringent emissions regulations. Efficient and clean combustion requires thorough fuel air mixing. As to liquid fuels, effective atomization and generation of fine sprays are required to enable quick fuel evaporation and thus homogenous fuel and air mixing, achieving clean and efficient combustion. Rapid evaporation and uniform fuel-air mixing are achieved by fine sprays, which greatly lower emissions of pollutants such soot, carbon monoxide (CO), and nitrogen oxides (NO_x) [7,15]. Commonly seen

in combustion systems, air-blast (AB) atomizers inject fuel at relatively low velocities and atomizing air at high velocities, first creating a liquid core at the injector exit that later break into ligaments and droplets due to aerodynamic shear layer instabilities [16–18]. However, high-viscosity fuels like glycerol with significantly suppressed shear layer instabilities while interacting with surrounding air due to its high viscosity and surface tension, resulting in incomplete atomization, requiring preheating to decrease viscosity, yet burn incompletely with high pollutant emissions, leading to inefficiencies in operation and combustion [19–21].

When compared to conventional atomizers, the Flow-Blurring (FB) atomizer, which was first created by Ganán-Calvo, offers higher atomization capabilities and produces droplets with up to fifty times the surface area of AB atomizers [19]. It generates fine droplets, rather than a typical jet core of AB atomization, immediately at the injector exit [20]. This is because of the special design of FB atomizers, in which atomizing air (AA) circulates across an annular zone while liquid fuel flows through a central channel. The critical geometric parameters of the FB concept are that the center liquid channel inner diameter (D) must be equal to the exit orifice diameter, and the distance between the liquid flow tube exit and injector exit (H) must be equal to or less than 0.25 times of the center liquid channel diameter [19]. A fraction of AA enters the liquid channel just upstream, creating a turbulent two-phase flow and producing bubbles that burst when they leave the atomizer, generating tiny droplets due to a significant pressure drop [18]. This primary atomization is followed by a secondary atomization phase, where high-velocity AA further breaks droplets and ligaments. Jiang et al. (2015) observed that thin ligaments accompanied by many fine droplets are formed at the injector immediate exit for high viscosity glycerol (~>200 times more viscous than diesel) and subsequently go through secondary atomization [20]. Regardless of viscosity, FB can generate considerably finer sprays with a wider range of capabilities [7,21] compared to AB injectors. For example, it can produce droplets with a smaller diameter and more uniform size (for water SMD 5-25 for FB and 5-45 for AB) [22], as well as a shorter atomization complete length (for FB ~2.67D and AB > 50D from the injector exit) [23]. Compared to traditional AB injectors, the FB atomizer produces fine, steady sprays with much smaller droplet sizes and does not require fuel preheating, demonstrating exceptional atomization performance even with high-viscosity fuels [24].

The Swirl Burst (SB) injector, recently developed by our group by integrating swirling atomizing air (SAA) with the FB concept, significantly enhances secondary atomization efficiency and thus fuel evaporation, as well as fuel-air mixing [18,25–27]. Strong aerodynamic shear interactions are produced near the injector exit by the swirling motion of the atomizing air, which quickly breaks down ligaments and the large droplets produced during primary atomization into finer droplets [18,25]. In comparison to the FB injector, the SB injector's atomization length is likewise shorter - nearly half for a variety of high viscosity fluids, such as biodiesel (similar viscosity to diesel), straight vegetable oil (VO), and straight algae oil (AO) (~15-16 times more viscous than diesel) [25,26] - resulting in lean pre-mixed combustion (LPM) and a short flame length. Additionally, SB has greater combustion efficiency than FB. For VO, combustion completeness was 98% when using the SB injector and 95% while using the FB injector [18]. The SB injector's fine atomization capabilities were demonstrated by its extremely low CO (6–14 ppm) and NO_x (0–13 ppm) emissions even for straight AO combustion, which is nearly 16 times more viscous fuel than diesel [25].

In our previous study, SB injector achieved ultra-clean combustion of G/M blends in the HRR ratios of 50/50, 60/40, and 70/30, especially with almost complete combustion efficiencies (~99.5%) of 50/50 G/M at ALR of 1.5 at a constant HRR of 7kW [24]. Our SB injector also achieved ultra-clean combustion with CO concentration ≤ 2 ppm and ~0 ppm NOx concentration without preheating the viscous G/M 60/40 ratio (by HRR) blend, representing typical composition of crude glycerol [6], co-combusting with methane [28]. Near-zero emissions were achieved at ALRs of 2.0, 2.5, and 3.0, with ALR 2.5 selected as optimal due to its lower air input requirement than ALR 3 [28]. In this study, we extend that work by investigating the effect of simulated LFG which is made up of 50/50 CH_4/CO_2 by volume on the combustion of the 60/40 ratio of G/M by HRR using the SB injector. Without pre-heating, co-combustion behavior is evaluated via flame imaging, CO and NO_x concentrations in gas products, and temperature profiles of the exhaust and combustor wall. The current study also signifies the characteristics of dual-waste fuel combustion.

II. Research Objective

The objective of our current study is to analyze the effects of varying amounts of simulated LFG flowing through the combustion swirler on the combustion performance of dual waste fuel composition i.e., G/M (liquid) and LFG (gaseous) fuels utilizing the SB injector while maintaining a constant ALR of 2.5 for the liquid portion. Dual-waste fuel combustion is investigated with an LFG quantity ranging from 0 to 7 kW, without fuel nor air preheating. G/M 60/40 by HRR blend was used to represent waste crude glycerol. The study is conducted using simulated LFG with the CH_4 and CO_2 volumetric ratio of 50/50 in the fuel feed, a typical range under realistic conditions. The equivalence ratio and total HRR are kept constant at 0.75 and 7 kW respectively. The effect of the composition of the liquid and

gaseous fuels on dual waste fuel combustion are evaluated via flame images, concentration of CO, and NOx in the exhaust gas, and exhaust gas and combustor wall temperature.

III. Experimental Setup

The working principle and concept of SB are illustrated in Fig 1. To improve spray quality and combustion performance, the Swirl Burst (SB) injector utilizes a two-stage atomization process that combines swirling atomizing air (AA) with FB concept [18,25,27,29,30]. Under certain geometric conditions mentioned in introduction [19], atomizing air first enters an annular channel around the central liquid fuel tube and partially bifurcates, allowing a small amount of air to return to the liquid tube tip. In the liquid tube tip, this AA backflow quickly produces a bubbly two-phase zone. A quick drop in pressure causes the bubbles to expand and burst as they exit the injector and generate fine droplets, which is defined as the primary atomization. The second stage improves shear interactions between air and liquid by allowing the residual atomizing air to escape through specially designed swirling grooves in the chamfered injector orifice. The secondary breakup of any ligaments and bigger droplets, via shear layer instabilities between the two phases, is greatly facilitated by this swirling action, which further reduces droplet size [27,29,30].

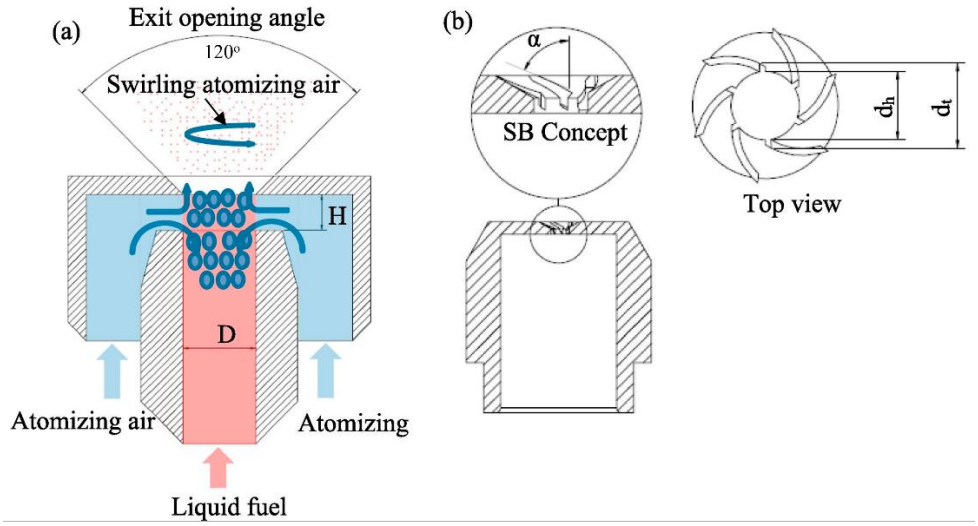

Fig. 1 (a) Working principle of SB injector, (b) SB concept [18,25,29]

The injector swirl number (ISN), representing swirl intensity, is defined by the three parameters that define the geometry of these swirling grooves: hub diameter (d_h), tip diameter (d_t), and swirl vane angle (α) [27,29–31]. It is a non-dimensional number representing the axial flux of swirl momentum divided by the axial flux of axial momentum times equivalent nozzle radius and determined by Equation (1) [31]. To ensure fine atomization and effective combustion, the current study uses an SB injector configuration with an internal liquid tube diameter (D) of 1.5 mm, a gap (H) of 0.375 mm, and an injector swirl number (ISN) of 2.4 [24,31].

$$ISN = \frac{2}{3} \times \frac{1-(d_h/d_t)^3}{1-(d_h/d_t)^2} \times tan\,\alpha \quad (1)$$

As shown in Fig. 2, a lab-scale 7kW swirl stabilized gas turbine combustor was employed for our current study. The compositions of G/M ratio and CH_4/CO_2 in LFG are kept constant at 60/40 by HRR and 50/50 by volume respectively. The liquid HRR composition ratio and gaseous fuel volume ratio are decided to represent the waste crude glycerol [8–10,28] and LFG [13] at their general realistic condition. A comparison of the related properties of pure glycerol and methanol with their blend and methane is provided in Table 1. The effect of varying amounts of LFG ranging from 0 to 7 kW on the combustion performance of non-preheated 60/40 (by HRR) G/M blend is studied. Then the amount of HRR contributed by the liquid-gaseous waste fuel varies throughout the experiment. The compressed air is separated into primary air (PA) and atomizing air (AA) after passing through water traps and filters to ensure a dry, clean air supply to the combustor. The Alicat MC-series Mass Flow Controller (MFC) regulates the PA and AA supply with an uncertainty of 0.8% of the reading and ± 0.2% of the full range. The MFC model numbers for PA and AA are MCP-250SLPM-D and MCP-100SLPM-D, respectively, with a range of 0-250 and 0-100 SLPM respectively. The combustor was preheated with methane gas before the experiment's start. Methane flowed through a valve from

the methane tank, and the MFC, model number MCP-50SLPM-D, controlled the flow between 0 and 50 SLPM with an uncertainty of 0.8% of the reading and ± 0.2% of the full range. After methane and PA are mixed, the mixture is sent to the quartz combustor via a 45º curved vane swirler with swirl number (SN) of 0.77. The combustor's cylindrical quartz tube is 45 cm in length and 7.62 cm in diameter. A peristaltic pump, the Cole-Parmer Masterflex L/S (EW-77921-75), with a range of 0-88 mLPM and an uncertainty of ± 0.1% of the reading, was used to pump the liquid fuel to the injector. Between the injector and the fuel pump, a pulsation damper was employed. The ISN is 2.4.

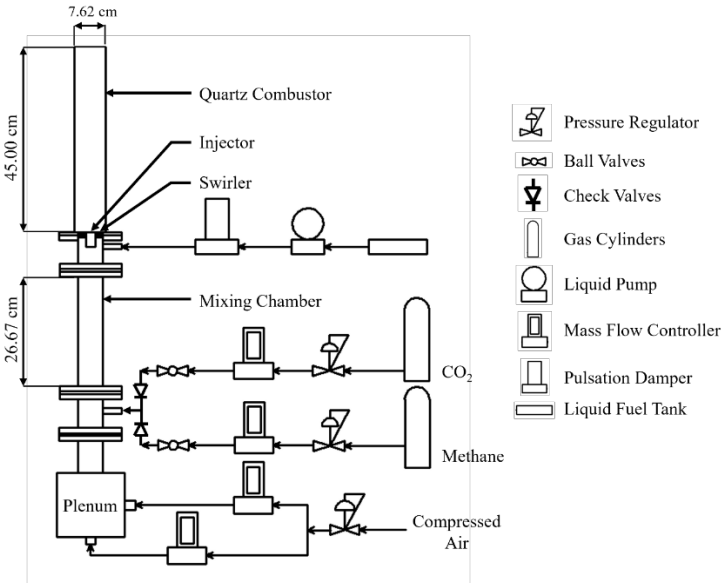

Fig. 2 Schematic diagram of the experimental set-up

The ENERAC (700 series) emission gas analyzer was used to detect the concentrations of CO and NOx in the exhaust gas to examine global combustion characteristics. For NOx detection, the resolution was 0.1 ppm, the uncertainty was less than ±1% of the reading, and the range was 0-150 ppm and 0-1500 ppm (dual mode). For CO detection, the precision was 0.1 ppm, the uncertainty was ±1-2% of the reading, and the range was 0-150 ppm and 0-2000 ppm (dual mode). The lower range mode was used for both CO and NOx detection as the emission was near zero during the experiments. The exit gas temperature was measured at 1 inch upstream of the combustor exit in the radial direction of the quartz combustor tube using a K-type thermocouple with a range of 0-1100ºC and an uncertainty of 2ºC. An LS-84D thermometer with a J-type thermocouple (Omega HPS-HT-J-12-SMP-M) with a range of 0-760ºC and an uncertainty of (±0.5% of reading + 0.7 ºC) was used to monitor the surface temperature of the quartz combustor tube.

Table 1 Selected properties of the fuels used [10,29,32,33].

Property	Methane	Methanol	Glycerol	G/M of 60/40 Blend
Chemical Formula	CH_4	CH_4O	$C_3H_8O_3$	N/A
Lower heating value, LHV (MJ/kg)	48	19.90	15.80	17.22
Density at 25ºC (kg/m^3)	0.77	791	1260	1045.46
Kinematic Viscosity at 25ºC (mm^2/s)	17.07	0.59	965.8	2
Auto-ignition temperature (ºC)	650	464	370	N/A
Vaporization temperature (ºC)	- 156	64.70	290	N/A
Heat of vaporization (kJ/kg)	215-276	726.10	662.00	N/A
Stoichiometric air/fuel ratio (mol/mol)	17	7.14	16.66	10.92

IV. Results and Discussion

Flame images for the co-combustion of the dual waste fuel with varying composition of liquid (G/M)-gaseous (LFG) fuels at a constant 7 kW HRR are shown in Figure 3. The flame lift-off height gradually decreases as the LFG

HRR rises from 0 to 7 kW. The highest lift-off (~10 cm) is seen in the pure liquid waste fuel - G/M blend flame. When methane from LFG is introduced, the flame anchors closer to the swirler, lowering the lift-off height to about 5 cm at 4 kW of LFG. By 7 kW LFG, the flame finally anchors at the swirler outlet. At the same time, flame length reduces from about 14 cm (pure G/M) to around 5 cm (7 kW LFG), suggesting that the flame structures are more compact and radially broader. This transition reflects improved combustion reaction speed and dynamics driven by the high reactivity of methane, which enhances thermal feedback and promotes rapid vaporization of the G/M blend. Faster droplet vaporization leads to more uniform fuel-air mixing, enabling earlier ignition and shorter, and more stabilized flames.

However, carbon dioxide adversely affects combustion efficiency and significantly decreases the laminar burning speed of methane-air mixtures due to its high heat capacity and chemical effects [34]. Increased carbon dioxide concentration from Fig. 3(a) –(m) leads to increased flame thickness, thus the observed broader flames with higher LFG component, i.e. more CO_2, and reduced flame temperature [35,36]. While methane acts as combustion promoter, carbon dioxide acts as combustion moderator.

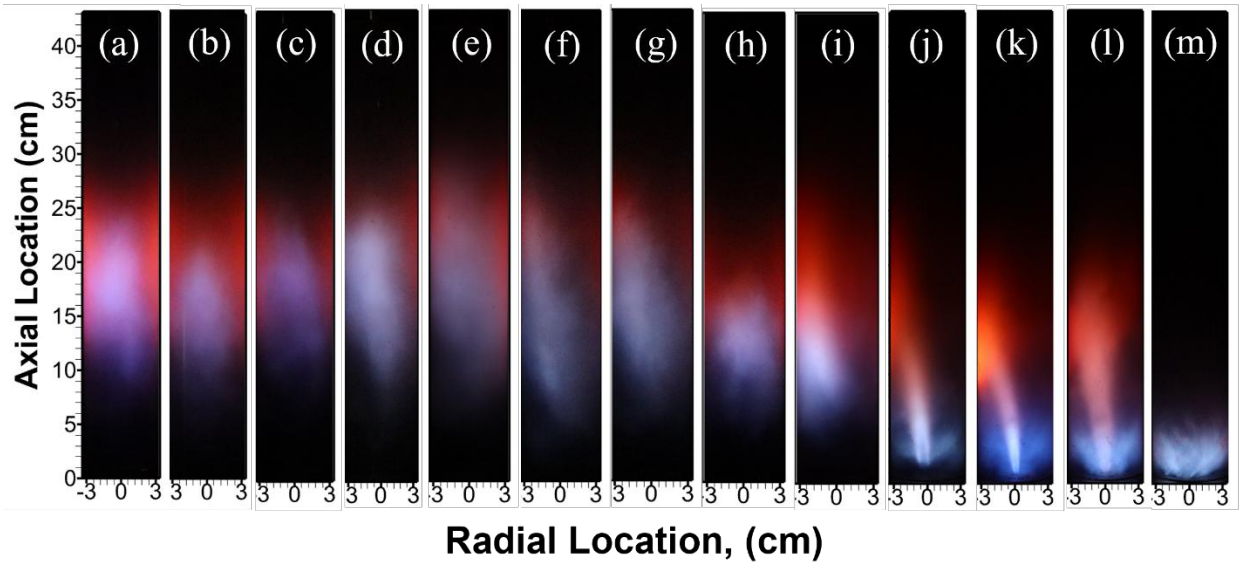

Fig. 3 Flame images for (a) pure-liquid G/M of 60/40, and dual waste fuel combustion of G/M 60/40-simulated LFG with quantity of (b) 1 kW, (c) 1.5 kW, (d) 2 kW, (e) 2.5 kW, (f) 3 kW, (g) 3.5 kW, (h) 4 kW, (i) 4.5 kW, (j) 5 kW, (k) 5.5 kW, (l) 6 kW, (m) 7 kW at a constant ER of 0.75, ALR of 2.5 and total HRR of 7 kW using SB injector.

The combined effect of methane and carbon dioxide on dual waste fuel co-combustion will be further evaluated by the temperature and emission profiles at the combustion exit in this study. The HRR of the swirl stabilized gas turbine combustor was also maintained at 7.0 kW with ALR 2.5 and the equivalence ratio 0.75.

V. Conclusion

The current research investigates the effect of simulated LFG on the global combustion characteristics of dual-waste fuel composed of 60/40 G/M blend by HRR (liquid), representing crude glycerol, and simulated LFG (gaseous fuel) by utilizing the fuel-flexible SB injector with ultra-fine atomization capability. Methane and carbon dioxide have completely opposite effects on combustion performance. Visual flame images have qualitatively illustrated in Fig. 3(a) – (m). Since emission regulations are becoming stringent all over the world, global combustion characteristics in terms of CO, NOx emissions will also be investigated for the different quantity of LFG in combustion of G/M blend. Efficiently and cleanly burning G/M will reduce the cost of glycerol extraction from crude glycerol biofuel, and waste crude glycerol along with the waste biogas LFG can also be utilized to generate power with the reduction of waste processing cost and environmental impact.

Acknowledgments

The current research is funded by the Startup fund of Baylor University and NSF CIVIC award No. 2228311 and No. 2322319 co-funded by US National Science Foundation and Department of Energy. We would also like to express our gratitude to Mr. Ashely Orr who helped manufacture the combustion system and Mr. Joseph Breerwood for helping set up the system.

References

[1] Leung, D. Y., Wu, X., and Leung, M. K. H., "A Review on Biodiesel Production Using Catalyzed Transesterification," *Applied energy*, Vol. 87, No. 4, 2010, pp. 1083–1095.

[2] Gutiérrez-Arnillas, E., Álvarez, M. S., Deive, F. J., Rodríguez, A., and Sanromán, M. Á., "New Horizons in the Enzymatic Production of Biodiesel Using Neoteric Solvents," *Renewable Energy*, Vol. 98, 2016, pp. 92–100.

[3] Pires, J. C., "COP21: The Algae Opportunity?," *Renewable and Sustainable Energy Reviews*, Vol. 79, 2017, pp. 867–877.

[4] Pasha, M. K., Dai, L., Liu, D., Guo, M., and Du, W., "An Overview to Process Design, Simulation and Sustainability Evaluation of Biodiesel Production," *Biotechnology for Biofuels*, Vol. 14, 2021, pp. 1–23.

[5] "UFOP. Report on Global Market Supply: 2019/2020," 2020.

[6] Quispe, C. A., Coronado, C. J., and Carvalho Jr, J. A., "Glycerol: Production, Consumption, Prices, Characterization and New Trends in Combustion," *Renewable and sustainable energy reviews*, Vol. 27, 2013, pp. 475–493.

[7] Jiang, L., and Agrawal, A. K., "Combustion of Straight Glycerol with/without Methane Using a Fuel-Flexible, Low-Emissions Burner," *Fuel*, Vol. 136, 2014, pp. 177–184.

[8] McNutt, J., and Yang, J., "Utilization of the Residual Glycerol from Biodiesel Production for Renewable Energy Generation," *Renewable and Sustainable Energy Reviews*, Vol. 71, 2017, pp. 63–76.

[9] Zhang, J., Wang, Y., Muldoon, V. L., and Deng, S., "Crude Glycerol and Glycerol as Fuels and Fuel Additives in Combustion Applications," *Renewable and Sustainable Energy Reviews*, Vol. 159, 2022, p. 112206.

[10] Agwu, O., Valera-Medina, A., Katrašnik, T., and Seljak, T., "Flame Characteristics of Glycerol/Methanol Blends in a Swirl-Stabilised Gas Turbine Burner," *Fuel*, Vol. 290, 2021, p. 119968. https://doi.org/10.1016/j.fuel.2020.119968

[11] Deka, T. J., Osman, A. I., Baruah, D. C., and Rooney, D. W., "Methanol Fuel Production, Utilization, and Techno-Economy: A Review," *Environmental Chemistry Letters*, Vol. 20, No. 6, 2022, pp. 3525–3554.

[12] Zeng, W., Liu, J., Ma, H., Liu, Y., and Liu, A., "Experimental Study on the Flame Propagation and Laminar Combustion Characteristics of Landfill Gas," *Energy*, Vol. 158, 2018, pp. 437–448.

[13] Kohn, M. P., Lee, J., Basinger, M. L., and Castaldi, M. J., "Performance of an Internal Combustion Engine Operating on Landfill Gas and the Effect of Syngas Addition," *Industrial & engineering chemistry research*, Vol. 50, No. 6, 2011, pp. 3570–3579.

[14] Qin, W., Egolfopoulos, F. N., and Tsotsis, T. T., "Fundamental and Environmental Aspects of Landfill Gas Utilization for Power Generation," *Chemical Engineering Journal*, Vol. 82, Nos. 1–3, 2001, pp. 157–172.

[15] Jiang, L., Agrawal, A. K., and Taylor, R. P., "Clean Combustion of Different Liquid Fuels Using a Novel Injector," *Experimental thermal and fluid science*, Vol. 57, 2014, pp. 275–284.

[16] Lefebvre, A. H., "Airblast Atomization," *Progress in Energy and Combustion Science*, Vol. 6, No. 3, 1980, pp. 233–261.

[17] Simmons, B. M., and Agrawal, A. K., "Spray Characteristics of a Flow-Blurring Atomizer," *Atomization and Sprays*, Vol. 20, No. 9, 2010.

[18] Akinyemi, O. S., and Jiang, L., "Development and Combustion Characterization of a Novel Twin-Fluid Fuel Injector in a Swirl-Stabilized Gas Turbine Burner Operating on Straight Vegetable Oil," *Experimental Thermal and Fluid Science*, Vol. 102, 2019, pp. 279–290.

[19] Gañán-Calvo, A. M., "Enhanced Liquid Atomization: From Flow-Focusing to Flow-Blurring," *Applied physics letters*, Vol. 86, No. 21, 2005.

[20] Jiang, L., and Agrawal, A. K., "Investigation of Glycerol Atomization in the Near-Field of a Flow-Blurring Injector Using Time-Resolved PIV and High-Speed Visualization," *Flow, Turbulence and Combustion*, Vol. 94, 2015, pp. 323–338.

[21] Qavi, I., Jiang, L., and Akinyemi, O. S., "Near-Field Spray Characterization of a High-Viscosity Alternative Jet Fuel Blend C-3 Using a Flow Blurring Injector," *fuel*, Vol. 293, 2021, p. 120350.

[22] Simmons, B. M., Panchasara, H. V., and Agrawal, A. K., "A Comparison of Air-Blast and Flow-Blurring Injectors Using Phase Doppler Particle Analyzer Technique," Vol. 48838, 2009, pp. 981–992.
[23] Jiang, L., and Agrawal, A. K., "Spray Features in the near Field of a Flow-Blurring Injector Investigated by High-Speed Visualization and Time-Resolved PIV," *Experiments in Fluids*, Vol. 56, 2015, pp. 1–13.
[24] Hall, T., Williams, D., Islam, S. R., Patel, I., Chakmakjian, C., and Jiang, L., "Clean Co-Combustion of Glycerol and Methanol Blends Using a Novel Fuel-Flexible Injector," *Fuel*, Vol. 371, 2024, p. 132125.
[25] Akinyemi, O. S., Jiang, L., Hernandez, R., McIntyre, C., and Holmes, W., "Combustion of Straight Algae Oil in a Swirl-Stabilized Burner Using a Novel Twin-Fluid Injector," *Fuel*, Vol. 241, 2019, pp. 176–187.
[26] Jiang, L., Akinyemi, O. S., and Danh, V., "Investigation of Combustion Characteristics of Straight Vegetable Oil for a Novel Twin-Fluid Fuel Injector," 2017.
[27] Danh, V., Akinyemi, O. S., Taylor, C. E., Frank, J. T., and Jiang, L., "Effect of Injector Swirl Number on Near-Field Spray Characteristics of a Novel Twin-Fluid Injector," *Experiments in Fluids*, Vol. 60, 2019, pp. 1–17.
[28] Islam, S. R., Patel, I., and Jiang, L., "Effect of Methane on Combustion of Glycerol and Methanol Blends Using a Novel Swirl Burst Injector in a Model Dual-Fuel Gas Turbine Combustor," *Clean Technologies*, Vol. 6, No. 4, 2024, pp. 1445–1464.
[29] Jiang, L., Hall, T., Williams, D., and Swinney, R., "Global Combustion Characteristics of Glycerol and Methanol Blends Using a Novel Fuel-Flexible Injector," National Harbor, MD & Online, 2023. https://doi.org/10.2514/6.2023-0495
[30] Danh, V., Jiang, L., and Akinyemi, O. S., "Investigation of Water Spray Characteristics in the near Field of a Novel Swirl Burst Injector," *Experimental Thermal and Fluid Science*, Vol. 102, 2019, pp. 376–386.
[31] Lilley, D. G., "Swirl Flows in Combustion: A Review," *AIAA journal*, Vol. 15, No. 8, 1977, pp. 1063–1078.
[32] Y., B. H., and Banapurmath, N. R., "Effect of CNG Manifold Injection on the Performance, Combustion and Emission Characteristics of a CNG -Biodiesel Dual Fuel Operation/Bir Manifolda Enjekte Edilen CNG-Biyodizel Çift Yakıt Çalışmasının Perf.,Yanma ve Emisyon Karakteristikleri Üzerine Etkisi," *International Journal of Automotive Engineering and Technologies*, Vol. 4, No. 4, 2016, p. 223. https://doi.org/10.18245/ijaet.46045
[33] Banapurmath, N. R., Marikatti, M. K., Hunashyal, A. M., and Tewari, P. G., "Combustion Characteristics of a Four-Stroke CI Engine Operated on Honge and Jatropha Oil Methyl Ester–Ethanol Blends When Directly Injected and Dual Fuelled with CNG Induction," *International Journal of Sustainable Engineering*, Vol. 4, No. 2, 2011, pp. 145–152. https://doi.org/10.1080/19397038.2010.540680
[34] Wang, Z., Yelishala, S. C., Yu, G., Metghalchi, H., and Levendis, Y. A., "Effects of Carbon Dioxide on Laminar Burning Speed and Flame Instability of Methane/Air and Propane/Air Mixtures: A Literature Review," *Energy & Fuels*, Vol. 33, No. 10, 2019, pp. 9403–9418.
[35] Feng, W., Shibo, L., Yizhuo, H., and Huiqiao, J., "The Chemical Effect of CO2 on the Methane Laminar Flame Speed in O2/CO2 Atmosphere," Vol. 186, 2018, pp. 012050.
[36] Mortazavi, H., Wang, Y., Ma, Z., and Zhang, Y., "The Investigation of CO2 Effect on the Characteristics of a Methane Diffusion Flame," *Elsevier*, Vol. 92, 2018, pp. 97–102. https://doi.org/10.1016/j.expthermflusci.2017.11.005

Investigation of Effect of Fluid Properties on Near-Field Spray Characteristics of a Two-Phase Swirl Burst Injector

Md Shakil Ahmed[1], Presley Mogote[2], Kamel Fezzaa[3], Samuel Clark[4] and Lulin Jiang[5]*

[1,2,5]*Department of Mechanical Engineering, Baylor University, Waco, TX 76798, USA*
[3,4]*X-Ray Imaging Group, Advanced Photon Source, Argonne National Lab, Argonne, IL 60439, USA*

Effective atomization dictates clean and efficient liquid fuel combustion. A novel twin-fluid swirl burst injector combining reverse internal and external swirls (SBCR) injector has previously produced fine and stable sprays for water at the injector immediate exit, rather than a typical jet of conventional atomizers that are highly sensitive to slight fuel property variations. Based on the superior SBCR atomization, this study investigates the effect of fluid properties on the SBCR spray behavior at a constant air-to-liquid mass ratio (ALR) of 2.0. Three working fluids were chosen to reflect a wide range of viscosities and surface tensions characteristic of conventional and bio-derived fuels: 100% water, 100% glycerol and a 50%/50% glycerol/water blend by mass. These fluids were selected because of their differing rheological characteristics as well as their applicability in real-world combustion systems looking for sustainable substitutes for fuels generated from fossil fuels. Under the same operating conditions, droplet size distribution, breakup dynamics, and spray stability will be evaluated using high-speed X-ray imaging and frequency-domain analysis. This study will examine the critical role of fluid properties in governing spray behavior and highlight the SBCR injector's robust performance across a wide range of rheologies. The study supports SBCR configuration as a promising candidate for future low-emission, fuel-flexible combustion systems capable of handling distinct fossil fuels and next-generation alternative fuels.

I. Nomenclature

ALR	=	Air-to-Liquid Mass Ratio
D	=	inner diameter of liquid tube and injector exit orifice
D_t	=	outer diameter of grooved surface
D_h	=	inner diameter of grooved surface
α	=	angle of swirl imparted to the atomizing air at the liquid tube tip
H	=	gap height between liquid tube and exit orifice
AB	=	Air Blast
PS	=	Pressure-Swirl
FB	=	Flow Blurring

[1,2] Graduate Research Assistant, Department of Mechanical Engineering, Baylor University
[3] Supporting Author, Physicist at Argonne National Laboratory
[4] Supporting Author, Advanced Photon Source Scientist at Argonne National Laboratory
[5] Assistant Professor, Department of Mechanical Engineering, Baylor University, and AIAA Senior member
* Corresponding Author Email: Lulin_Jiang@baylor.edu

AA = atomizing air
SB = Swirl Burst
ISN = Injector Swirl Number
SBP = Swirl Burst Primary with enhanced primary atomization
SBS = Swirl Burst Secondary with enhanced secondary aotmization
SBCR = Swirl Burst injector combining reverse internal and external swirls
SMD = Sauter Mean Diameter
FFT = Fast Fourier Transformation

II. Introduction

Global energy demands are rising because of widespread population increase and rising living standards in many areas. Growing worldwide energy usage presents problems for energy security and greatly contributes to environmental deterioration [1]. Because of their affordability, sustainability, and lower carbon footprint, alternative fuels - especially bio-derived ones like glycerol - have grown in popularity as worries about the depletion of fossil fuels and environmental degradation grow on a worldwide scale. However, due to its high viscosity and autoignition temperature, glycerol, a by-product of the manufacturing of biodiesel, is difficult to use directly in combustion systems without undergoing significant preprocessing or chemical modification due to the limited atomization capability of conventional atomizers [2,3].

When used with viscous fuels, conventional air-blast (AB) and pressure-swirl (PS) injectors, which mostly rely on shear-layer instabilities to break up fuel streams/films discharged from the injector orifice, are not very effective. Fuels like glycerol have high viscosities, which greatly reduce the shear-driven atomization mechanism and cause inadequate fuel-air mixing and inefficient combustion [4]. Insufficient atomization of viscous fuels lead to inconsistent droplet size distribution with large droplets, which undergo incomplete fuel pervaporation and result in poor fuel air mixing. Consequently, it leads to incomplete and/or diffusion combustion emitting pollutants and decreasing combustion efficiency. Thus, fuel preheating and air preconditioning were necessary in many earlier experiments to address these issues, which increased system complexity and energy costs as well as decreased operational efficiency.

Using internal two-phase interactions and bubble-bursting events slightly upstream the injector exit, flow-blurring (FB) atomization proved to be a reliable substitute that could produce finer sprays [5]. Without requiring fuel or air preheating, FB injectors have achieved fine atomization across a variety of fuels, including straight glycerol and straight vegetable oil [3,6], showing its significantly higher fuel property independence than that of the conventional AB or PS atomizers. Compared to the conventional AB injector atomizing liquid by shear layer instabilities, the FB atomization involves primary atomization by bubble bursting and liquid column breakup due to a sudden pressure drop at the injector exit, and the secondary atomization by shear layer instabilities between the high-velocity air and the liquid droplets in the near field [7]. As a result, FB injectors are now seen as potentially viable options for fuel-flexible combustion systems. Nevertheless, restrictions were noted even with FB injectors, where high-viscosity fuels were more likely to cause ligament persistence and reduced breakup efficiency [3].

To overcome these residual difficulties, the first version of Swirl Burst (SB) injector concept was designed to enhance secondary atomization, called Swirl Burst Secondary (SBS). By incorporating swirl-inducing geometries at the chamfered FB injector exit, the SB design enhances atomization through intensified shear-layer instabilities and thus improved breakup of large droplets [8]. Furthermore, the Swirl Burst Injector combining reverse internal and external swirls (SBCR) has a reverse-oriented internal swirl that counteracts the external swirl. The internal and external swirls are to enhance the primary and secondary atomization respectively. The atomizing air (AA)'s radial and tangential velocity are increased by this interaction, improving the internal and external two-phase mixing. Consequently, the spray stabilizes from our previous study, fine and consistent droplet dispersion across the spray field for water is achieved by the SBCR injector [9].

This study expands on these developments by systematically investigating how physical characteristics of the fluid—viscosity, surface tension, and density—affect near-field spray characteristics and temporal stability in the SBCR injector under a controlled ALR of 2.0. The study will quantitatively investigate spray characteristics using high-speed X-ray imaging, Cumulative Density Function (CDF) plots, Sauter Mean Diameter (SMD) contouring, and spray dynamics by Fast Fourier Transform (FFT) frequency-domain analysis, using three working fluids of increasing viscosity: 100% water, 50%/50% glycerol/water, and 100% glycerol. The findings will provide critical insight into how the SBCR injector can facilitate fuel-flexible, clean, and stable combustion with a range of liquid fuel types.

III. Objectives

Driven by the achieved ultra-fine and fast atomization of water using the SBCR,, the current study aims to quantify how different fuel physical properties (viscosity, surface tension and density) affect near-field spray dynamics and characteristics for the SBCR injector at a given ALR of 2.0. Under the same geometric and flow parameters, the major goal is to evaluate the effects of three different working fluids: 100% water, 50%/50% glycerol/water, and 100% glycerol on the Sauter Mean Diameter (SMD), droplet size distribution, and frequency-domain spray fluctuations. Spray stability will be observed using FFT-based spray fluctuation analysis in conjunction with high-speed X-ray imaging. This experimental study will help achieve the broader goal of stable, efficient combustion using fuel-flexible atomizer designs by benchmarking the SBCR injector's adaptability across fuel types.

IV. Experimental Setup

Figure 1(a) illustrates the FB and SB design and working principle. The SBS injector incorporates a radial element of AA into the liquid stream from the injector nozzle by combining swirling grooves onto the injector orifice exit. This injector works on the same concept as the FB injector in terms of primary atomization mechanism, which is achieved by internal bubbling and bubble bursting [10]. In order for the SB injector to function, the inner piece must be suspended inside the injector frame and the *D* to *H* ratio must be 4:1 or below [10].

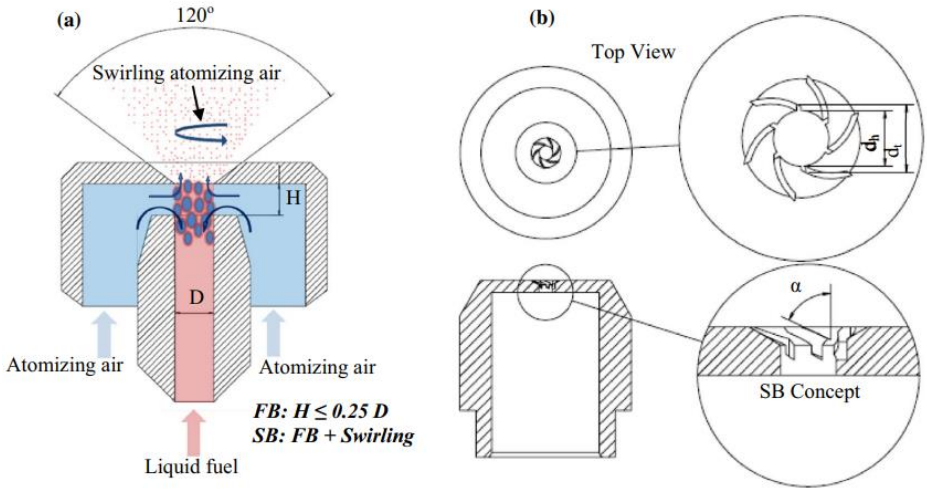

Figure 1: (a) Working principle of the FB and SB injector, (b) Swirl-burst concept [8].

When the aforementioned geometrical conditions are met, the atomizing gas gets divided into two portions at the stagnation plane developed at the annular gap (*H*) between the liquid tube tip and the injector exit orifice [10]. A vortex that improves the bifurcation process and boosts fine atomization is created when the AA is guided through the swirling grooves and acquires a tangential velocity with respect to the inner liquid tube. Because the air and air-liquid mixture have different velocity vectors, the pressure of the air-liquid mixture decreases near the injector exit, causing shear layer instabilities. The Injector Swirl Number (ISN) was created using the guiding design factors to regulate the swirl's curvature by earlier researchers [11]. Eq. (1) defines the ISN:

$$ISN = \frac{2}{3} \times \frac{1-(d_h/d_t)^3}{1-(d_h/d_t)^2} \times \tan\alpha \quad (1)$$

where d_t is the grooves' tip diameter, d_h is the diameter of the hub, which is roughly equivalent to the diameter of the exit orifice, and α is the swirl grooves' exit angle, which is the angle between the tangent line to the exit of the groove at the inner wall in relation to the spray axis. This angle roughly corresponds to the angle at which air exits the groove [12]. *D*=1.5 mm, *H*=0.375 mm, injector opening angle=120 degrees, α=71.6 degrees, and ISN=2.6 are the important geometrical parameters. The SBCR injector, which includes swirl grooves into both the inner and outer components, has combined the same key geometries as the Swirl Burst Primary with improved primary atomization (SBP) and

Swirl Burst Secondary (SBS) injectors, as seen in Fig. 2. The swirl which assists in secondary atomization in the SBCR injector is oriented in the opposite direction from the internal swirl that contribute to primary atomization.

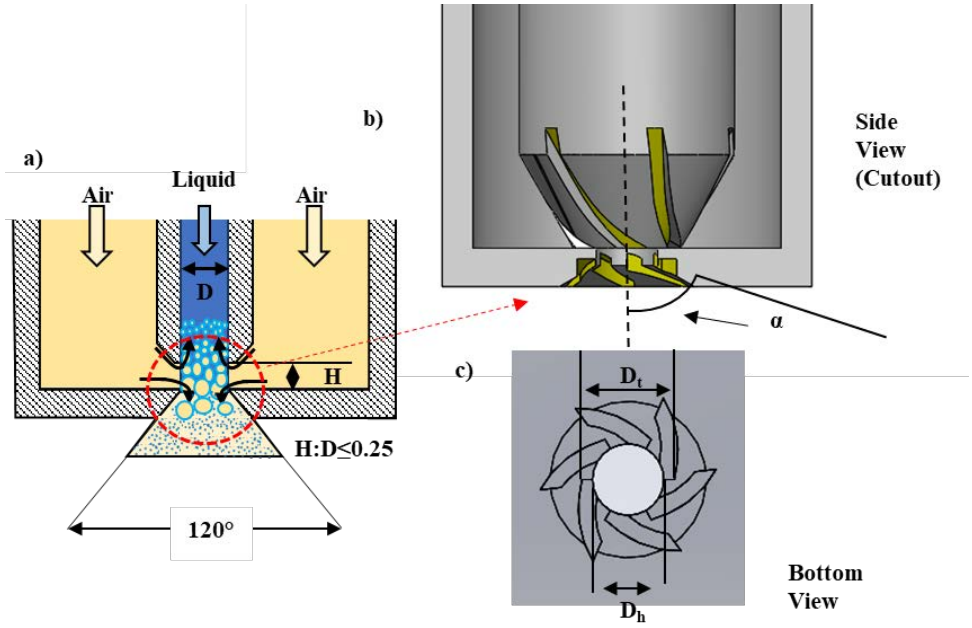

Figure 2: (a) SBCR bubble bursting atomizing visualization and (b, c) visual and important parameters [9].

High-resolution X-ray imaging is used in the experimental setup to record precise near-field spray behavior. A ¼" inner diameter (ID) flexible tube (rated for -68°F to 140°F, 180 psi) and a ~¼" ID welded steel tube (rated for -65°F to 800°F, 3,700 psi at 72°F) regulate and supply the compressed air to the injector after it has been conditioned by filters and a water trap [9]. An Alicat Mass Flow Controller (Model MCR-250SLPM-D) with ±0.8% reading accuracy and ±0.2% full-scale error is used to precisely manage airflow. A Cole-Parmer Digital Peristaltic Pump (Masterflex L/S Model 07522-30) supplies the liquid phase, which travels through a ¼" OD welded steel tube and a ½" OD rubber hose that is rated for temperatures between 25°F and 150°F and 350 psi [9]. Smooth flow is ensured by a custom-made pulsation dampener. To reduce contamination, an acrylic spray chamber encloses the injector. In addition to having windows for polyimide (Kapton) film for X-ray transparency, the chamber has specific ports for injecting inert air to keep the film from fogging during spray imaging [9]. A Shimadzu HPV-X2 high-speed camera (Serial No. 1778057L0122) with a temporal resolution of 110 ns at 5 MHz and exposure of 500 ns at 100 kHz is used in the imaging setup [9]. The X-ray system records 128 images each sequence with a spatial resolution of 3 μm/pixel over a field of view of 0.75 mm × 1.2 mm [9]. 5 MHz imaging is made possible via a 3.3 cm period undulator with a 15 mm gap [9]. Fast-moving droplets are efficiently frozen by the extremely short pulse duration, reducing motion blur for precise analysis.

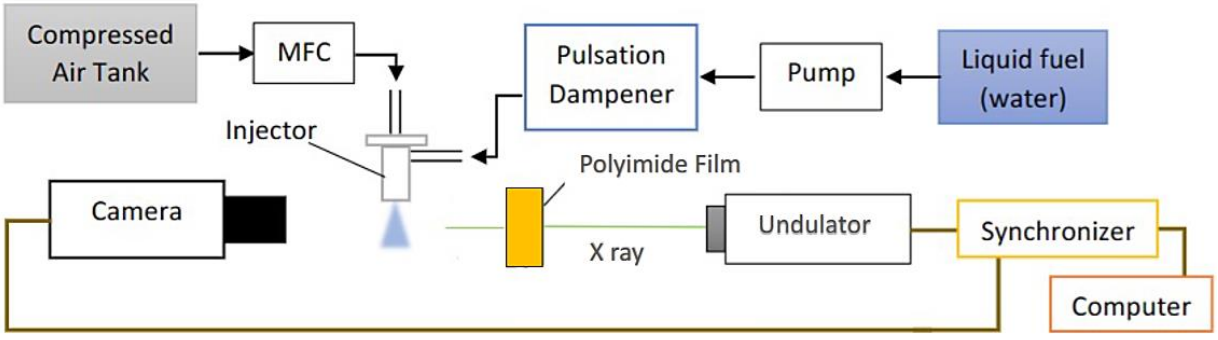

Figure 3: Experimental setup diagram [9].

ImageJ software with a variety of plug-ins and macros is used in the image processing procedure. The Retinex filter is used to improve the contrast and color restoration of raw X-ray images, and then the BaSiC plugin is used to correct the illumination [9]. The median Z-Project and subtraction method is used to eliminate lens static distortions [9]. The CSBDeep plugin's Noise2Void function is used to remove background noise by training a custom de-noising model [9]. The TrackMate plugin for droplet tracking and data export is then used to threshold and analyze the cleaned photos [9]. To evaluate spray characteristics and stability, MATLAB programs subsequently transformed the data into droplet distribution plots, Sauter Mean Diameter (SMD) contour maps, and Fourier transforms etc. Table showing the flow rates is given below.

Table 1: Experimental flow rates

Injector Exit D = 1.5 mm			
Type of Fluid	**Liquid Flow Rate (mLPM)**	**Air Flow Rate (sLPM)**	**ALR**
100% Water	12	19.96	2
50%/50% Glycerol/Water	12	22.57	
100% Glycerol	12	25.26	

V. Results and Discussion

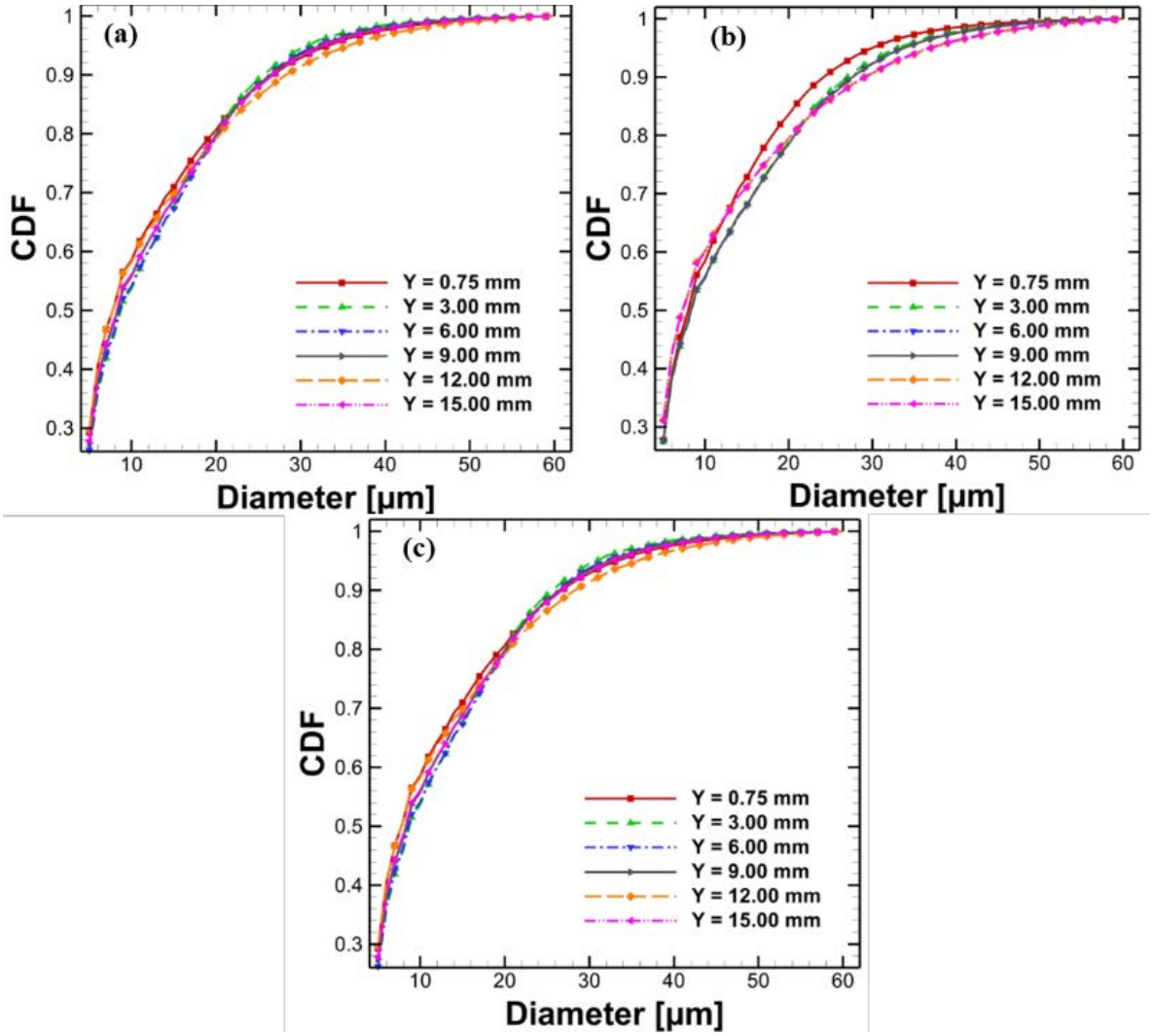

Figure 4: Cumulative density function (CDF) profile for (a) 100% Water, (b) 50%/50% Glycerol/Water & (c) 100% Glycerol at an ALR of 2.00 for SBCR injector.

Figure 4 shows the cumulative density function (CDF) profiles which are based on the droplet count for three different fluid types at an ALR of 2.00 for the SBCR injector. From the plots, 90% droplets are below ~28 μm for all the fluids at all the axial locations. This consistent trend indicates that the SBCR injector effectively generates fine sprays, demonstrating its robust atomization performance independent of fuel properties. The ability to maintain such fine droplet characteristics across varying fluid properties highlights the injector's versatility and effectiveness due to efficient atomization. The SBCR injector's capacity to consistently deliver fine sprays across various fluid types is especially advantageous for applications involving high-viscosity or bio-derived fuels, where conventional atomizers often fail to achieve comparable spray quality. Overall, the plots validate the SBCR injector's superior atomization performance and its potential for broad applicability in advanced combustion and spray-based systems.

VI. Conclusion

Motivated by the growing demand for fuel-flexible, low-emission combustion technologies, this study proposes an in-depth analysis into the effect of fluid properties on the spray performance of the SBCR injector at a fixed ALR of 2.00. The study uses water and bio-derived fuels to examine atomization issues that arise in real-world applications

by choosing fluids with a broad variety of viscosities and surface tensions, specifically 100% water, 50%/50% glycerol/water, and 100% glycerol. The study will measure droplet size distributions and spray dynamics by combining frequency-domain analysis and high-speed X-ray imaging. This proposed study will advance knowledge of the connection between twin-fluid swirl-assisted injectors' atomization efficiency and fuel physical characteristics. These results are anticipated to help the broader goal of incorporating alternative fuels into future energy solutions with enhanced stability and lower emissions, as well as direct the best use of SBCR designs for advanced combustion systems.

Acknowledgements

This research is funded by the Startup fund of Baylor University and NSF CIVIC award No. 2228311 and No. 2322319. This work is being conducted at Advanced Photon Source (APS) beamline 32-ID at Argonne National Lab based on the awarded beamtime under the GUP #80526. We would like to thank Mrs. Rachel Swinney for assisting with data collection, and Mr. Alex L. Deriy, the Beamline Instrumentation Specialist, who helped facilitate the easy and efficient experimental setup. We also sincerely appreciate Mr. Presley Mogote, Mr. John Cary, Mrs. Karly Jackson, and Mr. Curtis Jackson's assistance on injector SolidWorks design, manufacturing, and/or experimental setup.

References

[1] M. S. Ahmed, R. Karal, B. K. Das, and A. Das, "Experimental investigation of cooling, wind velocity, and dust deposition effects on solar PV performance in a tropical climate in Bangladesh," *Case Stud. Therm. Eng.*, vol. 50, p. 103409, Oct. 2023, doi: 10.1016/j.csite.2023.103409.

[2] L. Jiang and A. K. Agrawal, "Combustion of straight glycerol with/without methane using a fuel-flexible, low-emissions burner," *Fuel*, vol. 136, pp. 177–184, Nov. 2014, doi: 10.1016/j.fuel.2014.07.027.

[3] L. Jiang and A. K. Agrawal, "Investigation of Glycerol Atomization in the Near-Field of a Flow-Blurring Injector using Time-Resolved PIV and High-Speed Visualization," *Flow Turbul. Combust.*, vol. 94, no. 2, pp. 323–338, Mar. 2015, doi: 10.1007/s10494-014-9572-2.

[4] I. Qavi and L. Jiang, "Optical Characterization of Near-Field Sprays for Various Alternative and Conventional Jet Fuels Using a Flow-Blurring Injector," *Flow Turbul. Combust.*, vol. 108, no. 2, pp. 599–624, Feb. 2022, doi: 10.1007/s10494-021-00276-9.

[5] A. Gañán-Calvo, "Enhanced liquid atomization: From flow-focusing to flow-blurring," *Appl. Phys. Lett.*, vol. 86, pp. 214101–214101, May 2005, doi: 10.1063/1.1931057.

[6] B. M. Simmons and A. K. Agrawal, "Flow Blurring Atomization for Low-Emission Combustion of Liquid Biofuels," *Combust. Sci. Technol.*, vol. 184, no. 5, pp. 660–675, May 2012, doi: 10.1080/00102202.2012.660222.

[7] J. Breerwood, L. Jiang, and M. S. Ahmed, "Near-field spray characteristics and steadiness of a novel twin-fluid injector with enhanced primary atomization," *J. Aerosol Sci.*, vol. 180, p. 106402, 2024, doi: https://doi.org/10.1016/j.jaerosci.2024.106402.

[8] V. Danh, O. S. Akinyemi, C. E. Taylor, J. T. Frank, and L. Jiang, "Effect of injector swirl number on near-field spray characteristics of a novel twin-fluid injector," *Exp. Fluids*, vol. 60, no. 5, p. 80, 2019a, doi: 10.1007/s00348-019-2721-6.

[9] M. S. Ahmed, J. Cary, K. Fezzaa, S. Clark, S. T. McClain, and L. Jiang, "Effect of Internal and External Swirls on Near-Field Spray Characteristics of Swirl Burst Injectors Using High-Speed X-Ray Imaging," in *AIAA SCITECH 2024 Forum*, American Institute of Aeronautics and Astronautics. doi: 10.2514/6.2024-0218.

[10] O. S. Akinyemi and L. Jiang, "Development and combustion characterization of a novel twin-fluid fuel injector in a swirl-stabilized gas turbine burner operating on straight vegetable oil," *Exp. Therm. Fluid Sci.*, vol. 102, pp. 279–290, Apr. 2019, doi: 10.1016/j.expthermflusci.2018.11.014.

[11] B. Khandelwal, D. Lili, and V. Sethi, "Design and study on performance of axial swirler for annular combustor by changing different design parameters," *J. Energy Inst.*, vol. 87, no. 4, pp. 372–382, Nov. 2014, doi: 10.1016/j.joei.2014.03.022.

[12] A. K. Gupta, D. G. Lilley, and N. Syred, *Swirl flows*. 1984. Accessed: May 20, 2025. [Online]. Available: https://ui.adsabs.harvard.edu/abs/1984tw...book.....G